Distribution Agreement

In presenting this thesis or dissertation as a partial fulfillment of the requirements for an advanced degree from Emory University, I hereby grant to Emory University and its agents the non-exclusive license to archive, make accessible, and display my thesis or dissertation in whole or in part in all forms of media, now or hereafter known, including display on the world wide web. I understand that I may select some access restrictions as part of the online submission of this thesis or dissertation. I retain all ownership rights to the copyright of the thesis or dissertation. I also retain the right to use in future works (such as articles or books) all or part of this thesis or dissertation.

Signature:

_____	_____
Mooeung Kim	Date

Mechanistic Study on Multi-Electron Processes in POM Catalysis

By

Mooeung Kim
Doctor of Philosophy

Chemistry

_____
Craig L. Hill, Ph.D.
Advisor

_____
Brian Dyer, Ph.D.
Committee Member

_____
Cora MacBeth, Ph.D.
Committee Member

Accepted:

_____
Lisa A. Tedesco, Ph.D.
Dean of the James T. Laney School of Graduate Studies

_____
Date

Mechanistic Study on Multi-Electron Processes in POM Catalysis

By

Mooeung Kim
B.S. Hanyang University, Korea, 2011
M.S. Hanyang University, Korea, 2013

Advisor: Craig L. Hill, Ph.D.

An abstract of
a dissertation submitted to the Faculty of the
James T. Laney School of Graduate Studies of Emory University
in partial fulfillment of the requirements for the degree of
Doctor of Philosophy
in Chemistry
2018

Abstract

Mechanistic Study on Multi-Electron Processes in POM Catalysis

By

Mooeung Kim

Polyoxometalate (POM)-based catalytic oxidations have been attracting great attention and are even used in several commercialized POM-dependent processes owing to their distinctive natures, especially high stability toward oxidative and hydrolytic degradation as well as capability to transfer multiple electrons without structural alterations. POM-based aerobic oxidation generally comprise two steps: (1) oxidation of a substrate catalyzed by the form of POM and (2) the counterpart, reoxidation of reduced POM by O_2. The latter step is usually slower than the former, and thus is rate-limiting, so that is generally considered the key reaction in POM-catalyzed O_2-based oxidations. In addition, the development of efficient water oxidation catalysts (WOCs) has been challenging. The fact that water oxidation is a multi-electron process has led to utilizing POMs as WOCs. Cobalt-containing species including POMs, CoO_x and others are known to be among the most active WOCs. However, understanding the behavior and mechanism of aqueous cobalt is necessary due to the lack of detailed investigations on aqueous cobalt. Given these facts, this dissertation is mainly on the focus of two parts: (1) O_2-based POM_{red} reoxidation to make it more efficient and (2) a thorough analysis on aqueous cobalt WOCs.

The reoxidation process is investigated in Chapters 2 through 4. The first part describes Cu catalysis of the reoxidation process. Chapter 2 addresses the fact that trace amounts of Cu efficiently catalyze oxidation of the one-electron-reduced Keggin heteropolytungstates, $SiW_{12}O_{40}^{5-}$. Chapter 3 involves further advances using both Cu(II) and Fe(II) as a more efficient POM_{red} reoxidation catalyst, and Chapter 4 describes aerobic (O_2-based) reoxidation of reduced POMs that have much higher potentials by nitrous acid.

The last chapter addresses the true catalysts in catalytic water oxidation using aqueous cobalt and $[Co_4(H_2O)_2(VW_9O_{34})_2]^{10-}$: key catalytic species and mechanisms are elucidated. Double-mixing stopped-flow kinetics and systematic computational calculations ascertain the possible active catalysts in water oxidation by aqueous solutions of cobalt ion, Co(II), that are present in many types of water oxidation catalysts.

Mechanistic Study on Multi-Electron Processes in POM Catalysis

By

Mooeung Kim
B.S. Hanyang University, Korea, 2011
M.S. Hanyang University, Korea, 2013

Advisor: Craig L. Hill, Ph.D.

A dissertation submitted to the Faculty of the
James T. Laney School of Graduate Studies of Emory University
in partial fulfillment of the requirements for the degree of
Doctor of Philosophy
in Chemistry
2018

Acknowledgments

I very much cherish everyone I have met, everything I have known, everywhere I have been, and all the time I have spent in pursuit of my doctoral degree here at Emory. I could take priceless experiences at Emory with full of appreciation to everyone who has been with me.

My deepest appreciation and utmost respect go first to my advisor, Dr. Craig L. Hill. He accepted me to join the Hill group, even my research was not focused on Inorganic Chemistry. This was one of the best moments in my Emory life. As my mentor and advisor, I have never met such a distinguished, caring professor, who has provided me not only scientific guidance but also the way how to make life wonderful. Dr. Hill also encouraged me to be more positive, interact with more people, to be more confident in myself. His constant motivation has made me feel recognized and mentally stronger. Without his vital support and assistance, it would have been impossible to make my life successful at Emory.

I would like to express my gratitude to Dr. Brian Dyer who interviewed and provided me an opportunity to study at Emory University. His advanced inorganic chemistry class laid the groundwork for my subsequent research. I made progress in my research and was motivated under his guidance and advice for the annual reports as my committee member.

I am grateful to Dr. Christopher C. Scarborough, who accepted to be on my committee. I sincerely had the pleasure to talk with him. I still remember the joyful moments in his class and we played soccer together.

I also wish to show my warm thank to Dr. Cora MacBeth. When I had to handle the situation to choose my committee member again, she accepted to be my committee without hesitation. Her great personality makes me have a more positive attitude towards research and even life.

I would like to offer my very special appreciation to Dr. Yurii V. Geletii, who has been my true mentor and another supervisor. It is very fortunate to me that I could work with this brilliant scientist of great knowledge. His remarkable intelligence in kinetics has been

helpful to my overall research indeed. He has provided me invaluable scientific assistance as well as meaningful information for a better life. I will never forget his representative wording “Don’t trust anyone except ME”, and I will keep that in mind.

I owe a debt of gratitude to Dr. Giovanni Gadda who is a professor in Department of Chemistry at Georgia State University. He welcomed and allowed me to use his double mixing stopped-flow system for which I am grateful. I also thank his student, Daniel Ouedraogo, who kindly helped me to use the instrument.

I really appreciate all the past and present Hill group members: Dr. Zhen Lou, Dr. Guibo Zhu, Dr. Chongchao Zhao, Dr. James W. Vickers, Dr. Hongjin Lv, Dr. Elliot Glass, Dr. Weiwei Guo, Jordan Sumliner, Dr. Marika Wieliczko, Dr. Sarah Lauinger, Kevin Sullivan, Daniel Collins-Wildman, Ben Yin, Torie Snider, Philip Zhu, Juncheng Yang, Yimu Hu, Dr. Masoumeh Chamack, Meilin Tao, and others. I owe my special gratitude to Leslie Chauvin, who has inspired me to live confidently and wisely. With these nice people, my life has been truly valuable, and I won’t forget any single moment at Emory.

Additional sincere thanks will be to all of my friends who have supported me in many ways. I cannot imagine this achievement without you all.

Nobody has been more important to me in my life than my beloved family, whose love and support are with me in whatever I do. Words could never be enough to express my gratitude to my family. I deeply wish my family good health and endless happiness.

Last but not least, I want to express my appreciation to Emory University for providing a valuable opportunity to study and strengthen my personal development.

Table of Contents

List of Figures

List of Schemes

List of Tables

List of Symbols and Abbreviations

A	absorbance
AlVW11$_{ox}$	α-$AlVW_{11}O_{40}^{6-}$
AlVW11$_{red}$	α-$AlVW_{11}O_{40}^{7-}$
AlW12$_{ox}$	α-$AlW_{12}O_{40}^{5-}$
AlW12$_{red}$	α-$AlW_{12}O_{40}^{6-}$
atm	standard atmosphere, unit of pressure
bpy	2,2'-bipyridine
Co_4P_2	$Na_{10}[Co_4(H_2O)_2(\alpha\text{-}PW_9O_{34})_2]$
Co_4V_2	$Na_{10}[Co_4(H_2O)_2(VW_9O_{34})_2]$
CPET	concerted proton-electron transfer
CT	charge transfer
CV	cyclic voltammogram
CWA	chemical warfare agent
D	dielectric constant of reaction medium
DFT	density functional theory
DMF	dimethylformamide
DMP	2,9-dimethyl-1,10-phenanthroline (neocuproine)
e	elementary charge
$E°$	standard potential
E_{app}	apparent (observed) reduction potential
E_s	standard potential at a specific condition

EtOH	ethanol, C_2H_5OH
e^-	electron
ETPT	electron transfer proton transfer
F	Faraday constant
g	gram(s)
h	hour(s)
HOMO	highest occupied molecular orbital
HPA	heteropoly acid
I	ionic strength
IR	infrared
IVCT	intervalence charge transfer
K_a	acid dissociation constant
k_{app}	apparent rate constant (observed rate constant)
kcal	kilocalorie (10^3 calories)
K_{sp}	solubility product constant
k_n	rate constant for reaction n
K_n	equilibrium constant for reaction n
LMCT	ligand-to-metal charge transfer
LUMO	lowest unoccupied molecular orbital
M	molarity
MCR	Marcus cross relation
min	minute(s)
mM	millimolar (10^{-3} molar)

mol	mole
mV	millivolt (10^{-3} volt)
N_A	Avogadro constant
NaB_i	sodium borate buffer
NHE	normal hydrogen electrode
nm	nanometer (10^{-9} meter)
NO_x	nitrogen oxide
OAc^-	acetate, CH_3COO^-
PCET	proton-coupled electron transfer
pH	potential of hydrogen, a measure of the acidity or alkalinity of a solution
POM	polyoxometalate
POM_{ox}	oxidized polyoxometalate
POM_{red}	reduced polyoxometalate
$PVW11_{ox}$	α-$PVW_{11}O_{40}^{4-}$
$PVW11_{red}$	α-$PVW_{11}O_{40}^{5-}$
$PW12_{ox}$	α-$PW_{12}O_{40}^{3-}$
$PW12_{red}$	α-$PW_{12}O_{40}^{4-}$
R	gas constant
RIXS	resonant inelastic X-ray scattering
rls	rate-limiting step
r_n	reaction rate for reaction n
RSNO	S-nitrosothiol

$[Ru(bpy)_3]^{2+}$	Tris(2,2'-bipyridyl)dichlororuthenium(II) hexahydrate
$[Ru(bpy)_3]^{3+}$	Tris(2,2′-bipyridyl)triperchlororuthenium(III)
Ru_4P_2	$Cs_9[Ru_4O_5(OH)(OH_2)_4(\gamma\text{-}PW_{10}O_{36})_2]$
Ru_4Si_2	$Rb_8K_2[Ru_4(\mu\text{-}O)_4(\mu\text{-}OH)_2(H_2O)_4(\gamma\text{-}SiW_{10}O_{36})_2]$
$SiW12_{ox}$	$\alpha\text{-}SiW_{12}O_{40}^{4-}$
$SiW12_{red}$	$\alpha\text{-}SiW_{12}O_{40}^{5-}$
s	second(s)
SCE	saturated calomel electrode
Sub	substrate
Sub_{ox}	oxidized substrate
$SiVW11_{ox}$	$\alpha\text{-}SiVW_{11}O_{40}^{5-}$
$SiVW11_{red}$	$\alpha\text{-}SiVW_{11}O_{40}^{6-}$
T	temperature
t	reaction time
TIC	toxic industrial chemical
TOF	turnover frequency
TON	turnover number
UV	ultraviolet
V	volt, electric potential
vis	visible
W_n	Coulombic working term
XAS	X-ray absorption spectroscopy
Z	collision frequency

z_n	charge of species n
Å	angstrom (10^{-10} meters)
β	formation constant
°	degree(s)
°C	degrees Celsius
ε	molar absorptivity or molar extinction coefficient
ε_0	vacuum permittivity constant
ε_n	molar extinction coefficient at wavelength n
λ	wavelength
λ_n	reorganization energy of reaction n
μ	ionic strength (Debye-Hückel equation)
μM	micromolar (10^{-6} molar)

Chapter 1

Introduction: Polyoxometalates in Redox Chemistry

1.1 Fundamental Overview of Polyoxometalates

Polyoxometalates (POMs) are defined as early transition metal oxyanion clusters.[1-4] These clusters can be formed by aggregation and condensation with the formation of transition metal oxo species in aqueous media. POMs are generally based on addenda atoms at their highest oxidation states (d^0) such as V(V), Nb(V), Mo(VI), Ta(V), or W(VI), and may contain various heteroatoms (e.g. Al, Si, P, Ge, or As) depending on the coordination geometries (tetrahedral, octahedral, or square pyramidal). These structures are classified into two families: "isopolyanions", composed of only one metal (addenda atom) and oxygen atoms, and "heteropolyanions", which also contain one or more heteroatoms in the polyanion unit.[5] The latter are generally more hydrolytically stable than the former. The spontaneous condensation from precursors (metal oxyanions and the heteroatom) into POMs is carefully controlled by acidity, concentration, ionic strength, ratio of addenda oxyanion and heteroatom, reaction time, solvent, and temperature, etc. These synthetic conditions can give rise to a wide diversity of functional properties belonging to the structural and compositional differences in POMs.[6] Despite the high tunability of POMs, the clusters are oxidatively and thermally stable, and most are also hydrolytically stable over a substantial pH range. The addition of alkali metal counter cations (e.g. Li^+, Na^+, K^+, Rb^+, Cs^+) to aqueous solutions can lead to isolation and purification of POMs via crystallization.

The very first POM was discovered by Berzelius in 1826, ammonium phosphomolybdate ($(NH_4)_3PMo_{12}O_{40}$).[7] The structure of this POM, however, was not determined due to a lack of analytical techniques at the time. Thanks to the invention of X-ray diffraction, the α-Keggin structure was identified in 1934,[8,9] and this led to the

extensive development of new POM compounds, an enterprise that has continued to date. There are a multitude of reports targeted change in the chemical, structural and physical properties of POMs by addition of other atoms or groups. Some representative structural families such as Lindqvist, Keggin (separately shown in Figure 1.2 in more detail), Well-Dawson, Crown (also known as the "Wheel"), and Preyssler structures are illustrated in Figure 1.1. Dramatic contributions to development of new POM structures have given rise

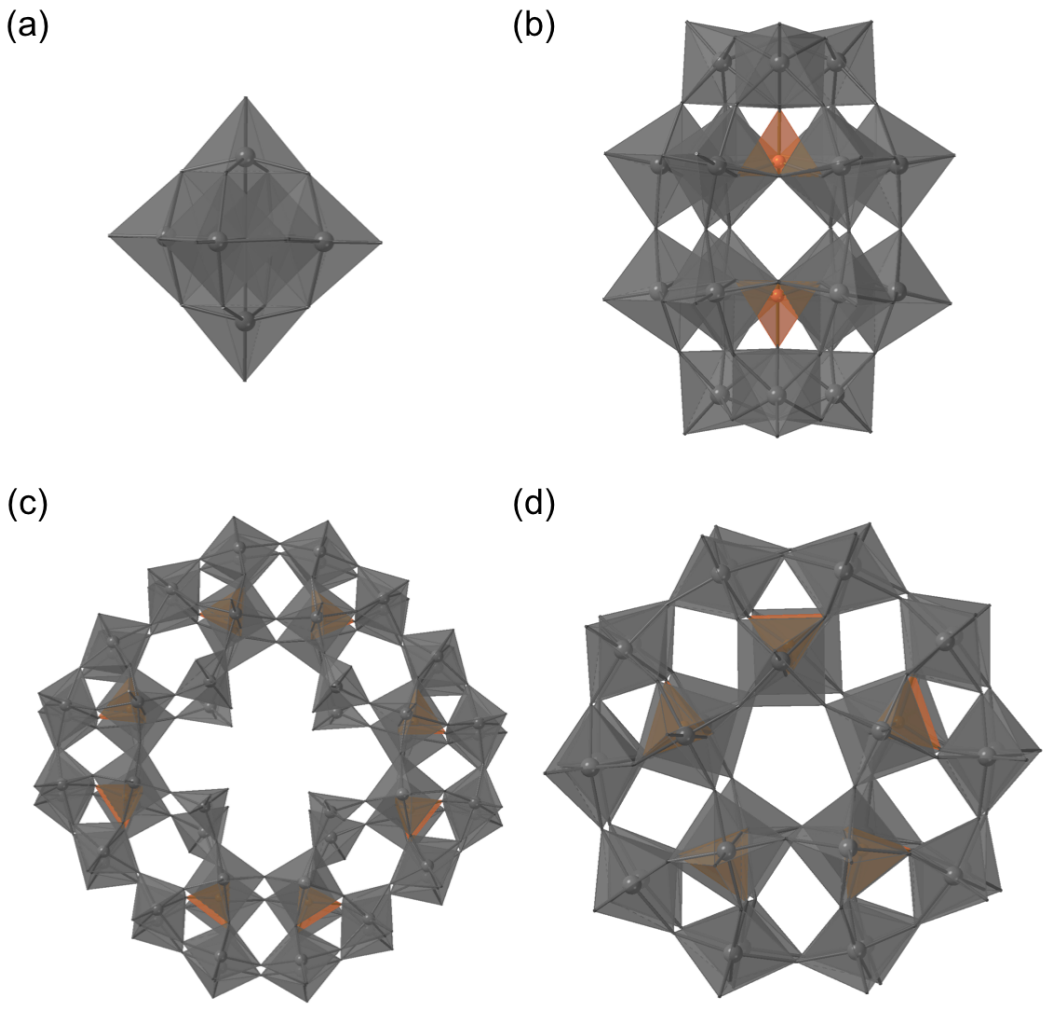

Figure 1.1. Representative polyhedral structures of polyoxometalates: (a) Lindqvist, (b) Wells-Dawson, (c) crown (or wheel), and (d) Preyssler structures.

to breakthroughs in various fields, mainly catalysis, materials, medicines, energy, and chemical/biochemical analysis, etc.[10,11]

One of the most important and well-studied POMs is the Keggin structure with a general formula of $[XM_{12}O_{40}]^{n-}$, where X (heteroatom) is commonly P^{V}, Si^{IV}, or Al^{III}, and M is Mo or W. This plenary structure is composed of 12 octahedral metal oxyanions surrounding a tetrahedral heteroatom-oxygen unit in center, giving an overall tetrahedral geometry based on the central heteroatom tetrahedron. This structure contains four M_3O_{13} units (grouped by three MO_6 units) that are corner- and edge-shared with other units. This representative and traditional structure is referred to a α-Keggin structure, and has total five isomers presented in Figure 1.2. The 60° rotation of M_3O_{13} clusters provides the other four

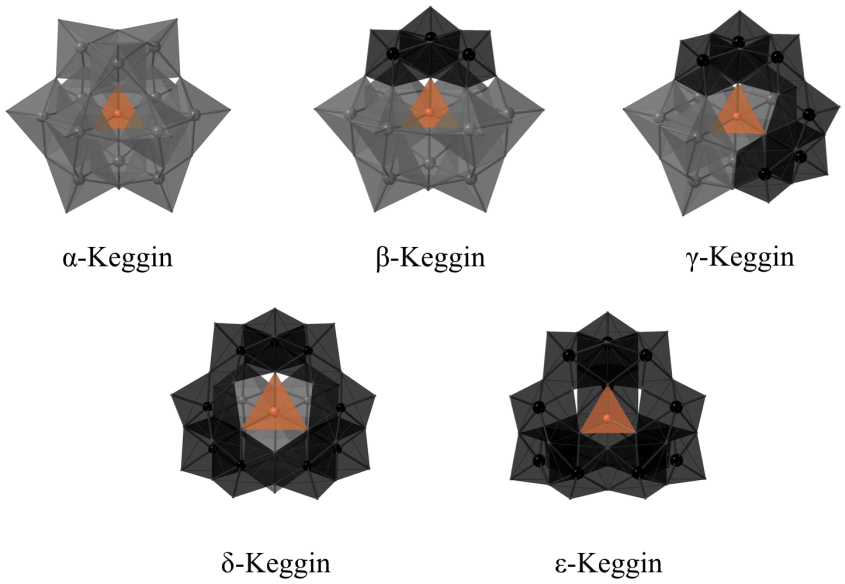

Figure 1.2. Polyhedral structures of the Keggin POM isomers. Orange, XO_4 tetrahedra; grey, MO_6 octahedra; black, M_3O_{13} units rotated by 60°.

possible isomers (β, γ, δ, and ε). The most thermodynamically stable isomer is the α-Keggin structure, and only three (α, β, and γ) have been effectively characterized and synthesized of the five theoretically possible five isomers. Several properties of these isomer forms have been scrutinized and compared in terms of their stabilities, structures, and energies.[12-20] Therefore, the α-Keggin POM, unless otherwise noted, will be discussed without any notations in this study due to its dominant stability.

Given that numerous properties of POMs have been documented, the compounds have been broadly applied to several fields including materials,[21-30] medicine,[31-38] some others,[11,39-43] and dominantly, catalysis.[44-50] In context with both fundamental research catalytic applications of POMs, I now discuss general POM properties.

1.2 General Properties of Polyoxometalates

It is the remarkable variety of POM structures, in part, that has led to the versatile properties and applications of POMs noted above. POMs have characteristic properties influenced by their size, shape, composition, acidity, charge density, solubility, and redox potentials. The notable property of POMs, mainly heteropoly acids (HPAs), is strong acid behavior in solution.[1] This acid properties were examined in detail by utilizing Hammett acidity constants and dissociation constants for HPAs in aqueous and several organic solvents.[51-53] Kozhevnikov reported that $H_3PW_{12}O_{40}$ is the strongest acid among HPA family, and even stronger than the usual mineral acids (e.g. H_2SO_4, HCl, HNO_3) based on the dissociation constants in acetone.[54] The acidity combined with the catalytic oxidation activity of HPAs, has led to the development of selective organic transformations utilizing

HPAs as acid catalysts,[55,56] and several of these (e.g. hydration of olefins, oxidation of methacrolein, polymerization of tetrahydrofuran, etc) have been commercialized.[57,44,45]

POMs have photochemical activity as well. The excitation of POMs involves charge transfer (CT) from oxygen atom to fully oxidized (d^0) transition metal center (LMCT) under the irradiation of UV or near-visible light. These LMCT bands, assigned as $O_{2p} \rightarrow W_{5d}$ or Mo_{4d}, are in the UV region.[58] The photo-excited LMCT bands involve the promotion of an electron from oxygen centered orbitals (HOMOs) and to empty metal orbitals (LUMOs).[59] The excited state of the CT species is a better oxidant than the ground state and frequently has radical character.[60] The reduced POMs resulting from quenching of the CT excited POMs are commonly intense blue in color. As a consequence, they are commonly called "heteropoly blues",[61-68] while the oxidized POMs are almost always colorless or pale yellow. The blue color of the reduced POMs results from an intervalence CT (IVCT) band around 700 nm in the electronic absorption spectrum (Figure 1.3).[66-68]

One of the most important properties of POMs, along with their photochemical ones, is the capability to accept or release one or more electrons without any changes (or decomposition) in their structures under the appropriate conditions. As mentioned in the previous section, POMs contain transition metals in their highest oxidation states, so that can oxidize many other compounds. Thus POM redox properties are pervasively important in POM chemistry,[11] and will be discussed in context with POM-based oxidation catalysis in this chapter.

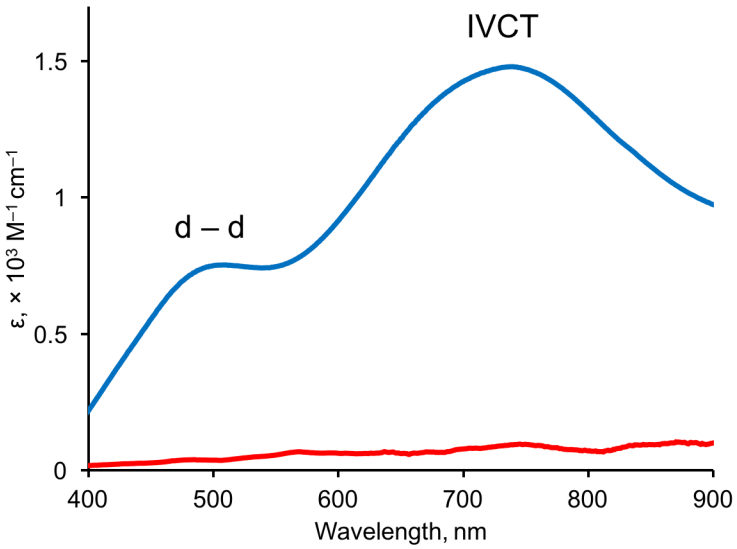

Figure 1.3. The representative absorption spectra of $[SiW_{12}O_{40}]^{4-}$ (oxidized form, red line) and $[SiW_{12}O_{40}]^{5-}$ (one electron reduced form, blue line) in 50 mM sodium sulfate buffer. The labels represent electronic transitions.

1.3 Applications of POM Catalysis

1.3.1 POM-Catalyzed Oxidation Processes

POMs have been extensively investigated in numerous fields, however, mostly in catalysis. The promising and distinctive properties of POMs, facilitating great thermal and oxidative stability (against oxidative decomposition) and extensive redox properties, have led to myriad investigations in POM-based catalysis. Organic compound oxidations by the environmentally benign oxidants, O_2 and H_2O_2 catalyzed by POMs (frequently heteropoly

acids) have considerable impact, and several of these selective hydrocarbon processes commercialized. Further advances in POM-catalyzed oxidation processes have been extensively reported in context with water oxidation and/or reduction.

The special volume of *Chemistry Reviews* on POMs was published in 1998.[10] POM-catalyzed oxidation reactions in the liquid-phase were reviewed by Kozhevnikov et al.[69] Heterogeneous POM-catalyzed oxidations were addressed by Misono et al.,[46] and Steckhan et al. reviewed the electrocatalytic oxidations by transition metal-substituted heteropolyanions with a mechanistic and kinetic perspectives.[47] Subsequently, Mizuno et al. reviewed catalytic hydrocarbon oxidation by H_2O_2.[70] Their review covers vanadium-based compounds and POMs in both homogeneous and heterogeneous catalysis in the liquid phase. Sun and Basset et al. have summarized numerous oxidation processes, especially the oxidation of light alkanes ($C_1 - C_4$) catalyzed by heteropoly compounds.[71] POM-catalyzed oxidations of hydrocarbons, arenes, alcohols, phenols and other organic compounds were recently reviewed by Yang et al.[50] The most active area in POM catalysis recently have been in water oxidation, largely now referred to as "water splitting", which reflects the major global research effort today on solar fuel generation (artificial photosynthesis). This area will be detailed in the next section.

The general mechanism of O_2-based POM-catalyzed oxidation reaction is shown in Scheme 1.1. The POMs are reduced by the substrate, which can be organic compounds, environmental pollutants, chemical warfare agents (CWAs), toxic industrial chemicals (TICs), or biological targets, etc., then the reduced POM is reoxidized by green oxidants, O_2 (or H_2O_2). Oxidative delignification (also known as wood pulp bleaching) is an

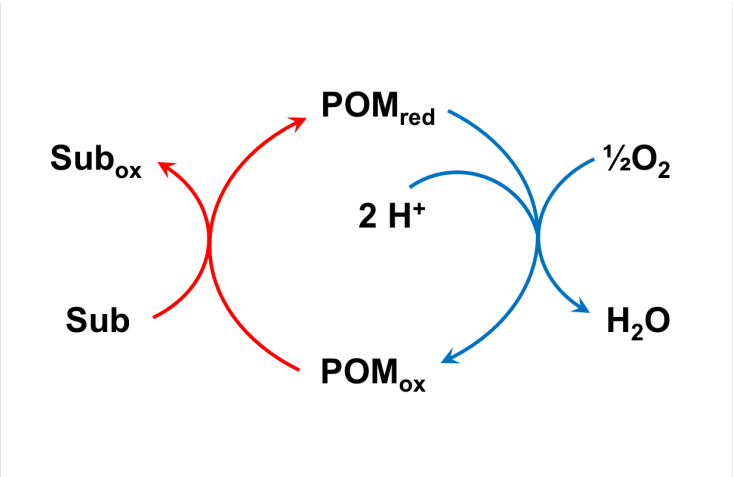

Scheme 1.1. The general two-step mechanism for oxidation of substrates by O_2 catalyzed by POMs.

excellent and well-studied example of POM-catalyzed O_2-based oxidation processes.[72-75] This chemistry can be achieved by utilizing POMs with O_2 because lignin has a lower redox potential than polysaccharides and, consequently, the former is more readily oxidized than the latter.[76] The two general steps in these O_2/air-based oxidations is illustrated in Scheme 1.1. One substrate (Sub) can be the lignin. The thermodynamic requirement for oxidative delignification is that the redox potential of POM should be higher than that of lignin but more negative than that of O_2 (O_2 to H_2O). Most POMs used in lignin oxidation are transition-metal-substituted Keggin POMs such as $[PV_2Mo_{10}O_{40}]^{5-}$, $[PVW_{11}O_{40}]^{4-}$, $[SiVW_{11}O_{40}]^{5-}$, $[SiMnW_{11}O_{40}]^{5-}$, and $[AlVW_{11}O_{40}]^{6-}$, etc.[72,77-80] Here the problem is that the oxidative removal of lignin is inefficient or nonexistent when using POMs with lower redox potentials. Alternatively, reoxidation of the reduced POM can be ineffective for the POMs with higher potentials.

Reoxidation of reduced POMs (the right blue part in Scheme 1.1) is generally considered as a rate-limiting step in overall O_2-based POM-catalyzed oxidation reactions. However, O_2 reduction to water, while thermodynamically favorable is frequently not kinetically favorable because O_2 is a ground state triplet. Moreover, one-electron reduction of O_2 generating superoxide is the most unfavorable step (the most negative reduction potential) in the overall four-electron reduction process. Given these facts, POM-based substrate oxidation, but more frequently, reduced POM reoxidation is a success-limiting phenomenon. Understanding the reoxidation process, however, has been much less investigated in terms of mechanistic and kinetic studies. Thanks to Weinstock's contributions to this chemistry, however, some detailed and consequently informative mechanistic studies have been documented.[81-83] The electron transfer (ET) process from the reduced POM to O_2 was systematically investigated using one electron-reduced Keggin heteropolytungstate anions (α-$X^{n+}W_{12}O_{40}^{(9-n)-}$, $X = Al^{3+}$, Si^{4+}, P^{5+}).[84] Detailed kinetics and mechanism studies, including the Marcus cross relation, indicate that the ET process occurs via an outer-sphere ET process. Additionally, the formation of protonated superoxide ($HO_2^{\bullet}$) originates through two consecutive steps; first, outer-sphere ET, followed by proton transfer (PT), named an ETPT mechanism, instead of simultaneous proton-coupled electron transfer (PCET) process. The advanced study confirmed that ETPT from the one-electron-reduced POM (here $[PW_{12}O_{40}]^{4-}$) to O_2 is converted to concerted proton-electron transfer (CPET) at higher concentrations of proton (in the range of 0.3 to 1.9 M), resulting the formation of $HO_2^{\bullet}$, while the ET proceeds via ETPT at lower proton concentrations (0.01 – 0.3 M).[85] A very recent review by Neumann and Weinstock addresses the use of

molecular oxygen in reactions mediated by polyoxometalates including in depth kinetic and mechanistic studies.[83]

1.3.2 POM Catalysis in Water Oxidation

Significant contributions and accomplishments in sustainable and renewable energy have given rise to breakthroughs to overcome world energy problems over the past decade. Solar is the one energy resource that has the capacity to power our civilization, and is thus of potential interest in various scientific fields.[86-88] Solar fuel generation requires catalysts for both water splitting reduction of H_2O or CO_2 (Scheme 1.2). The development of water oxidation catalysts (WOCs) is more challenging than for water reduction (proton reduction) because water oxidation is of a four-electron process requiring a high oxidizing potential (versus two-electron low-potential process for water reduction) and proceeds through a proton-coupled electron transfer (PCET) mechanism.

The performance of homogeneous WOCs is evaluated generally in two ways: "dark" and "light-driven" systems. The dark system mainly consists of a WOC, water, and sacrificial oxidant (commonly $[Ru(bpy)_3]^{3+}$) which can oxidize water to O_2 (Scheme 1.3

Oxidation	$2\ H_2O \rightarrow 4\ H^+ + 4\ e^- + O_2$	E^o = 1.23 V (vs. NHE)
Reduction	$4\ H^+ + 4\ e^- \rightarrow 2\ H_2$	E^o = 0.00 V (vs. NHE)
Net reaction	$2\ H_2O + h\nu \rightarrow 2\ H_2 + O_2$	

Scheme 1.2. Water splitting half reactions.

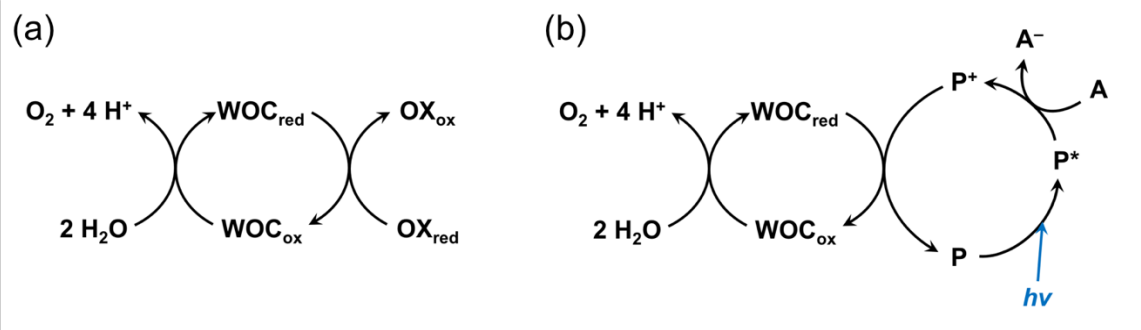

Scheme 1.3. Water oxidation catalytic cycles for (a) a "dark" system and (b) a "light-driven" system. OX, P, and A represent an oxidant, a photosensitizer, and a sacrificial electron acceptor, respectively.

(a)) in the absence of light. The other system, light-driven system, however, requires a photosensitizer (commonly $[Ru(bpy)_3]^{2+}$) and a sacrificial electron acceptor (commonly $S_2O_8^{2-}$) plus light (Scheme 1.3 (b)). After irradiation, the excited photosensitizer is quenched by a sacrificial electron acceptor, generating the oxidant, $[Ru(bpy)_3]^{3+}$, which in turn, oxidizes the WOC.

Great efforts to design better solar fuel systems have led to significant intellectual as well as potentially practical insights in WOC chemistry. A large number of WOCs have been reported in context with homogeneous, heterogeneous and electrochemical systems in the past few years.[89-103] POMs are excellent candidates for both homogeneous and heterogeneous WOCs as they possess hydrolytic, oxidative and thermal stability as well as rich and tunable multi-electron redox chemistry. Good WOCs and other multi-electron-transfer catalysts should exhibit the ability for redox levelling, high stability, selectivity, and high catalytic performance.[104] These evident guidelines led to the development of a

POM with a tetraruthenium-oxo core, $[Ru_4(\mu\text{-}O)_4(\mu\text{-}OH)_2(H_2O)_4(\gamma\text{-}SiW_{10}O_{36})_2]^{10-}$ (**Ru_4Si_2**), the first molecular and carbon-free WOC (crystal structure in Figure 1.4 (a)) in 2008.[105,106] The homogeneous catalytic water oxidation activity of **Ru_4Si_2** was examined by Hill group, using $[Ru(bpy)_3]^{3+}$ as an oxidant in phosphate buffer at pH 7.2.[105] Later, they evaluated catalytic water oxidation performance of **Ru_4Si_2** in a light-driven system utilizing $[Ru(bpy)_3]^{2+}$ and $S_2O_8^{2-}$ as a photosensitizer and a sacrificial electron acceptor, respectively.[107] Further advanced studies have probed the stability, mechanism, catalytic activities under certain conditions.[108-114] Among other efforts, **Ru_4Si_2** was compared with the P-centered structural analogue, $Cs_9[(\gamma\text{-}PW_{10}O_{36})_2Ru^{IV}_4O_5(OH)(OH_2)_4]$ (**Ru_4P_2**),[115] which is also a good WOC with extensive hydrolytic stability. All these activities have led to confirmation of the marked WOC performance of this class of compounds.[116,117,113,118-121]

A tetracobalt-substituted polytungstate, $[Co_4(H_2O)_2(PW_9O_{34})_2]^{10-}$ (**Co_4P_2**), was a breakthrough in the area of molecular water oxidation catalysts (crystal structure in Figure 1.4 (b)).[122,123] This earth-abundant metal-containing POM can catalyze water oxidation with exceptional efficiency in the dark system providing a turnover frequency (TOF) of 5 s^{-1} in phosphate buffer at pH 8.0. Consequently, substantial interest in **Co_4P_2** have given rise to further advances in analysis, mechanistic studies, and catalytic activities under a range of conditions.[124-131] Several reviews provide details from various perspectives.[104,91,132]

In addition to **Co_4P_2**, our group reported an exceptionally fast molecular water oxidation catalyst, which is an analogue of **Co_4P_2** with a replacement of P to V, $[Co_4(H_2O)_2(VW_9O_{34})_2]^{10-}$ (**Co_4V_2**) (crystal structure in Figure 1.4 (c)).[133] **Co_4V_2** showed a TOF value ~ 1000 s^{-1} in 80 mM borate buffer at pH 9.0 under the dark system conditions. Additionally, **Co_4V_2** produces a twice higher yield of O_2 relative to **Co_4P_2** using light-driven photochemical conditions. Folkman and Finke provided additional stability studies of **Co_4V_2**, suggesting decomposition of **Co_4V_2**, resulting in the formation of CoO_x film (possibly from oxidation of Co^{2+}(aq) impurities), and that Co^{2+} is a most likely water oxidation catalyst under electrochemical conditions.[134] However, the hydrolytic stability of **Co_4V_2** is still in debate, yet the catalytic water oxidation activity of **Co_4V_2** was not

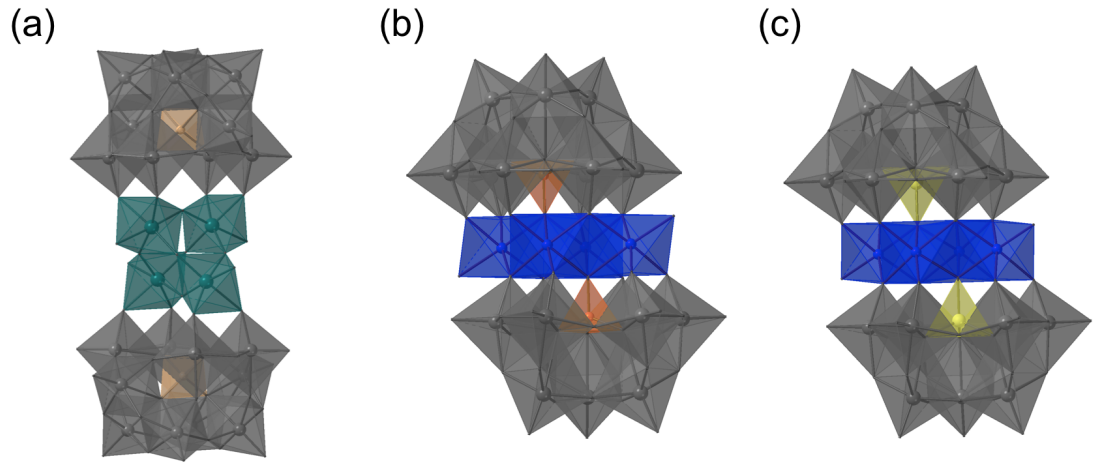

Figure 1.4. Crystal structures of the representative POM water oxidation catalysts in polyhedral representation: (a) $[\{Ru_4O_4(OH)_2(H_2O)_4\}(\gamma\text{-}SiW_{10}O_{36})_2]^{10-}$, (b) $[Co_4(H_2O)_2(PW_9O_{34})_2]^{10-}$, (c) $[Co_4(H_2O)_2(VW_9O_{34})_2]^{10-}$. Color: Si, light brown; P, orange; V, yellow; Co, blue; Ru, dark cyan; W, grey.

specifically investigated by them. Separately, the mechanistic of **Co_4V_2**-catalyzed water oxidation was elucidated recently by DFT calculations.[130] The d orbital coupling between V and Co results in an increase in the oxidation potential of the Co centers and results in better performance of **Co_4V_2** versus **Co_4P_2** in water oxidation. A very recent study addressed the difference in electronic structure between **Co_4P_2** and **Co_4V_2** using soft X-ray absorption (XAS) and resonant inelastic X-ray scattering (RIXS) spectroscopies, confirming the higher water oxidation catalytic activity of **Co_4V_2**.[135]

1.4 Goal of This Work and Outline

The main objective of this dissertation is to understand the kinetics and mechanisms of key POM reactions to make more efficient POM catalysis. First, I focus on the catalysis of reduced POM reoxidation, as this is central to many POM-catalyzed redox processes, including those using O_2 as the terminal oxidant. Later on, I investigated cobalt species, including Co-containing POMs, as water oxidation catalysts. The various experimental techniques such as a stopped-flow kinetics, and other spectroscopic methods have been employed to achieve our goal. The experimental results and proposed mechanistic study are supported by computational studies.

Chapter 2 reports the catalytic oxidation of reduced POMs by O_2, which is a challenging step in POM catalysis and usually must be facile to make the overall catalysis efficient. This study is mainly focused on the behavior of aqueous Cu^{2+} as a co-catalyst for the oxidation of reduced Keggin heteropolytungstates by O_2 in an acidic aqueous environment. Thorough kinetic and mechanistic studies concur with the implications of our experimental results. Chapter 3 reports that the rate of reduced POM reoxidation by

O_2 for POMs with higher reduction potentials is rapid and effective when both Cu(II) and Fe(II) are also present as co-catalysts. The role of copper and iron in the catalysis and the catalytic pathway are established with experiments as well as computational studies.

In Chapter 4, nitrous acid is used to enhance the catalytic efficiency in POM_{red} oxidation for practical purposes. The series of one electron-reduced vanadium, V(IV), -substituted Keggin heteropolytungstates possessing much higher reduction potentials are investigated. In addition, the effect of heteroatoms in POM_{red} oxidation is addressed by electrochemical and computational studies.

Chapter 5 reports identification of the true water oxidation catalysts in WOC systems that contain some cobalt-containing species including Co-POM (especially **Co_4V_2**) and aqueous Co(II). Additionally, understanding the role of aqueous cobalt species as a WOC is addressed. This research focusses on homogeneous water oxidation conditions and the distribution of aggregated Co complexes on reaction of Co(II) with $[Ru(bpy)_3]^{3+}$. This work identifies the true WOCs, and involves supporting experiments that use a double-mixing stopped-flow kinetics system and complementary computational studies.

1.5 References

(1) Pope, M. T. *Heteropoly and Isopoly Oxometalates*; Springer-Verlag: Berlin, 1983.

(2) *Polyoxometalates: From Platonic Solids to Anti-retroviral Activity*; Pope, M. T.; Müller, A., Eds.; Kluwer Academic Publishers: Dordrecht, Netherlands, 1993.

(3) *Polyoxometalate Chemistry From Topology via Self-Assembly to Applications*; Pope, M. T.; Müller, A., Eds.; Kluwer Academic Publishers: Dordrecht, 2001.

(4) Borrás-Almenar, J. J.; Coronado, E.; Müller, A.; Pope, M. T. *Polyoxometalate Molecular Science. Proceedings of the NATO Advanced Study Institute, Tenerife, Spain from 25 August to 4 September 2001*; Kluwer Academic Publishers: Dordrecht, 2003.

(5) Pope, M. T. In *Comprehensive Coordination Chemistry II: From Biology to Nanotechnology*; Wedd, A. G., Ed.; Elsevier Ltd.: Oxford, UK, 2004; Vol. 4.

(6) Hill, C. L. In *Comprehensive Coordination Chemistry-II: From Biology to Nanotechnology*; Wedd, A. G., Ed.; Elsevier Ltd.: Oxford, UK, 2004; Vol. 4.

(7) Berzelius, J. J. *Poggendorfs Ann. Phys. Chem.* **1826,** *6*, 369.

(8) Keggin, J. F. *Nature* **1933,** *131*, 908.

(9) Keggin, J. F. *Proc. R. Soc. Lond. A* **1934,** *144*, 75.

(10) Hill, C. L. *Chem. Rev.* **1998,** *98*, 1.

(11) Katsoulis, D. E. *Chem. Rev.* **1998,** *98*, 359.

(12) Matsumoto, K. Y.; Kobayashi, A.; Sasaki, Y. *Bull. Chem. Soc. Jpn.* **1975,** *48*, 3146.

(13) Pope, M. T.; O'Donnell, S. E.; Prados, R. A. *J. Chem. Soc., Chem. Commun.* **1975**, 22.

(14) Thouvenot, R.; Fournier, M.; Franck, R.; Rocchiccioli-Deltcheff, C. *Inorg. Chem.* **1984,** *23*, 598.

(15) Wang, S. H.; Jansen, S. A. *Chem. Mater.* **1994,** *6*, 2130.

(16) Weinstock, I. A.; Cowan, J. J.; Barbuzzi, E. M. G.; Zeng, H.; Hill, C. L. *J. Am. Chem. Soc.* **1999,** *121*, 4608.

(17) Cowan, J. J.; Bailey, A. J.; Heintz, R. A.; Do, B. T.; Hardcastle, K. I.; Hill, C. L.; Weinstock, I. A. *Inorg. Chem.* **2001,** *40*, 6666.

(18) Neiwert, W. A.; Cowan, J. J.; Hardcastle, K. I.; Hill, C. L.; Weinstock, I. A. *Inorg. Chem.* **2002,** *41*, 6950.

(19) Sundaram, K. M.; Neiwert, W. A.; Hill, C. L.; Weinstock, I. A. *Inorg. Chem.* **2006,** *45*, 958.

(20) Zhang, F.-Q.; Zhang, X.-M.; Wu, H.-S.; Jiao, H. *J. Phys. Chem. A* **2007,** *111*, 159.

(21) Coronado, E.; Gómez-García, C. J. *Chem. Rev.* **1998,** *98*, 273.

(22) Müller, A.; Peters, F.; Pope, M. T.; Gatteschi, D. *Chem. Rev.* **1998,** *98*, 239.

(23) Yamase, T. *Chem. Rev.* **1998,** *98*, 307.

(24) Sanchez, C.; Soler-Illia, G. J. d. A. A.; Ribot, F.; Lalot, T.; Mayer, C. R.; Cabuil, V. *Chem. Mater.* **2001,** *13*, 3061.

(25) Coronado, E.; Giménez-Saiz, C.; Gómez-García, C. J. *Coord. Chem. Rev.* **2005,** *249*, 1776.

(26) Akutagawa, T.; Endo, D.; Noro, S.-I.; Cronin, L.; Nakamura, T. *Coord. Chem. Rev.* **2007,** *251*, 2547.

(27) Long, D.-L.; Burkholder, E.; Cronin, L. *Chem. Soc. Rev.* **2007,** *36*, 105.

(28) Proust, A.; Thouvenot, R.; Gouzerh, P. *Chem. Commun.* **2008**, 1837.

(29) Dolbecq, A.; Dumas, E.; Mayer, C. R.; Mialane, P. *Chem. Rev.* **2010,** *110*, 6009.

(30) Song, Y.-F.; Tsunashima, R. *Chem. Soc. Rev.* **2012,** *41*, 7384.

(31) Rhule, J. T.; Hill, C. L.; Judd, D. A.; Schinazi, R. F. *Chem. Rev.* **1998,** *98*, 327.

(32) Shigeta, S.; Mori, S.; Kodama, E.; Kodama, J.; Takahashi, K.; Yamase, T. *Antiviral Res.* **2003,** *58*, 265.

(33) Hasenknopf, B. *Front. Biosci.* **2005,** *10*, 275.

(34) Lee, I. S.; Long, J. R.; Prusiner, S. B.; Safar, J. G. *J. Am. Chem. Soc.* **2005,** *127*, 13802.

(35) Wille, H.; Shanmugam, M.; Murugesu, M.; Ollesch, J.; Stubbs, G.; Long, J. R.; Safar, J. G.; Prusiner, S. B. *Proc. Natl. Acad. Sci.* **2009,** *106*, 3740.

(36) Vanhaecht, S.; Absillis, G.; Parac-Vogt, T. N. *Dalton Trans.* **2012,** *41*, 10028.

(37) Stroobants, K.; Moelants, E.; Ly, H. G. T.; Proost, P.; Bartik, K.; Parac-Vogt, T. N. *Chem.Eur. J.* **2013,** *19*, 2848.

(38) Gao, N.; Sun, H.; Dong, K.; Ren, J.; Duan, T.; Xu, C.; Qu, X. *Nat. Commun.* **2014,** *5*, 3422.

(39) Long, D.-L.; Tsunashima, R.; Cronin, L. *Angew. Chem. Int. Ed.* **2010,** *49*, 1736.

(40) Clemente-Juan, J. M.; Coronado, E.; Gaita-Arino, A. *Chem. Soc. Rev.* **2012,** *41*, 7464.

(41) Miras, H. N.; Yan, J.; Long, D.-L.; Cronin, L. *Chem. Soc. Rev.* **2012,** *41*, 7403.

(42) Wang, Y.; Weinstock, I. A. *Chem. Soc. Rev.* **2012,** *41*, 7479.

(43) Zheng, S.-T.; Yang, G.-Y. *Chem. Soc. Rev.* **2012,** *41*, 7623.

(44) Misono, M. In *Polyoxometalates: From Platonic Solids to Anti-retroviral Activity*; Pope, M. T.;Müller, A., Eds.; Kluwer Academic Publishers: Dordrecht, Netherlands, 1993.

(45) Misono, M. *Mol. Eng.* **1993,** *3*, 193.

(46) Mizuno, N.; Misono, M. *Chem. Rev.* **1998,** *98*, 199.

(47) Sadakane, M.; Steckhan, E. *Chem. Rev.* **1998,** *98*, 219.

(48) Kozhevnikov, I. V. *Catalysis by Polyoxometalates*; Wiley: Chichester, England, 2002.

(49) Hill, C. L. *J. Mol. Catal. A: Chem.* **2007 Special Issue,** *262*, 1.

(50) Wang, S.-S.; Yang, G.-Y. *Chem. Rev.* **2015,** *115*, 4893.

(51) Kozhevnikov, I. V.; Matveev, K. I. *Russ. Chem. Rev.* **1982,** *51*, 1075.

(52) Kozhevnikov, I. V.; Khankhasaeva, S. T.; Kulikov, S. M. *Kinet. Catal.* **1988,** *29*, 76.

(53) Ono, Y. In *Perspective in Catalysis*; Thomas, J. M.;Zamaraev, K. I., Eds.; Blackwell: Oxford, UK, 1992.

(54) Kozhevnikov, I. V. *Russ. Chem. Rev.* **1987,** *56*, 811.

(55) Kozhevnikov, I. V. *Applied Catalysis A: General* **2003,** *256*, 3.

(56) Bielański, A.; Lubańska, A.; Micek-Ilnicka, A.; Poźniczek, J. *Coord. Chem. Rev.* **2005,** *249*, 2222.

(57) Misono, M.; Nojiri, N. *Appl. Catal.* **1990,** *64*, 1.

(58) Hill, C. L.; Prosser-McCartha, C. M. In *Photosensitization and Photocatalysis Using Inorganic and Organometallic Compounds*; Kalyanasundaram, K.;Grätzel, M., Eds.; Kluwer Academic Publishers: Dordrecht, 1993; Vol. 14.

(59) Duncan, D. C.; Netzel; L., T.; Hill, C. L. *Inorg. Chem.* **1995,** *34*, 4640.

(60) Papaconstantinou, E. *Chem. Soc. Rev.* **1989,** *18*, 1.

(61) Pope, M. T.; Varga, G. M. *Inorg. Chem.* **1966,** *5*, 1249.

(62) Papaconstantinou, E.; Pope, M. T. *Inorg. Chem.* **1967,** *6*, 1152.

(63) Pope, M. T.; Papaconstantinou, E. *Inorg. Chem.* **1967,** *6*, 1147.

(64) Papaconstantinou, E.; Pope, M. T. *Inorg. Chem.* **1970,** *9*, 667.

(65) Varga, G. M.; Papaconstantinou, E.; Pope, M. T. *Inorg. Chem.* **1970,** *9*, 662.

(66) Pope, M. T. *Inorg. Chem.* **1972,** *11*, 1973.

(67) Prados, R. A.; Meiklejohn, P. T.; Pope, M. T. *J. Am. Chem. Soc.* **1974,** *96*, 1261.

(68) Altenau, J.; Pope, M. T.; Prados, R. A.; So, H. *Inorg. Chem.* **1975,** *14*, 417.

(69) Kozhevnikov, I. V. *Chem. Rev.* **1998,** *98*, 171.

(70) Mizuno, N.; Kamata, K. *Coord. Chem. Rev.* **2011,** *255*, 2358.

(71) Sun, M.; Zhang, J.; Putaj, P.; Caps, V.; Lefebvre, F.; Pelletier, J.; Basset, J.M. *Chem. Rev.* **2014,** *114*, 981.

(72) Weinstock, I. A.; Atalla, R. H.; Reiner, R. S.; Moen, M. A.; Hammel, K. E.; Houtman, C. J.; Hill, C. L. *New J. Chem.* **1996,** *20*, 269.

(73) Weinstock, I. A.; Atalla, R. H.; Reiner, R. S.; Moen, M. A.; Hammel, K. E.; Houtman, C. J.; Hill, C. L.; Harrup, M. K. *J. Mol. Catal. A: Chem.* **1997,** *116*, 59.

(74) Gaspar, A. R.; Gamelas, J. A. F.; Evtuguin, D. V.; Pascoal Neto, C. *Green Chem.* **2007,** *9*, 717.

(75) Bujanovic, B.; Ralph, S.; Reiner, R.; Hirth, K.; Atalla, R. *Materials* **2010,** *3*.

(76) Weinstock, I. A.; Hill, C. L.; Minor, J. L. Second European Workshop on Lignocellulosics and Pulp, Grenoble, France, 1992; p 33.

(77) Weinstock, I.; Atalla, R. H.; Reiner, R. S.; Houtman, C. J.; Hill, C. L. *Holz Forschung* **1998,** *52*, 304.

(78) Weinstock, I.; Hammel, K. E.; Moen, M. A.; Landucci, L. L.; Ralph, S.; Sullivan, C. E.; Reiner, R. S. *Holz Forschung* **1998,** *52*, 311.

(79) Weinstock, I. A.; Barbuzzi, E. M. G.; Wemple, M. W.; Cowan, J. J.; Reiner, R. S.; Sonnen, D. M.; Heintz, R. A.; Bond, J. S.; Hill, C. L. *Nature* **2001,** *414*, 191.

(80) Weinstock, I.; Barbuzzi, E. M. G.; Sonnen, D. M.; Hill, C. L. In *Advancing Sustainability through Green Chemistry and Engineering*; Lankey, R. L.;Anastas, P. T., Eds.; American Chemical Society: Washington, D. C., 2002.

(81) Weinstock, I. A. *Chem. Rev.* **1998,** *98*, 113.

(82) Snir, O.; Wang, Y.; Weinstock, I. A. *Isr. J. Chem.* **2011,** *51*, 247.

(83) Weinstock, I. A.; Schreiber, R. E.; Neumann, R. *Chem. Rev.* **2018**, *118*, 2680.

(84) Geletii, Y. V.; Hill, C. L.; Atalla, R. H.; Weinstock, I. A. *J. Am. Chem. Soc.* **2006,** *128*, 17033.

(85) Snir, O.; Wang, Y.; Tuckerman, M. E.; Geletii, Y. V.; Weinstock, I. A. *J. Am. Chem. Soc.* **2010,** *132*, 11678.

(86) Lewis, N. S.; Nocera, D. G. *Proc. Natl. Acad. Sci.* **2006,** *103*, 15729.

(87) Gray, H. B. *Nat. Chem.* **2009,** *1*, 112.

(88) Chu, S.; Cui, Y.; Liu, N. *Nat. Mater.* **2017,** *16*, 16.

(89) Deng, X.; Tüysüz, H. *ACS Catal.* **2014,** *4*, 3701.

(90) Fukuzumi, S.; Hong, D. *Eur. J. Inorg. Chem.* **2014,** *4*, 645.

(91) Sumliner, J. M.; Lv, H.; Fielden, J.; Geletii, Y. V.; Hill, C. L. *Eur. J. Inorg. Chem.* **2014,** *4*, 635.

(92) Blakemore, J. D.; Crabtree, R. H.; Brudvig, G. W. *Chem. Rev.* **2015,** *115*, 12974.

(93) Han, L.; Dong, S.; Wang, E. *Adv. Mater.* **2016,** *28*, 9266.

(94) Hunter, B. M.; Gray, H. B.; Müller, A. M. *Chem. Rev.* **2016,** *116*, 14120.

(95) Shen, S.; Lindley, S. A.; Chen, X.; Zhang, J. Z. *Energy Environ. Sci.* **2016,** *9*, 2744.

(96) Garrido-Barros, P.; Gimbert-Surinach, C.; Matheu, R.; Sala, X.; Llobet, A. *Chem. Soc. Rev.* **2017,** *46*, 6088.

(97) Li, J.; Güttinger, R.; Moré, R.; Song, F.; Wan, W.; Patzke, G. R. *Chem. Soc. Rev.* **2017,** *46*, 6124.

(98) Materna, K. L.; Crabtree, R. H.; Brudvig, G. W. *Chem. Soc. Rev.* **2017,** *46*, 6099.

(99) Meyer, T. J.; Sheridan, M. V.; Sherman, B. D. *Chem. Soc. Rev.* **2017,** *46*, 6148.

(100) Reier, T.; Nong, H. N.; Teschner, D.; Schlögl, R.; Strasser, P. *Adv. Energy Mater.* **2017,** *7*, 1601275.

(101) Roger, I.; Shipman, M. A.; Symes, M. D. *Nat. Rev. Chem.* **2017,** *1*, 0003.

(102) Stevens, M. B.; Enman, L. J.; Batchellor, A. S.; Cosby, M. R.; Vise, A. E.; Trang, C. D. M.; Boettcher, S. W. *Chem. Mater.* **2017,** *29*, 120.

(103) Tahir, M.; Pan, L.; Idrees, F.; Zhang, X.; Wang, L.; Zou, J.-J.; Wang, Z. L. *Nano Energy* **2017,** *37*, 136.

(104) Lv, H.; Geletii, Y. V.; Zhao, C.; Vickers, J. W.; Zhu, G.; Luo, Z.; Song, J.; Lian, T.; Musaev, D. G.; Hill, C. L. *Chem. Soc. Rev.* **2012,** *41*, 7572.

(105) Geletii, Y. V.; Botar, B.; Kögerler, P.; Hillesheim, D. A.; Musaev, D. G.; Hill, C. L. *Angew. Chem. Int. Ed.* **2008,** *47*, 3896.

(106) Sartorel, A.; Carraro, M.; Scorrano, G.; Zorzi, R. D.; Geremia, S.; McDaniel, N. D.; Bernhard, S.; Bonchio, M. *J. Am. Chem. Soc.* **2008,** *130*, 5006.

(107) Geletii, Y. V.; Huang, Z.; Hou, Y.; Musaev, D. G.; Lian, T.; Hill, C. L. *J. Am. Chem. Soc.* **2009,** *131*, 7522.

(108) Geletii, Y. V.; Besson, C.; Hou, Y.; Yin, Q.; Musaev, D. G.; Quinonero, D.; Cao, R.; Hardcastle, K. I.; Proust, A.; Kögerler, P.et al. *J. Am. Chem. Soc.* **2009,** *131*, 17360.

(109) Kuznetsov, A. E.; Geletii, Y. V.; Hill, C. L.; Morokuma, K.; Musaev, D. G. *J. Am. Chem. Soc.* **2009,** *131*, 6844.

(110) Sartorel, A.; Miro, P.; Salvadori, E.; Romain, S.; Carraro, M.; Scorrano, G.; Valentin, M. D.; Llobet, A.; Bo, C.; Bonchio, M. *J. Am. Chem. Soc.* **2009,** *131*, 16051.

(111) Quiñonero, D.; Kaledin, A. L.; Kuznetsov, A. E.; Geletii, Y. V.; Besson, C.; Hill, C. L.; Musaev, D. G. *J. Phys. Chem. A* **2010,** *114*, 535.

(112) Piccinin, S.; Fabris, S. *Phys. Chem. Chem. Phys.* **2011,** *13*, 7666.

(113) Piccinin, S.; Sartorel, A.; Aquilanti, G.; Goldoni, A.; Bonchio, M.; Fabris, S. *Proc. Natl. Acad. Sci.* **2013,** *110*, 4917.

(114) Piccinin, S.; Fabris, S. *Inorganics* **2015,** *3*.

(115) Besson, C.; Huang, Z.; Geletii, Y. V.; Lense, S.; Hardcastle, K. I.; Musaev, D. G.; Lian, T.; Proust, A.; Hill, C. L. *Chem. Commun.* **2010**, 2784.

(116) Toma, F. M.; Sartorel, A.; Iurlo, M.; Carraro, M.; Parisse, P.; Maccato, C.; Rapino, S.; Gonzalez, B. R.; Amenitsch, H.; Ros, T. D.et al. *Nat. Chem.* **2010,** *2*, 826.

(117) Guo, S.-X.; Liu, Y.; Lee, C.-Y.; Bond, A. M.; Zhang, J.; Geletii, Y. V.; Hill, C. L. *Energy Environ. Sci.* **2013,** *6*, 2654.

(118) Quintana, M.; López, A. M.; Rapino, S.; Toma, F. M.; Iurlo, M.; Carraro, M.; Sartorel, A.; Maccato, C.; Ke, X.; Bittencourt, C.et al. *ACS Nano* **2013,** *7*, 811.

(119) Fielden, J.; Sumliner, J. M.; Han, N.; Geletii, Y. V.; Xiang, X.; Musaev, D. G.; Lian, T.; Hill, C. L. *Chem. Sci.* **2015,** *6*, 5531.

(120) Lauinger, S. M.; Sumliner, J. M.; Yin, Q.; Xu, Z.; Liang, G.; Glass, E. N.; Lian, T.; Hill, C. L. *Chem. Mater.* **2015,** *27*, 5886.

(121) Lauinger, S. M.; Piercy, B. D.; Li, W.; Yin, Q.; Collins-Wildman, D. L.; Glass, E. N.; Losego, M. D.; Wang, D.; Geletii, Y. V.; Hill, C. L. *ACS Appl. Mater. Interfaces* **2017,** *9*, 35048.

(122) Yin, Q.; Tan, J. M.; Besson, C.; Geletii, Y. V.; Musaev, D. G.; Kuznetsov, A. E.; Luo, Z.; Hardcastle, K. I.; Hill, C. L. *Science* **2010,** *328*, 342.

(123) Huang, Z.; Luo, Z.; Geletii, Y. V.; Vickers, J.; Yin, Q.; Wu, D.; Hou, Y.; Ding, Y.; Song, J.; Musaev, D. G.et al. *J. Am. Chem. Soc.* **2011,** *133*, 2068.

(124) Steinmiller, E. M. P.; Choi, K.-S. *Proc. Natl. Acad. Sci.* **2009,** *106*, 20633.

(125) Stracke, J. J.; Finke, R. G. *J. Am. Chem. Soc.* **2011,** *133*, 14872.

(126) Stracke, J. J.; Finke, R. G. *ACS Catal.* **2013,** *3*, 1209.

(127) Schiwon, R.; Klingan, K.; Dau, H.; Limberg, C. *Chem. Commun.* **2014,** *50*, 100.

(128) Stracke, J. J.; Finke, R. G. *ACS Catal.* **2014,** *4*, 79.

(129) Goberna-Ferrón, S.; Soriano-López, J.; Galán-Mascarós, J. R.; Nyman, M. *Eur. J. Inorg. Chem.* **2015,** *17*, 2833.

(130) Soriano-López, J.; Musaev, D. G.; Hill, C. L.; Galán-Mascarós, J. R.; Carbó, J. J.; Poblet, J. M. *J. Catal.* **2017,** *350*, 56.

(131) Wieliczko, M.; Geletii, Y. V.; Bacsa, J.; Musaev, D. G.; Hill, C. L. *J. Cluster Sci.* **2017,** *28*, 839.

(132) Sumliner, J. M.; Vickers, J. W.; Lv, H.; Geletii, Y. V.; Hill, C. L. In *Molecular Water Oxidation Catalysts: A Key Topic for New Sustainable Energy Conversion Schemes*; Llobet, A., Ed.; John Wiley & Sons, Ltd., 2014; Vol. First Edition.

(133) Lv, H.; Song, J.; Geletii, Y. V.; Vickers, J. W.; Sumliner, J. M.; Musaev, D. G.; Kögerler, P.; Zhuk, P. F.; Bacsa, J.; Zhu, G.et al. *J. Am. Chem. Soc.* **2014,** *136*, 9268.

(134) Folkman, S. J.; Finke, R. G. *ACS Catal.* **2017,** *7*, 7.

(135) Liu, B.; Glass, E. N.; Wang, R.-P.; Cui, Y.-T.; Harada, Y.; Huang, D.-J.; Schuppler, S.; Hill, C. L.; de Groot, F. M. F. *Phys. Chem. Chem. Phys.* **2018,** *20*, 4554.

Chapter 2

Cu(II)-Catalyzed Oxidation of Reduced Keggin Heteropolytungstates with Dioxygen in Aqueous Medium

With Ira A. Weinstock, Yurii V. Geletii and Craig L. Hill

Reproduced in part with permission from *ACS Catal.*, **2015**, *5* (12), 7048–7054.

2.1 Introduction

A multitude of polyoxometalate (POM)-catalyzed O_2-based oxidation reactions have been studied and several of these processes have been commercialized.[1-13] These are a sub-set of catalytic O_2-based oxidation processes that continue to be heavily investigated because of their environmental attractiveness and potential low cost.[14-17] POMs afford several advantages as oxidation catalysts, including the ability to address the low reactivity of O_2 in the ground-state, readily store a single electron at a controllable potential, and function as highly effective ligands (carbon-free, multidentate and synthetically tunable) for d-electron-metal(s) active sites.[5,8-10,12,18-21] A central feature of these O_2/air-based oxidation processes is the reaction of the reduced POM (POM_{red}) with O_2.[7,11,22-25] This step is frequently much slower than oxidation of the substrate by the oxidized (resting oxidation state) POM (POM_{ox}) to form POM_{red}.[6,22-27] Given this fact, it is surprising that major efforts have not been expended to find catalysts for this bottleneck $POM_{red} + O_2$ step.

While the overall reduction of O_2 to water by POM_{red} is known to be a complex sequence of electron transfer (ET) steps with intermediate formation of $O_2^{-\bullet}/HO_2^{\bullet}$ and H_2O_2,[28] comprehensive experimental and theoretical studies have unequivocally demonstrated that the first step of $POM_{red} + O_2$ proceeds via an outer-sphere ET mechanism,[28] eq 2.1:

$$POM_{red} + O_2 \rightarrow POM_{ox} + O_2^{-\bullet} \qquad (2.1)$$

Outer-sphere ET processes such as eq 2.1, however, are commonly slow. Cu ions have been previously noted to catalyze $POM_{red} + O_2$, but the authors focused their efforts on the inhibition of this reaction.[28] There are numerous examples where classical outer-sphere one-electron-transfer processes are actually catalyzed by submicromolar concentrations of

copper.[29,30] Trace amounts of copper efficiently catalyze the oxidation of cysteine and related thiols by hexacyanoferrate(III)[31] and thioglycolic acid by octacyanomolybdate(V).[32] Bagiyan et al. reported that oxidation of thiols by O_2 in neutral and alkaline solutions is catalyzed by Cu complexes.[33] Such complexes can be efficient in switching redox processes of coordination compounds from outer-sphere to multistep pathways involving the Cu(II)/Cu(I) couple. Additionally, Williams et al. documented that the decomposition of S-nitrosothiols (RSNO) to nitric oxide and disulfides in neutral aqueous solution is efficiently catalyzed by traces amounts of copper.[34]

In this Chapter, we herein examine the mechanism of this critical $POM_{red} + O_2$ step using the oxidized α-Keggin anions, α-$X^{n+}W_{12}O_{40}^{(8-n)-}$ (POM_{ox}) and their 1e^--reduced counterparts, α-$X^{n+}W_{12}O_{40}^{(9-n)-}$ (POM_{red}, where X = Al^{3+}, Si^{4+}, and P^{5+}, **AlW12$_{red}$**, **SiW12$_{red}$**, and **PW12$_{red}$**, respectively). These complexes have been selected for initial in-depth study because they are well known, thoroughly characterized and extensively studied.[35,36] They are also well behaved (stable, non-protonated and free of ion pairing over a wide range of pH and ionic-strength values in water). We report that $POM_{red} + O_2$ for these complexes (**AlW12$_{red}$**, **SiW12$_{red}$**, or **PW12$_{red}$** + O_2) is efficiently catalyzed by trace amounts of copper ions. The reaction kinetics are thoroughly studied and a reaction mechanism is proposed that quantitatively describes the experimental data.

2.2 Experimental

2.2.1 Materials

Fully oxidized α-Keggin ions (POM_{ox}), α-$K_5AlW_{12}O_{40}$,[35,37,38] and α-$K_4SiW_{12}O_{40}$,[39,40] were prepared using published methods; α-$Na_3PW_{12}O_{40}$ (+99.9%) was purchased from Sigma-Aldrich, Inc. The reduced Keggin ions, POM_{red} were prepared by constant-potential bulk electrolysis of 1 − 2 mM solutions of the parent POM_{ox} under Ar as described previously,[28,41] and subsequently stored under Ar. The ratio of $[POM_{red}]/[POM_{ox}]$ was controlled by the charge passed through the solution. All chemicals were of commercial quality unless otherwise specified. Sulfate buffer solutions were prepared using Barnstead Nanopure® quality water from Na_2SO_4 (99+%) and $NaHSO_4$ (99%) reagents purchased from Sigma-Aldrich. Copper sulfate (99.99+%) purchased from Sigma-Aldrich, was used as a source of Cu(II).

2.2.2 Electrochemistry

All electrochemical data were obtained using a BAS CV-50W electrochemical analyzer. Cyclic voltammograms (CVs) and bulk electrolysis were conducted at room temperature (24 ± 2 °C) as previously described[28,41] using an Ag/AgCl (3 M NaCl) BAS, glassy carbon, and Pt wire as the reference, working and counter electrodes, respectively. CVs were recorded in buffered solutions in the presence of 100 mM $NaClO_4$ as an electrolyte. A reticulated vitreous-carbon working electrode was used as a working electrode in bulk electrolyses to prepare aqueous solutions of POM_{red}. Extinction coefficients of the $1e^-$-reduced α-Keggin anions were previously reported: ε_{700} = (1.48 ± 0.1) × 10^3 and (1.56 ± 0.1) × 10^3 $M^{-1}cm^{-1}$ for **SiW12$_{red}$** and **PW12$_{red}$**, respectively.[28]

2.2.3 Kinetic Measurements

The reaction kinetics were followed using an SF-61 stopped-flow instrument (Hi-Tech Scientific, UK) measuring changes in absorbance at 700 nm with time. One feed syringe in the stopped-flow apparatus was filled with a deaerated solution of POM_{red}. These solutions were diluted, as needed, with O_2-free buffer/electrolyte solution. The second syringe was filled with Cu(II) in the same buffer/electrolyte solution but saturated with O_2 or air. The solubility of dioxygen in water with an ionic strength of 175 mM at 25 °C and 1 atm O_2 was taken as 1.15 mM.[28] In all stopped-flow kinetic measurements, the concentrations of O_2, POM_{red} and Cu(II) in the reaction mixture were twice lower than in the feed syringes. The initial reaction rates were obtained using an iterative (self-consistent) form of the method of initial rates. The fitting of kinetic curves was performed using COPASI 4.13 (Build 87) software (www.copasi.org).

2.3 Results and Discussion

2.3.1 Catalytic Effect of Cu(II)

The rate of $\mathbf{AlW12_{red}}$ oxidation by O_2 is significantly faster in the presence of Cu(II) (added as $CuSO_4$) over a wide range of pH (1.8 − 7.4). The reaction with $\mathbf{AlW12_{red}}$ is almost 25 faster if 38 μM Cu(II) is added at neutral pH as shown in Figure 2.1 (a). The reactions of reduced $\mathbf{SiW12_{red}}$ and $\mathbf{PW12_{red}}$ (henceforth POM_{red}) with O_2 are also catalyzed by copper ions.[28] Since these POM_{red} are unstable at neutral pH we moved to pH 2.0 (50 mM sodium sulphate buffer) containing 100 mM $NaClO_4$ to minimize the effect of ionic strength. The representative kinetic curves are shown in Figure 2.1 (b). The

reaction with **SiW12$_{red}$** proceeds 2 orders of magnitude faster if 10 μM Cu(II) is added (~3% based on [**SiW12$_{red}$**]$_0$). Here, the catalysis of **SiW12$_{red}$** and **PW12$_{red}$** will be discussed since they are oxidized directly by O_2 slower than **AlW12$_{red}$**. The transition

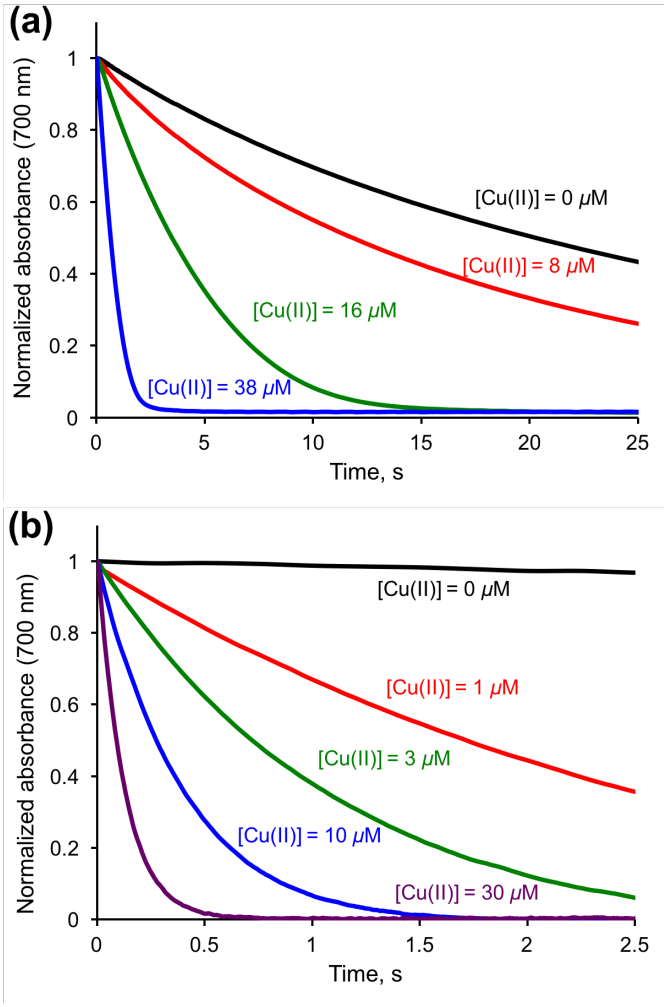

Figure 2.1. Effect of Cu(II) concentrations on kinetics of (a) **AlW12$_{red}$** and (b) **SiW12$_{red}$** oxidation by O_2 followed by the decrease of absorbance at 700 nm (the initial absorbance is normalized to 1.0). (a) [**AlW12$_{red}$**]$_0$ ~ 0.55 mM, [O_2]$_0$ = 0.58 mM, pH 7.2, 50 mM phosphate buffer, 100 mM $NaClO_4$, 25 °C. (b) [**SiW12$_{red}$**]$_0$ ~ 0.11 mM, [O_2]$_0$ = 0.12 mM, pH 2.0, 50 mM sulfate buffer, 100 mM $NaClO_4$, 25 °C.

metal cations Co(II), Fe(II), Mn(II), Ni(II), and Zn(II) (sulfate salts) were also screened for catalytic activity, but only the Cu salts were active.

2.3.2 Reaction Stoichiometry

Earlier we showed that the reaction between POM_{red} and H_2O_2 is much slower than with O_2 despite the greater driving force for reduction of H_2O_2 than for O_2.[28] Therefore, it was not a surprise that the product of the reaction between POM_{red} and O_2 proved to be H_2O_2, proceeding with the reaction stoichiometry in eq 2.2:

$$2\ POM_{red} + O_2 + 2\ H^+ \rightarrow 2\ POM_{ox} + H_2O_2 \qquad (2.2)$$

The addition of copper might alter the reaction stoichiometry due to copper catalyzed POM_{red} oxidation by H_2O_2. The kinetics of catalytic $\mathbf{SiW12_{red}}$ oxidation by O_2 at $[\mathbf{SiW12_{red}}]_0/[O_2]_0 > 4$ is shown in Figure 2.2. These data are consistent with the stoichiometry in eq 2.2. For example, 0.12 mM of $[O_2]_0$, is quickly and completely consumed by 0.42 or 1.05 mM of $[POM_{red}]_0$ in 0.54 and 1.2 s. In both cases the decrease in absorbance of POM_{red} as measured at 700 nm, ΔA, is about 0.34. For both cases, after completion of the reaction between POM_{red} and O_2, the absorbance decreases slowly. This process is assigned to the catalytic oxidation of POM_{red} by H_2O_2. At higher [Cu(II)], an additional amount of POM_{red} is consumed to reduce Cu(II) to Cu(I)/Cu(0). The reaction of $\mathbf{PW12_{red}}$ with O_2 is slower and two-phase kinetics (such as in Figure 2.2) is not clearly observed. Therefore, the kinetics of $\mathbf{PW12_{red}}$ consumption was studied at rather low conversion (20 – 50 %) of $\mathbf{PW12_{red}}$.

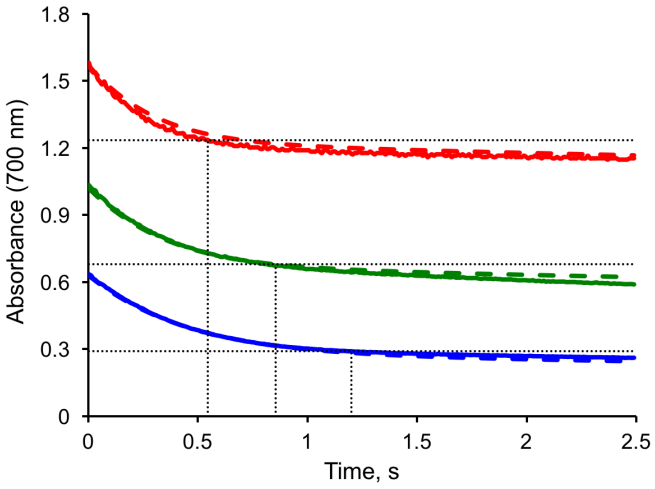

Figure 2.2. Kinetics of **SiW12$_{red}$** oxidation by O_2. Conditions: [**SiW12$_{red}$**]$_0$ ~ 1.05 (red), 0.69 (green), and 0.42 mM (blue), $[O_2]_0$ = 0.12 mM, [Cu(II)] = 10 μM, pH 2.0, 50 mM sodium sulfate buffer, 100 mM $NaClO_4$, 25 °C. Dotted lines indicate the reaction stoichiometry in eq 2.2. Dashed lines are the theoretical curves.

2.3.3 Dependence of the Initial Reaction Rate on [Cu(II)]$_0$, [POM$_{red}$]$_0$, and [O_2]$_0$

Earlier, it was shown that a direct reaction of POM_{red} with O_2 obeys the rate law in eq 2.3.[28]

$$-d[POM_{red}]/dt = k_3[POM_{red}]_0[O_2]_0 \qquad (2.3)$$

In the presence of copper the initial reaction rates are linearly dependent on [**SiW12$_{red}$**]$_0$ and [Cu(II)]$_0$, thus $-d[\mathbf{SiW12_{red}}]/dt = k_{app}(\mathbf{SiW12})[\mathbf{SiW12_{red}}]_0[Cu(II)]_0$, Figure 2.3 (a). In this case, the contribution of non-catalyzed pathway is negligible. From the slopes of the straight lines we determined k_{app}(**SiW12**) = 1.3×10^5 and 2.1×10^5 $M^{-1}s^{-1}$ for the experiments performed under air and O_2, respectively. From the data in Figure 2.3

(b) under O_2, the rate constant k_{app}(**SiW12**) = 2.4×10^5 $M^{-1}s^{-1}$, which is close to the value obtained from Figure 2.3 (a). The ratio for k_{app}(**SiW12**) obtained under O_2 and air and is about 2, but not 5 as expected for the first order reaction with respect to $[O_2]$. This indicates that the rate is weakly dependent on $[O_2]$ at high $[O_2]$, which is consistent with the eq 2.17 (reaction rate law).

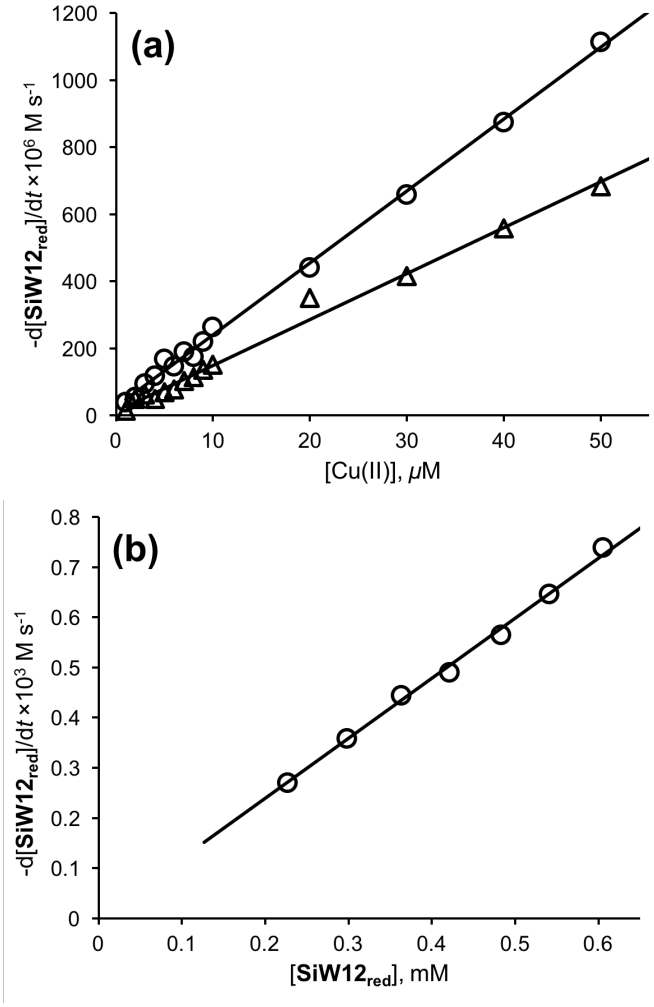

Figure 2.3. (a) Dependence of initial rate ($-d[\mathbf{SiW12_{red}}]_0/dt$) on $[Cu(II)]_0$ at 0.12 mM (Δ), and 0.58 mM (○) $[O_2]_0$, $[\mathbf{SiW12_{red}}]_0$ ~ 0.1 mM. (b) Dependence of initial rate ($-d[\mathbf{SiW12_{red}}]_0/dt$) on $[\mathbf{SiW12_{red}}]_0$ at 0.58 mM $[O_2]_0$ at 5 μM [Cu(II)]. Conditions: 50 mM sodium sulfate buffer; 100 mM $NaClO_4$; pH 2.0, 25 °C.

The same procedure was conducted for **PW12$_{red}$**. In the presence of copper the initial rates are linearly dependent on [Cu(II)]$_0$ (Figure 2.4) and for **PW12$_{red}$**, k_{app}(**PW12**) = 65 $M^{-1}s^{-1}$. The slopes for the reactions under dioxygen and under air are the same, which means that the rate of **PW12$_{red}$** oxidation is effectively independent on [O_2].

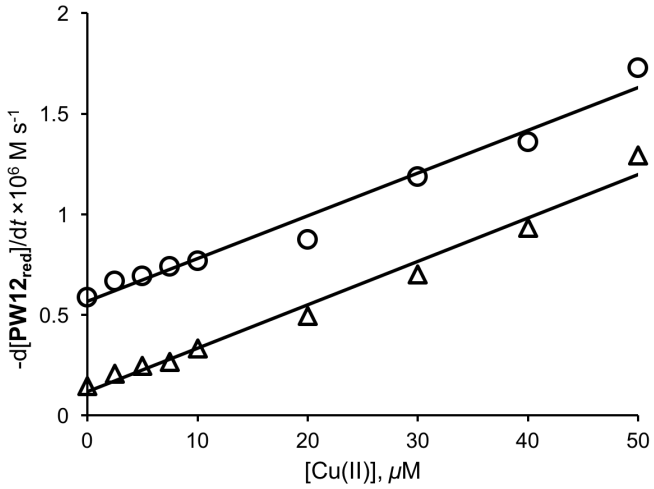

Figure 2.4. Dependence of initial rate (−d[**PW12$_{red}$**]/dt) on [Cu(II)]$_0$ at different initial concentrations of O_2. Conditions : ([O_2]$_0$) = 0.12 mM (Δ), and 0.58 mM (○) at pH = 2.0 and at 25 °C; 50 mM sodium sulfate buffer; 100 mM $NaClO_4$; [**PW12$_{red}$**]$_0$ ~ 0.33 mM.

2.3.4 Quantification of Contamination by Cu(II)

In previous studies, we and other groups reported that utilization of Cu-free aqueous electrolyte solutions is highly problematic because Cu ions are always present as trace contaminants.[28,30,42] Here we estimated the concentration of Cu contamination in our solutions. Neocuproine, 2,9-dimethyl-1,10-phenanthroline (DMP), was employed to

quantify the presence of potential trace Cu(II). DMP forms the hydrolytically stable complex, $[Cu(DMP)_2]^{+}$ [43,44] ($\log\beta_2 = 19.1$). DMP is partly protonated at low pH ($pK_a = 5.85$). This complex has a high reduction potential: 580 mV *versus* SCE in DMF,[45] and therefore cannot be oxidized by O_2 thus facilitating a separate catalytic cycle. Consequently, the addition of 10 − 40 fold excess of DMP over copper completely inhibits the catalysis by Cu(II). The theoretical initial rates were calculated based on eq 2.3. The speciation of Cu(II) complexes at pH 2.0 in the presence of DMP was calculated using HySS2009 software (http://www.hyperquad.co.uk/hyss.htm). Agreement between the theoretical and experimental data was achieved at Cu(II) contamination ~ 0.1 μM (Figure 2.5).

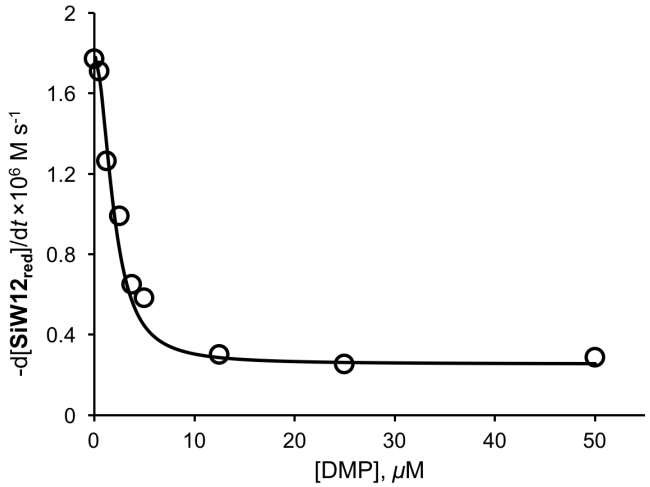

Figure 2.5. Initial rates of $\mathbf{SiW12_{red}}$ oxidation by O_2 at different neocuproine concentrations. The circles represent the experimental data, and the solid line is calculated data for a Cu(II) contamination ~ 0.1 μM. Conditions: pH 2.0, 50 mM sodium sulfate buffer, 100 mM $NaClO_4$, 25 °C, $[O_2]_0 = 0.12$ mM; $[\mathbf{SiW12_{red}}]_0 \sim 0.17$ mM.

2.3.5 Reaction Mechanism and Kinetic Model

The catalytic effect of Cu(II) on autoxidation of transition metals by O_2 under acidic conditions is described in the literature for several systems: autoxidation involving U^{5+},[46] Fe^{2+},[47,48] U^{4+},[49] and V^{3+}.[50] In the first system the catalysis is based on the thermodynamically favorable reduction of Cu(II) by UO_2^+ yielding Cu(I), which is rapidly re-oxidized by O_2. In the second case the equilibrium in eq 2.4 is significantly shifted to the left:

$$Fe^{2+} + Cu^{2+} \rightleftarrows Fe^{3+} + Cu^{+} \qquad (2.4)$$

The reduction potentials of the $\mathbf{PW12_{ox}/PW12_{red}}$ and $\mathbf{SiW12_{ox}/SiW12_{red}}$ couples are 255 mV and 55 mV, respectively.[28] The reduction potential of Cu^{2+}_{aq}/Cu^{+}_{aq} is 153 mV, thus the reduction of Cu^{2+}_{aq} is slightly favorable thermodynamically for $\mathbf{SiW12_{red}}$ and unfavorable for $\mathbf{PW12_{red}}$. In sulfate (or phosphate) buffer Cu^{2+}_{aq} forms $CuSO_4$ (or $CuH_2PO_4^+$) with a pK_a = 2.3 for $CuSO_4$ (and 0.1 for $CuH_2PO_4^+$).[51,52] These equilibria probably decrease the reduction potentials of Cu(II)/Cu(I) couples in buffered solutions. The speciation of Cu(II) and Cu(I) complexes will depend on the nature and concentration of buffer (sulfate or phosphate); this could well result in different reaction kinetics in different buffers.

Based on our data and literature data, we propose eqs 2.5 – 2.11 as the mechanism for copper-catalyzed reaction of POM_{red} with O_2.

$$POM_{red} + O_2 + H^+ \rightarrow POM_{ox} + HO_2^{\bullet} \qquad k_5(\mathbf{SiW12}) = 8.5\ M^{-1}s^{-1} \qquad [ref\ ^{28}] \qquad (2.5)$$

$$k_5(\mathbf{PW12}) = 1.4\ M^{-1}s^{-1}$$

$$POM_{red} + HO_2^{\bullet} + H^+ \rightarrow POM_{ox} + H_2O_2 \qquad k_6 = 2 \times 10^8\ M^{-1}s^{-1} \qquad [ref\ ^{28}] \qquad (2.6)$$

$$POM_{red} + Cu(II) \rightleftarrows POM_{ox} + Cu(I) \qquad K_7 = k_7/k_{-7} \qquad (2.7)$$

$$Cu(I) + O_2 + H^+ \rightleftarrows Cu(II) + HO_2^{\bullet} \qquad k_8 = 4.6 \times 10^5\ M^{-1}s^{-1} \quad [ref\ ^{53}]$$

$$k_{-8} = 5 \times 10^7\ M^{-1}s^{-1} \quad [ref\ ^{54}] \qquad (2.8)$$

$$Cu(I) + H_2O_2 \rightarrow Cu(II) + HO^{\bullet} + HO^- \qquad k_9 = 5 \times 10^3\ M^{-1}s^{-1} \quad [ref\ ^{54}] \qquad (2.9)$$

$$HO^{\bullet} + Cu(I) + H^+ \rightarrow H_2O + Cu(II) \qquad \text{Fast}, > 10^9\ M^{-1}s^{-1} \qquad (2.10)$$

$$HO^{\bullet} + POM_{red} + H^+ \rightarrow H_2O + POM_{ox} \qquad \text{Fast}, > 10^9\ M^{-1}s^{-1} \qquad (2.11)$$

The reactions in eqs 2.5 − 2.11 are simplified; each reaction may proceed through several steps. As we have shown earlier, the rate-limiting step in eq 2.5 is an outer-sphere electron transfer from POM_{red} to O_2.[28] In general this reaction should be written as reversible, but the reverse reaction is much slower than the reaction in eq 2.6. The reaction in eq 2.7 may proceed through an outer- or an inner-sphere ET mechanism.[29] The reaction in eq 2.8 is likely to proceed through an intermediate complex of O_2 and Cu(I).[46] The overall reaction of POM_{red} oxidation by O_2 is first order with respect to $[Cu(II)]_0$, Figures 2.3 (a) and 2.4, therefore the reaction of Cu(I) with O_2 is written in a simplified form (eq 2.8). The reaction thermodynamics of eqs 2.5 – 2.11 imposes constraints on the reaction rate constants. The difference between $\Delta E_7°$ for the reactions of **SiW12** and **PW12** should be equal to $E_{15}°$(**PW12**) − $E_{15}°$(**SiW12**), where $E_{15}°$(**PW12**) and $E_{15}°$(**SiW12**) are the standard reduction potentials of **SiW12** and **PW12**, eq 2.15.

$$O_2 + e^- + H^+ \rightarrow HO_2^{\bullet} \qquad E_{12}° = 0.12\ V\ (NHE\ at\ pH\ 2) \qquad (2.12)$$

$$HO_2^{\bullet} + e^- + H^+ \rightarrow H_2O_2 \qquad E_{13}° = 1.44\ V\ (NHE\ at\ pH\ 2) \qquad (2.13)$$

$$Cu(II) + e^- \rightarrow Cu(I) \qquad E_{14}° \qquad (2.14)$$

$$POM_{ox} + e^- \rightarrow POM_{red} \qquad E_{15}° \qquad (2.15)$$

2.3.6 Derivation of the Reaction Rate Law

The equation for the initial reaction rate based on this mechanism is very complex. Therefore, we simplify the derivation of the initial rate by taking into account that in the beginning, eq 2.6 is much faster than the reverse reaction, eq 2.8 (commonly $[POM_{red}]_0 >> [Cu(II)]_0$) and the contribution of the reactions in eqs 2.9 – 2.11 is negligible. The reaction rate law is derived with assuming steady state conditions with respect to Cu(I) and $HO_2^{\bullet}$.

The reactions are carried out in buffered solutions, therefore $[H^+]$ is not included in the reaction rate laws.

$$-d[POM_{red}]/dt = k_5[POM_{red}][O_2] + k_6[POM_{red}][HO_2^{\cdot}] + k_7[POM_{red}]\left[Cu^{2+}{}_{aq}\right] - k_{-7}[POM_{ox}]\left[Cu^{+}{}_{aq}\right]$$

Under our typical experimental conditions the ratio of the rates in eq 2.6 and the reverse rates in eq 2.8 is equal to $k_6[POM_{red}] / k_{-8}[Cu^{2+}] >> 1$. Thus, the reverse reaction in eq 2.8 can be ignored.

Steady state conditions with respect to $[HO_2^{\bullet}]$

$$d[HO_2^{\cdot}]/dt = k_5[POM_{red}][O_2] - k_6[POM_{red}][HO_2^{\cdot}] + k_8\left[Cu^{+}{}_{aq}\right][O_2] = 0$$

$$[HO_2^{\cdot}] = \left(k_5[POM_{red}][O_2] + k_8\left[Cu^{+}{}_{aq}\right][O_2]\right)/k_6[POM_{red}]$$

$$-d[POM_{red}]/dt = 2k_5[POM_{red}][O_2] + k_7[POM_{red}]\left[Cu^{2+}{}_{aq}\right] - k_{-7}[POM_{ox}]\left[Cu^{+}{}_{aq}\right] + k_8\left[Cu^{+}{}_{aq}\right][O_2]$$

Steady state conditions with respect to $[Cu^{+}{}_{aq}]$

$$d\left[Cu^{+}{}_{aq}\right]/dt = k_7[POM_{red}]\left[Cu^{2+}{}_{aq}\right] - k_{-7}[POM_{ox}]\left[Cu^{+}{}_{aq}\right] - k_8\left[Cu^{+}{}_{aq}\right][O_2] = 0$$

$$k_7[\mathrm{POM_{red}}]\left[\mathrm{Cu^{2+}_{aq}}\right] = k_{-7}[\mathrm{POM_{ox}}]\left[\mathrm{Cu^{+}_{aq}}\right] + k_8\left[\mathrm{Cu^{+}_{aq}}\right][\mathrm{O_2}]$$

$$-\mathrm{d}[\mathrm{POM_{red}}]/\mathrm{d}t = 2k_5[\mathrm{POM_{red}}][\mathrm{O_2}] + 2k_8\left[\mathrm{Cu^{+}_{aq}}\right][\mathrm{O_2}]$$

Mass balance

$$[\mathrm{Cu}] = \left[\mathrm{Cu^{+}_{aq}}\right] + \left[\mathrm{Cu^{2+}_{aq}}\right]$$

$$\left[\mathrm{Cu^{+}_{aq}}\right] = [\mathrm{Cu}] - \left[\mathrm{Cu^{2+}_{aq}}\right]$$

$$\left[\mathrm{Cu^{+}_{aq}}\right] = k_7[\mathrm{POM_{red}}]\left[\mathrm{Cu^{2+}_{aq}}\right]/(k_{-7}[\mathrm{POM_{ox}}] + k_8[\mathrm{O_2}]) = [\mathrm{Cu}] - \left[\mathrm{Cu^{2+}_{aq}}\right]$$

$$\left[\mathrm{Cu^{2+}_{aq}}\right] = \frac{k_{-7}[\mathrm{POM_{ox}}][\mathrm{Cu}] + k_8[\mathrm{Cu}][\mathrm{O_2}]}{k_{-7}[\mathrm{POM_{ox}}] + k_7[\mathrm{POM_{red}}] + k_8[\mathrm{O_2}]}$$

After simple rearrangements, the rate law will be in eq 2.16:

$$(\mathrm{d}[\mathrm{POM_{red}}]/\mathrm{d}t)_0 = -2k_5[\mathrm{POM_{red}}]_0[\mathrm{O_2}]_0 - 2k_7[\mathrm{POM_{red}}]_0[\mathrm{Cu(II)}]_0(k_8[\mathrm{O_2}]_0) / (k_{-7}[\mathrm{POM_{ox}}]_0 + k_7[\mathrm{POM_{red}}]_0 + k_8[\mathrm{O_2}]_0) \quad (2.16)$$

If the non-catalyzed reaction is slow, then eq 2.16 simplifies to eq 2.17:

$$(\mathrm{d}[\mathrm{POM_{red}}]/\mathrm{d}t)_0 = -2k_7[\mathrm{POM_{red}}]_0[\mathrm{Cu(II)}]_0(k_8[\mathrm{O_2}]_0) / (k_{-7}[\mathrm{POM_{ox}}]_0 + k_7[\mathrm{POM_{red}}]_0 + k_8[\mathrm{O_2}]_0) \quad (2.17)$$

2.3.7 Reaction of $\mathrm{POM_{red}}$ with Cu(II) under Ar

Based on the experimental data in Figure 2.3 (a) and when $[\mathrm{POM_{ox}}]$ is small at the beginning of the reaction, $k_{-7}[\mathrm{POM_{ox}}]$, $k_7[\mathrm{POM_{red}}] << k_8[\mathrm{O_2}]$ can be assumed under $\mathrm{O_2}$, and the eq 2.17 simplifies to eq 2.18:

$$(\mathrm{d}[\mathrm{POM_{red}}]/\mathrm{d}t)_0 = -2k_7[\mathrm{POM_{red}}]_0[\mathrm{Cu(II)}]_0 \quad (2.18)$$

which gives k_7(**SiW12**) = k_{app}(**SiW12**)/2 ~ 1.1 × 10^5 $M^{-1}s^{-1}$ and k_7(**PW12**) = k_{app}(**PW12**)/2 ~ 33 $M^{-1}s^{-1}$. Since these values were calculated from a simplified reaction rate law, they should be considered as rough estimates. To obtain more accurate data, the kinetics of $\mathbf{SiW12_{red}}$ and $\mathbf{PW12_{red}}$ with Cu(II) under Ar was examined.

The initial part of the decrease of absorbance at 700 nm is presented in Figure 2.6. The theoretical rate for the reaction in eq 2.7 at the reaction time t is given.

$$(d[POM_{red}]/dt)_t = -k_7[POM_{red}]_t[Cu(II)]_t + k_{-7}[POM]_t[Cu(I)]_t$$

The reaction stoichiometry $\Delta[POM_{red}]/\Delta[Cu(II)]$ in the excess of POM_{red} was found to be > 1 due to the further reduction of Cu(I) by POM_{red}. Therefore, the initial reaction rates at different initial concentrations of POM_{ox} and POM_{red} were measured and were plotted as a function $[POM_{red}]_t$ in Figures 2.7 and 2.8. The Solver sub-program of Microsoft Excel was used to fit the experimental data with k_7 and k_{-7} as variable parameters. This leads to the

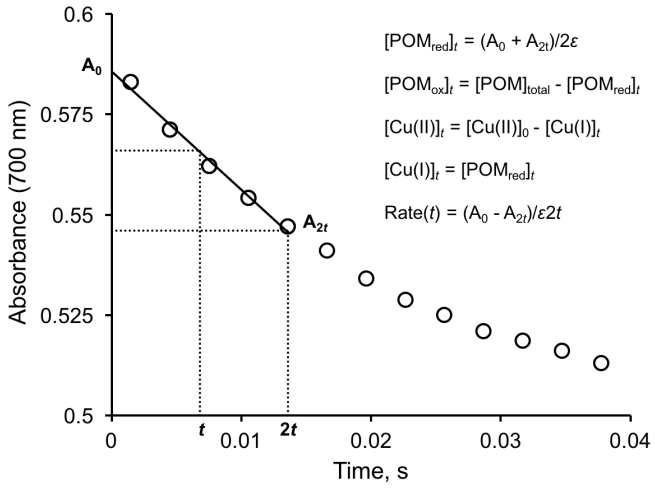

Figure 2.6. The initial decrease in absorbance at 700 nm (kinetics of $\mathbf{SiW12_{red}}$ oxidation). Conditions: [$\mathbf{SiW12_{red}}$]$_0$ ~ 0.4 mM, [Cu(II)] = 50 μM, pH 2.0, 50 mM sodium sulfate buffer, 100 mM $NaClO_4$, 25 °C.

following values: k_7(**SiW12**) ~ 1.9×10^5 $M^{-1}s^{-1}$, k_{-7}(**SiW12**) ~ 2×10^4 $M^{-1}s^{-1}$, K_7(**SiW12**) = 9.6, and k_7(**PW12**) = 17 $M^{-1}s^{-1}$, k_{-7}(**PW12**) = 7×10^3 $M^{-1}s^{-1}$, K_7(**PW12**) ~ 2.5×10^{-3}.

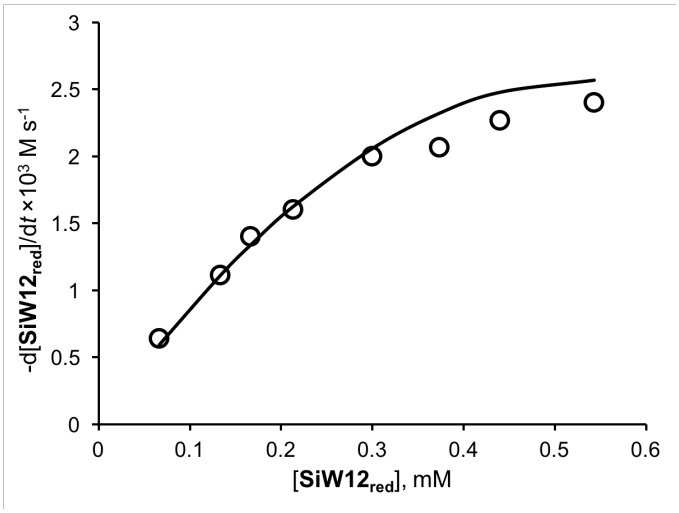

Figure 2.7. Initial rates of $\mathbf{SiW12_{red}}$ oxidation by 0.05 mM Cu(II) under Ar. Conditions: pH 2.0, 50 mM sulfate buffer, 100 mM $NaClO_4$, 25 °C. Black solid line is theoretical. k_7(**SiW12**) = 1.9×10^5 $M^{-1}s^{-1}$, k_{-7}(**SiW12**) = 2.0×10^4 $M^{-1}s^{-1}$, K_7(**SiW12**) = 9.6.

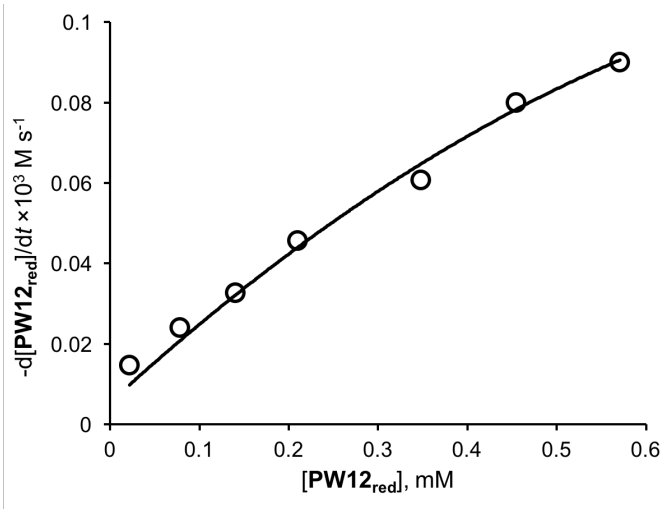

Figure 2.8. Initial rates of $\mathbf{PW12_{red}}$ oxidation by 0.5 mM Cu(II) under Ar. Conditions: pH 2.0, 50 mM sulfate buffer, 100 mM $NaClO_4$, 25 °C. Black solid line is theoretical. k_7(**PW12**) = 17 $M^{-1}s^{-1}$, k_{-7}(**PW12**) = 7×10^3 $M^{-1}s^{-1}$, K_7(**PW12**) ~ 2.5×10^{-3}.

2.3.8 General Discussion

Finally, we performed the global fitting of whole experimental kinetic curves (20 curves) for both **SiW12** and **PW12** to the reaction mechanism in eqs 2.5 – 2.11 with variable parameters k_7(**SiW12**), k_{-7}(**SiW12**), k_7(**PW12**), k_{-7}(**PW12**), k_8, and k_{-8} and k_9. The values of k_7(**SiW12**), k_{-7}(**SiW12**), k_7(**PW12**), and k_{-7}(**PW12**) were varied in a narrow range around the values estimated from eq 2.17 and from data on the reactions of Cu(II) with POM_{red}. The analysis of data showed that the results of fitting are very weakly dependent on k_9. Therefore we used $k_9 = 5 \times 10^3$ $M^{-1}s^{-1}$.[54] The results of fitting are given in Figure 2.9 (not all fitted curves are shown) and in Figure 2.2. The quantitative agreement with experimental data was achieved with $k_8 = (4.1 \pm 0.5) \times 10^5$ $M^{-1}s^{-1}$, $k_{-8} = (3.8 \pm 0.5) \times 10^6$ $M^{-1}s^{-1}$, k_7(**SiW12**) = $(1.8 \pm 0.3) \times 10^5$ $M^{-1}s^{-1}$, k_{-7}(**SiW12**) = $(1.9 \pm 0.3) \times 10^4$ $M^{-1}s^{-1}$,

K_7(**SiW12**) = 9.5 ± 1.5 and k_7(**PW12**) = (57 ± 10) $M^{-1}s^{-1}$, k_{-7}(**PW12**) = (1.3 ± 0.2) × 10^5 $M^{-1}s^{-1}$, K_7(**PW12**) = (4.4 ± 1.0) × 10^{-4}. As mentioned above, the thermodynamics requires that (RT/F) ln(K_7(**PW12**)/K_7(**SiW12**)) should be equal to the experimental electrochemical values (E_{15}°(**PW12**) − E_{15}°(**SiW12**)) = 0.2 V. The value of K_7(**SiW12**)/K_7(**PW12**) from the fitting is 9.5/(4.4 × 10^{-4}) = 2.2 × 10^4, which gives (RT/F) ln(K_7(**SiW12**)/K_7(**PW12**)) =

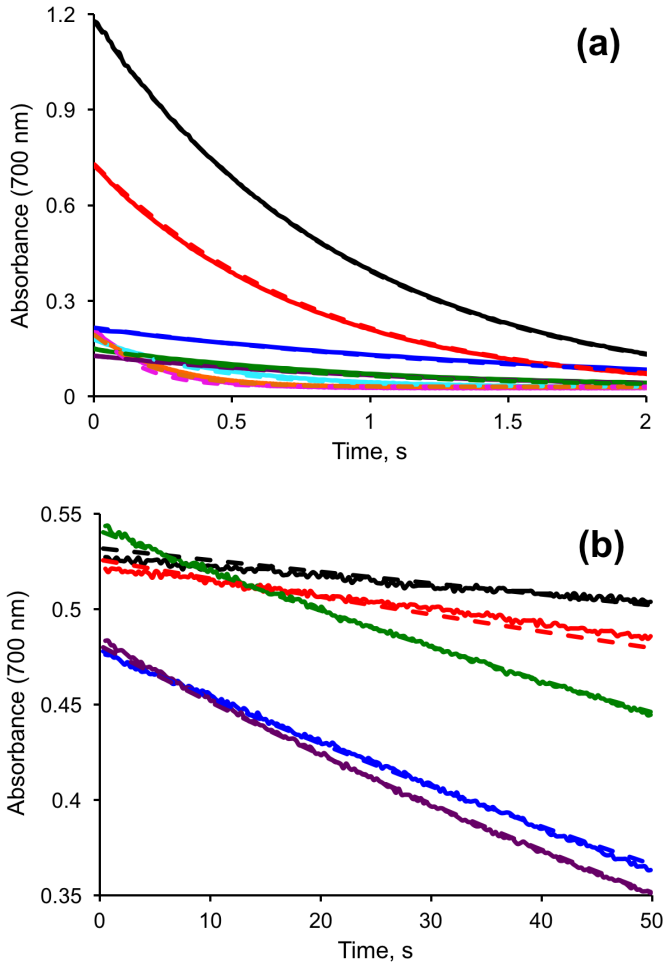

Figure 2.9. Kinetics of (a) **SiW12$_{red}$** and (b) **PW12$_{red}$** oxidation by O_2. Conditions: pH 2.0, 50 mM sodium sulfate buffer, 100 mM $NaClO_4$, 25 °C. Solid lines indicate the experimental curves. Dashed lines are the theoretical curves.

0.059 log(2.2 × 10^4) = 0.25 V. The Nernst law applied to the eq 2.7 is (RT/F) ln(K_7(**SiW12**)) = 0.059 log(9.5) = 0.058 = $E_{14}°$ − $E_{15}°$(**SiW12**) (0.055 V), resulting in $E_{14}°$ = 0.11 and 0.06 V based on K_7(**PW12**) (eq 2.14), which gives an average value of 0.09 V. This estimated number is slightly lower than that of 0.153 V for aqueous the Cu(II)/Cu(I) couple due to the effect of sulfate anion and/or ionic strength.

The kinetic model of catalytic oxidation of [POM_{red}] by O_2 in eqs 2.5 – 2.11 quantitatively describes the experimental data. The significant increase in the rate is achieved by replacement of the slow outer-sphere electron transfer reaction in eq 2.5 by much faster reactions in eqs 2.7 and 2.8. Under typical experimental conditions the reaction in eq 2.7 is the rate-limiting step, which is much faster than the direct reaction in eq 2.5. In the reaction in eq 2.5 the formation of $O_2^{-\bullet}$ is the slowest step. The oxidation potential of $O_2/O_2^{-\bullet}$ = − 0.16 V, while that of Cu(II)/Cu(I) = 0.09 V. Thus, eq 2.7 is thermodynamically more favorable then eq 2.5 by 0.25 V. The combination of higher thermodynamic driving force and fast oxidation of Cu(I) by O_2 via an intermediate formation of {Cu(I)…O_2} results in the high activity of copper complexes for catalyzing oxidation of POM_{red} by O_2.

Evidently, the efficiency of catalysis should be dependent on the ligand(s) in Cu(II)/Cu(I) complexes. Since Cu^{2+}_{aq} forms $CuSO_4$ in sulfate buffer (pK_a = 2.3)[51] and $CuH_2PO_4^+$ in phosphate buffer (pK_a = 0.1)[52], one could expect a different catalytic activity in sulfate and phosphate buffers. Indeed, under similar conditions the catalytic reactions proceed faster in phosphate buffer, Figure 2.10.

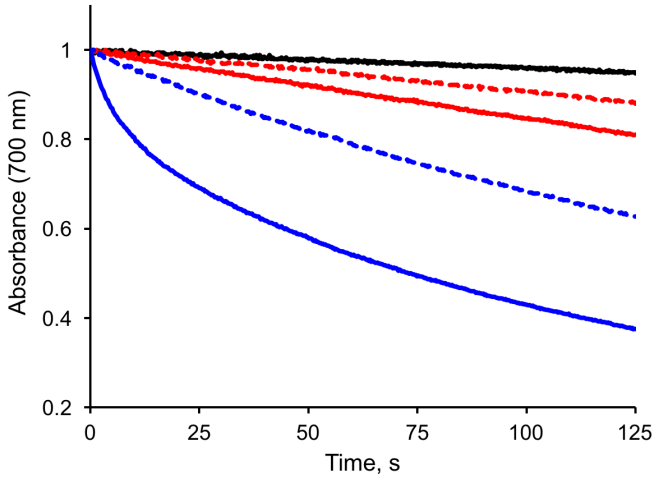

Figure 2.10. Kinetics of **PW12$_{red}$** oxidation by O_2 in sulfate and phosphate buffer. Conditions: [**PW12$_{red}$**]$_0$ ~ 0.4 mM, [O_2]$_0$ = 0.12 mM, [Cu(II)] = 0 (black), 10 (red), 50 (blue) μM, pH 2.0, 50 mM sodium sulfate buffer (dashed) and sodium phosphate buffer (solid), 100 mM $NaClO_4$, 25 °C.

2.4 Conclusions

The oxidation of reduced polyoxometalates by O_2 is of central importance in many POM-catalyzed oxidation processes ranging from those in academic laboratory studies to commercial processes. This study addresses the lack of rigorous mechanistic information about the catalysis of this generic type of process using the common Keggin structural class of POM and Cu(II), the most efficient hydrated 3d-metal ion for this catalysis. Other first-row-transition metal ions are far less active. Even micromolar concentrations of Cu(II)

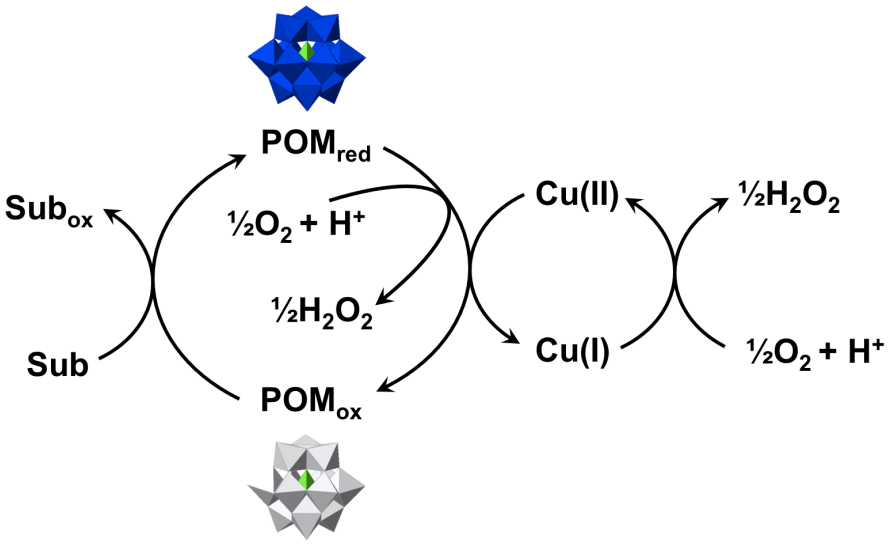

Scheme 2.1. Catalytic cycle of POM_{red} oxidation catalyzed by Cu(II).

species render the copper-catalyzed reaction of reduced POMs with O_2/air to be dominant under typical experimental conditions, in part because direct reaction of POM_{red} with O_2 is orders of magnitude slower. We have thoroughly studied the kinetics of the catalytic reaction at pH 2.0 in sulfate buffer and established the reaction mechanism which includes the reversible reduction of Cu(II) to Cu(I) by POM_{red} followed by fast re-oxidation of Cu(I) to Cu(II) by O_2 (Scheme 2.1). The reduction of Cu(II) by POM_{red} is typically the rate-limiting step but thermodynamically more favorable than direct outer-sphere electron transfer from POM_{red} to O_2. The proposed reaction mechanism quantitatively describes the experimental data.

2.5 References

(1) Misono, M. *Stud. Surf. Sci. Catal.* **1993,** *75*, 69.

(2) Hill, C. L.; Prosser-McCartha, C. M. *Coord. Chem. Rev.* **1995,** *143*, 407.

(3) Okuhara, T.; Mizuno, N.; Misono, M. *Adv. Catal.* **1996,** *41*, 113.

(4) Kozhevnikov, I. V. *Chem. Rev.* **1998,** *98*, 171.

(5) Chambers, R. C.; Hill, C. L. *Inorg. Chem.* **1989,** *28*, 2509.

(6) Harrup, M. K.; Hill, C. L. *Inorg. Chem.* **1994,** *33*, 5448.

(7) Hill, C. L. *J. Mol. Catal. A: Chem.* **1996,** *114*, 1.

(8) Neumann, R.; Dahan, M. *Nature* **1997,** *388*, 353.

(9) Hill, C. L.; Weinstock, I. A. *Nature (London)* **1997,** *388*, 332.

(10) Weinstock, I. A.; Barbuzzi, E. M. G.; Wemple, M. W.; Cowan, J. J.; Reiner, R. S.; Sonnen, D. M.; Heintz, R. A.; Bond, J. S.; Hill, C. L. *Nature* **2001,** *414*, 191.

(11) Hill, C. L. *J. Mol. Catal. A: Chem.* **2007 Special Issue,** *262*, 1.

(12) Snir, O.; Wang, Y.; Weinstock, I. A. *Isr. J. Chem.* **2011,** *51*, 247.

(13) Wang, S.-S.; Yang, G.-Y. *Chem. Rev.* **2015,** *115*, 4893.

(14) Punniyamurthy, T.; Velusamy, S.; Iqbal, J. *Chem. Rev.* **2005,** *105*, 2329.

(15) Piera, J.; ckvall, J.-E. B. *Angew. Chem. Int. Ed.* **2008,** *47*, 3506.

(16) Gligorich, K. M.; Sigman, M. S. *Chem. Commun.* **2009**, 3854.

(17) Shi, Z.; Zhang, C.; Tang, C.; Jiao, N. *Chem. Soc. Rev.* **2012,** *41*, 3381.

(18) Bonchio, M.; Carraro, M.; Sartorel, A.; Scorrano, G.; Kortz, U. *J. Mol. Catal. A: Chem.* **2006,** *251*, 93.

(19) Neumann, R.; Khenkin, A. M. *Chem. Commun.* **2006**, 2529.

(20) Neumann, R. *Inorg. Chem.* **2010,** *49*, 3594.

(21) Berardi, S.; Carraro, M.; Sartorel, A.; Modugno, G.; Bonchio, M. *Isr. J. Chem.* **2011,** *51*, 259.

(22) Hill, C. L. In *Comprehensive Coordination Chemistry-II: From Biology to Nanotechnology*; Wedd, A. G., Ed.; Elsevier Ltd.: Oxford, UK, 2004; Vol. 4.

(23) Duncan, D. C.; Hill, C. L. *J. Am. Chem. Soc.* **1997,** *119*, 243.

(24) Khenkin, A. M.; Neumann, R. *Angew. Chem. Int. Ed.* **2000,** *39*, 4088.

(25) Khenkin, A. M.; Weiner, L.; Wang, Y.; Neumann, R. *J. Am. Chem. Soc.* **2001,** *123*, 8531.

(26) Hill, C. L.; Gall, R. D. *J. Mol. Catal. A: Chem.* **1996,** *114*, 103.

(27) Neumann, R. *Mod. Oxidation Methods* **2004**, 223.

(28) Geletii, Y. V.; Hill, C. L.; Atalla, R. H.; Weinstock, I. A. *J. Am. Chem. Soc.* **2006,** *128*, 17033.

(29) Rorabacher, D. B. *Chem. Rev.* **2004,** *104*, 651.

(30) Wang, X.; Stanbury, D. M. *J. Phys. Chem. A* **2004,** *108*, 7637.

(31) Bridgart, G. J.; Fuller, M. W.; Wilson, I. R. *J. Chem. Soc., Dalton Trans.* **1973**, 1274.

(32) Saha, B.; Hung, M.; Stanbury, D. M. *Inorg. Chem.* **2002,** *41*, 5538.

(33) Bagiyan, G. A.; Koroleva, I. K.; Soroka, N. V.; Ufimtsev, A. V. *Russian Chemical Bulletin, Int. Ed.* **2003,** *52*, 1135.

(34) Dicks, A. P.; Swift, H. R.; Williams, D. L. H.; Butler, A. R.; Al-Sa'doni, H. H.; Cox, B. G. *J. Chem. Soc., Perkin Trans. 2* **1996**, 481.

(35) Cowan, J. J.; Bailey, A. J.; Heintz, R. A.; Do, B. T.; Hardcastle, K. I.; Hill, C. L.; Weinstock, I. A. *Inorg. Chem.* **2001,** *40*, 6666.

(36) Yang, B.; Pignatello, J. J.; Qu, D.; Xing, B. *J. Phys. Chem. A* **2015,** *119*, 1055.

(37) Weinstock, I. A.; Cowan, J. J.; Barbuzzi, E. M. G.; Zeng, H.; Hill, C. L. *J. Am. Chem. Soc.* **1999,** *121*, 4608.

(38) Cowan, J. J.; Hill, C. L.; Reiner, R. S.; Weinstock, I. A. In *Inorg. Synth.*; Coucouvanis, D., Ed.; John Wiley& Sons, Inc.: New York, 2002; Vol. 33.

(39) Pope, M. T.; Varga, G. M. *Inorg. Chem.* **1966,** *5*, 1249.

(40) Tézé, A.; Hervé, G. In *Inorg. Synth.*; Ginsberg, A. P., Ed.; John Wiley and Sons: New York, 1990; Vol. 27.

(41) Geletii, Y. V.; Weinstock, I. A. *J. Mol. Catal. A: Chem.* **2006,** *251*, 255.

(42) Geletii, Y. V.; Bailey, A. J.; Boring, E.; Hill, C. L. *J. Chem. Soc., Chem. Commun.* **2001**, 1484.

(43) James, B. R.; Williams, R. J. P. *J. Chem. Soc. A* **1961**, 2007.

(44) Proskurnin, M. A.; Chernysh, V. V.; Pakhomova, S. V.; Kononets, M. Y.; Sheshenev, A. A. *Talanta* **2002,** *57*, 831.

(45) McBryde, W. A. E. *A Critical Review of Equilibrium Data for Proton- and Metal Complexes of 1,10-phenanthroline,2,2-bipyridyl and Related Compounds*; Oxford: Pergamon Press, 1978, 1978.

(46) Bakac, A.; Espenson, J. H. *Inorg. Chem.* **1995,** *34*, 1730.

(47) Lamb, A. B.; Lucius W. Elder, J. *J. Am. Chem. Soc.* **1931,** *53*, 137.

(48) Cher, M.; Davidson, N. *J. Am. Chem. Soc.* **1955,** *77*, 793.

(49) Halpern, J.; Smith, J. G. *Can. J. Chem.* **1956,** *34*, 1419.

(50) Ramsey, J. B.; Sugimoto, R.; DeVorkin, H. *J. Am. Chem. Soc* **1941,** *63*, 3480.

(51) Davies, W. G.; Otter, R. J.; Prue, J. E. *Disc. Faraday Soc.* **1957,** *24*, 103.

(52) Aksu, S. *J. Electrochem. Soc.* **2009,** *156*, C387.

(53) Buxton, G. V.; Mulazzani, Q. G.; Ross, A. B. *J. Phys. Chem. Ref. Data* **1995,** *24*, 1055.

(54) Kozlov, Y. N.; Berdnikov, V. M. *Russian J. Phys. Chem. (Engl. Transl.)* **1973,** *47*, 338.

Chapter 3

Synergistic Oxidation of Reduced Keggin Heteropolytungstates by Dioxygen Catalyzed by a Combination of Copper and Iron

With Masoumeh Chamack, Yurii V. Geletii and Craig L. Hill

Reproduced in part with permission from *Inorg. Chem.*, **2018**, *57* (1), 311–318.

3.1 Introduction

Polyoxometalate (POM)-based redox processes underlie analytic methods such as phosphate determination,[1] POM-based high-charge-capacity batteries,[2] wet oxidation of organics,[3] and most importantly, catalysts for O_2-based oxidations.[3-15] Several of the last species have been commercialized.[6,16] O_2-based oxidation processes continue to be a mainstay in catalysis because of their green aspects and potential low cost.[17-22] As described in **Chapter 1**, POMs display several advantages as oxidation catalysts: they can serve as effective, reversibly-reducible, multidentate ligands for incorporation of one or more redox-active transition metals, which in turn, can help control the reactivity of ground-state triplet O_2.[3,8,11,12,14,23-26] A common barrier in these O_2/air-based oxidation processes is reaction of the reduced POM (POM_{red}) with O_2.[10,13,27-30,58] This step is usually slower than oxidation of the substrate by the resting oxidation state POM (POM_{ox}) to form the reduced POM.[9,27-32] Importantly, some of the most potentially useful POM oxidants (frequently those with the highest redox potentials such as the two targeted in this study, α-$PW_{12}O_{40}^{3-}$ and α-$SiVW_{11}O_{40}^{5-}$), are rendered marginally useful because their reduced forms *cannot* be reoxidized by O_2/air at a satisfactory rate or at all in the studies to date.

The overall reduction of O_2 to water by POM_{red} is a complex sequence of electron transfer (ET) steps that usually starts with a single outer-sphere ET process,[33] eq 3.1:

$$POM_{red} + O_2 \rightarrow POM_{ox} + O_2^{-\bullet} \qquad (3.1)$$

Outer-sphere ET processes such as in eq 3.1 are typically slow, but many can be catalyzed by very low concentrations of copper.[34,35] Examples of such copper-catalyzed oxidations are the reaction of thioglycolic acid by octacyanomolybdate(V) ,[36] cysteine with hexacyanoferrate(III),[37] and thiols with O_2 in neutral and alkaline media.[38] The availability

of the Cu(II)/Cu(I) couple converts these outer-sphere processes to inner-sphere ones involving several elementary processes.

According to **Chapter 2**, we demonstrated the highly efficient catalysis by submicromolar concentrations of Cu of the reaction between reduced Keggin polyoxometalates, POM_{red}, and dioxygen.[39] The mechanism of this $POM_{red} + O_2$ reaction specifically for the reduced α-Keggin anions, α-$X^{n+}W_{12}O_{40}^{(9-n)-}$ (X = Al^{3+}, Si^{4+}, and P^{5+}; **$AlW12_{red}$**, **$SiW12_{red}$**, and **$PW12_{red}$**, respectively) was studied in detail because these POMs have been thoroughly characterized and known to be quite stable, nonprotonated and non-ion-paired under the conditions in this paper and over a wide pH range.[14,40,41] Examination of the kinetics of this catalytic reaction at pH 2.0 in sulfate and phosphate buffers led to a proposed mechanism that entails the reversible reduction of Cu(II) to Cu(I) by POM_{red} followed by a fast re-oxidation of Cu(I) to Cu(II) by O_2.

This Chapter addresses a combination of copper and iron ions is a far more effective catalytic system for the O_2-based reoxidation of reduced POMs than just copper alone, and that this combination can catalyze reoxidation of more useful (more oxidizing, higher-potential) POMs: α-$PW_{12}O_{40}^{4-}$ (**$PW12_{red}$**) and α-$SiVW_{11}O_{40}^{6-}$ (**$SiVW11_{red}$**). The synergetic catalytic action of Cu and Fe in oxidation processes is rather rare and was discussed.[42] Mechanistic studies reveal that Cu(II) reacts with Fe(II) to form Cu(I) and Fe(III) followed by fast reaction of POM_{red} with Fe(III) and Cu(I) with O_2. In addition, Fe complexes catalyze the oxidation of POM_{red} by H_2O_2, resulting in an altered reaction stoichiometry.

3.2 Experimental

3.2.1 Materials

The fully oxidized α-Keggin ion (POM_{ox}), α-$Na_3PW_{12}O_{40}$ (+99.9%) was purchased from Sigma-Aldrich. POM_{red} was prepared by constant-potential bulk electrolysis of 1 – 2 mM parent POM_{ox} under Ar as described in previous studies,[33,39,43,44] and then stored under Ar. The [POM_{red}]/[POM_{ox}] ratio was controlled coulometrically (charge passed through the solution). The fully oxidized α-Keggin ion, α-$K_5SiVW_{11}O_{40}$ was prepared using published methods,[45] and the one-electron-reduced form, α-$K_6SiV^{IV}W_{11}O_{40}$ was prepared by using 1 molar equiv of $VOSO_4$ (≥99.99%) instead of $MnCl_2 \cdot 4H_2O$ as described in published methods.[46] $Cu(NO_3)_2$ (≥98 %), $CuSO_4$ (≥99.99%), $FeSO_4$ (99+%), and $Fe(NO_3)_3$ (98+%) were purchased from Sigma-Aldrich and used as the sources of Cu and Fe. We used 50 mM phosphate and sulfate buffers in this study. The 50 mM phosphate buffer at pH 1.8 is composed of 69 % H_3PO_4, 31 % $H_2PO_4^-$, and 0.00012 % HPO_4^{2-}, and that of sulfate buffer at pH 1.8 is 61 % HSO_4^-, 39 % SO_4^{2-}, and 0.00096 % H_2SO_4. All chemicals were commercial quality unless specified otherwise. Solutions were prepared using water from a Barnstead Nanopure® quality water; added salts and buffers were of the highest purity available.

3.2.2 Electrochemistry

The electrochemical data were collected by using a BAS CV-50W electrochemical system. Both cyclic voltammograms (CVs) and bulk electrolyses were recorded at room temperature (24 ± 2 °C) as previously described,[33,39,43,44] using Ag/AgCl (3 M NaCl) BAS, a glassy-carbon disk, and a Pt wire as the reference, working and counter electrodes,

respectively. CVs were recorded in buffered solutions containing 100 mM $NaNO_3$ or $NaClO_4$ electrolyte. The working electrode in bulk electrolyses was reticulated vitreous carbon. This was used to prepare aqueous solutions of POM_{red}. Extinction coefficients of $1e^-$-reduced α-Keggin anions were determined earlier ($\varepsilon_{700} = (1.56 \pm 0.1) \times 10^3\ M^{-1}cm^{-1}$ for **$PW12_{red}$**).[33]

3.2.3 Kinetic Measurements

A SF-61 instrument (Hi-Tech Scientific, U.K.) was used for all stopped-flow studies, and the reaction kinetics for **$PW12_{red}$** were monitored by the absorbance changes with time at 700 nm. The first feeding syringe in the stopped-flow apparatus contained a deaerated solution of POM_{red}. which was diluted, as appropriate, with O_2-free buffer/electrolyte solution. The second feeding syringe was filled with Cu(II) and/or Fe(II) (or Fe(III)) in the same buffer/electrolyte solution but saturated with O_2 or air. The solubility of dioxygen in water with an ionic strength of 175 mM at 25 °C and 1 atm O_2 was taken, as in previous studies, to be 1.15 mM.[33] In all stopped-flow kinetic measurements, the concentrations of O_2, POM_{red}, Fe(II) and Cu(II) in the reaction mixture were twice as low as those in the feeding syringes. For the reaction with **$PW12_{red}$** and H_2O_2, the first syringe was filled with the deaerated solution of **$PW12_{red}$** and catalyst(s), and the second syringe was filled with H_2O_2. For the reaction with **$SiVW11_{red}$** and H_2O_2, the first syringe was filled with the solution of **$SiVW11_{red}$** and catalyst(s), and the second syringe was filled with H_2O_2. For the reaction of **$SiVW11_{ox}$** and Fe(II), the first syringe was filled with the solution of **$SiVW11_{ox}$** and the second syringe was filled with Fe(II). The reaction progress was followed at 580 nm. The **$SiVW11_{red}$** oxidation by O_2 was

carried out in closed, thick-walled glass reaction vessels at 100 °C. After the desired reaction time, the vessels were quickly cooled by immersion in cold water. When the temperature reached 25 °C, the electrochemical potential of the solution was measured using an ORP meter (Mettler Toledo, Switzerland). The redox electrode was calibrated with ORP standard solution (Thermo Fisher Scientific). The plot of the electrode readings versus log([**SiVW11$_{ox}$**]/[**SiVW11$_{red}$**]) was found to be linear with a slope close to 0.059 V per decade in agreement with the Nernst law (Figure 3.1) and the standard reduction potential $E°$(**SiVW11$_{ox}$**/**SiVW11$_{red}$**) = 0.64 V (vs NHE). The fitting of kinetic curves, simulation of the reaction kinetics, and optimization of conditions were performed using COPASI 4.13 (Build 87) software (www.copasi.org).

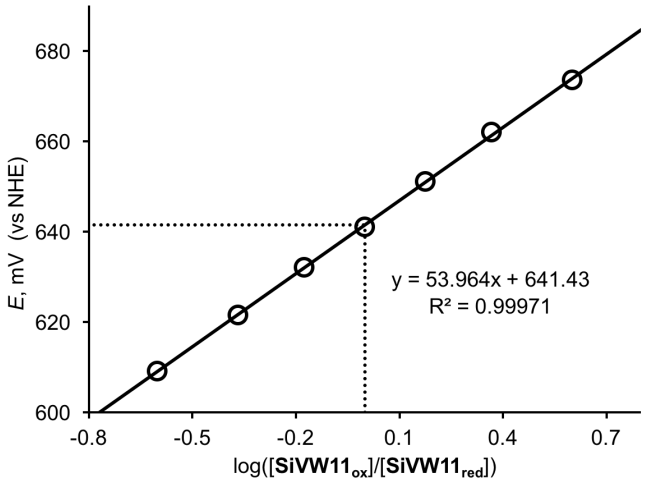

Figure 3.1. Dependence of solution electrochemical potentials as a function of [**SiVW11$_{ox}$**]/[**SiVW11$_{red}$**] ratio measured by Pt-redox electrode vs NHE in 0.1 M $NaNO_3$ at pH 1.8 adjusted by HNO_3.

3.2.4 Solubility of $FePO_4$

The ChemEq v3.1 software package with a built-in database was used to calculate the speciation under the experimental conditions. The solubility products are $pK_{sp} = 26.4$ for the mineral Strengite, $FePO_4 \bullet 2H_2O(s)$, and 21.6 for the amorphous $FePO_4$ (the most likely product in the experimental system).

The concentration of PO_4^{3-} in 50 mM phosphate buffer at pH 1.8 is $< 1 \times 10^{-18}$. The concentration of Fe(III) is < 0.5 mM under our experimental conditions. The concentration of free Fe^{3+}, calculated with ChemEq v3.1 in 50 mM phosphate buffer at pH 1.8 is 5×10^{-5} M. Thus, the formation of Strengite crystals is thermodynamically feasible. Importantly, however, the formation of solid $FePO_4$ is prohibitively slow. Under our experimental conditions, the initial rate law is $d[FePO_4]/dt = k[Fe^{3+}][PO_4^{3-}]$. The reaction rate constant $k < 10^{11}$ $M^{-1}s^{-1}$ (diffusion controlled), and the life-time of $[Fe^{3+}]$ is longer than $1/k[PO_4^{3-}] > 10^7$ s or > 4 months. Therefore, regardless of pK_{sp} value, our solutions are kinetically stable.

3.3 Results and Discussion

3.3.1 Synergetic Catalytic Effect of Cu(II) and Fe(II)

Recently, we have shown that trace amounts of Cu(II) efficiently catalyze oxidation of POM_{red} by O_2.[39] For example, the reaction with **AlW12$_{red}$** is almost 25 times faster if 38 μM Cu(II) is added at neutral pH, and the reaction with **SiW12$_{red}$** proceeds 2 orders of magnitude faster if 10 μM Cu(II) is added (~3% based on $[\mathbf{SiW12_{red}}]_0$). The catalytic cycle was proved to include two key reactions: the reduction of Cu(II) by POM_{red} followed

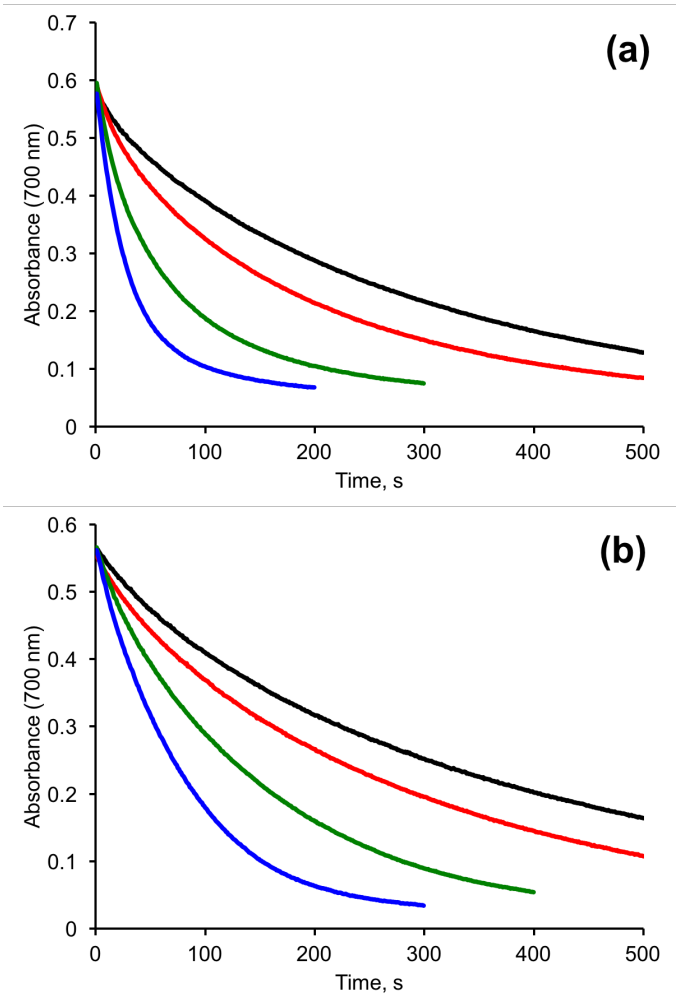

Figure 3.2. Effect of Fe(II) concentration on the kinetics of Cu(II)-catalyzed O_2-based oxidation of $\mathbf{PW12_{red}}$ in 50 mM (a) phosphate and (b) sulfate buffers, followed by the decrease of absorbance at 700 nm: $[\mathbf{PW12_{red}}]_0 \approx 0.4$ mM, $[O_2]_0 = 0.12$ mM, [Cu(II)] = 10 μM in all cases, [Fe(II)] = 0 (black), 25 (red), 50 (green), 125 (blue), μM, 100 mM $NaNO_3$, pH 1.8, 25 °C.

by fast reoxidation of Cu(I) by O_2. Unfortunately, for POMs with high reduction potentials, the reduction of Cu(II) becomes thermodynamically unfavorable and the catalysis by Cu ions is inefficient. Since the oxidation of Fe(II) by dioxygen is known to be catalyzed by Cu,[47] and the reduction potential of the Fe(III)/Fe(II) couple is higher, we reasoned that a combination of Fe and Cu ions might catalyze O_2-based reoxidation of POM_{red} with a less negative reduction potential. Indeed, we have found **$PW12_{red}$** is reoxidized by O_2 significantly faster in the presence of both Cu(II) and Fe(II) (added as $CuSO_4$ and $FeSO_4$) at pH 1.8 as shown in Figure 3.2. This is a significant finding because many families of POMs for potential use as catalysts for O_2/air-based oxidations are not effective because the O_2-based reoxidation does not proceed or proceeds too slowly to be useful.

3.3.2 Reaction Stoichiometry

In a previous study,[39] we established that H_2O_2 was the relatively stable reaction product of POM_{red} oxidation by O_2 catalyzed by copper. Significantly, in the presence of Fe and Cu ions, hydrogen peroxide efficiently oxidizes POM_{red} as shown in Figure 3.3 (a). In the absence of Cu, the reaction is also fast, only slightly slower than that in the presence of Cu (Figure 3.3 (b)). Such behavior indicates that Fe is a much more efficient catalyst of POM_{red} oxidation by H_2O_2, and the reaction is mostly catalyzed by Fe(II). Thus, in the presence of both copper and iron, the reaction product, H_2O_2, is unstable and further oxidizes POM_{red}. Therefore, we studied the oxidation of reduced POM by hydrogen peroxide in the presence of both Fe and Cu.

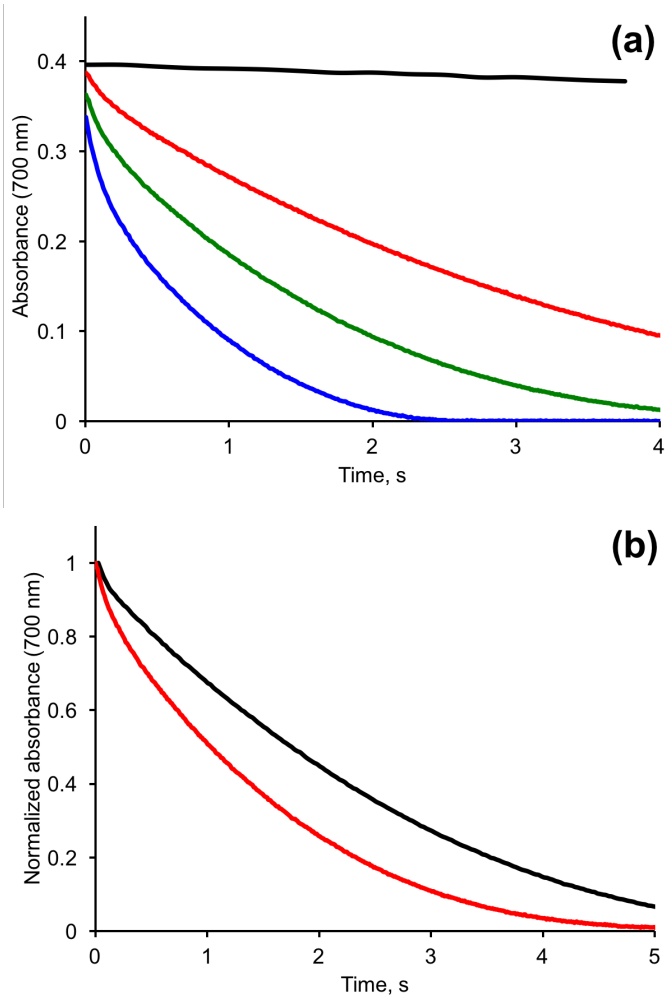

Figure 3.3. (a) Effect of Fe(II) concentration on the kinetics of Cu(II)-catalyzed oxidation of $\mathbf{PW12_{red}}$ by H_2O_2 followed by the decrease in absorbance at 700 nm: [Cu(II)] = 10 μM in all cases; [Fe(II)] = 0 (black), 31 (red), 62 (green), 125 (blue) μM, $[\mathbf{PW12_{red}}]_0 \approx 0.27$ mM, $[H_2O_2]_0 = 0.5$ mM, pH 1.8, 50 mM phosphate buffer, 100 mM $NaNO_3$, 25 °C under Ar. (b) Effect of Cu(II) concentrations on the kinetics of $\mathbf{PW12_{red}}$ oxidation by H_2O_2 followed by the decrease in absorbance at 700 nm in the presence of 62 μM Fe(II): [Cu(II)] = 0 (black), 10 (red) μM, $[\mathbf{PW12_{red}}]_0 \approx 0.27$ mM, $[H_2O_2]_0 = 0.5$ mM, 50 mM phosphate buffer, 100 mM $NaNO_3$, pH 1.8, 25 °C under Ar.

In the absence of Fe ions, the total amount of consumed POM per initial concentration of O_2, $\Delta[\mathbf{PW12_{red}}]/[O_2] \approx 2.0$ and therefore hydrogen peroxide is the reaction product. If the reaction is carried out in the presence of Fe ions under conditions where $[\mathbf{PW12_{red}}]_0/[O_2]_0 > 4$, then the reaction stoichiometry, $\Delta[\mathbf{PW12_{red}}]/[O_2]$, is between 2.0 and 4.0, indicating that H_2O_2 oxidizes $\mathbf{PW12_{red}}$ further. In Figure 3.11 (General Discussion), we show the final yield of H_2O_2 in the presence of Fe(II).

3.3.3 Initial Reaction Rates

Traditionally, kinetic studies include the analysis of initial reaction rates to establish the reaction rate law. For complex reaction mechanisms, however, derivation of the rate law is impossible without numerous assumptions and simplifications, such as the concept of the steady state. Achieving steady-state conditions may take a relatively long time and often can be seen in the very beginning of the kinetic curves. Indeed, the initial parts of the kinetic curves in this study cannot be described by a straight line. An exemplary curve is given in Figure 3.4. This results in uncertainty in measurements of the initial rates. Therefore, we performed the digital fitting of kinetic curves. Since the reaction mechanism includes relatively large numbers of reactions, we felt that the thermodynamic analysis would help to restrict the number and the range of variable parameters.

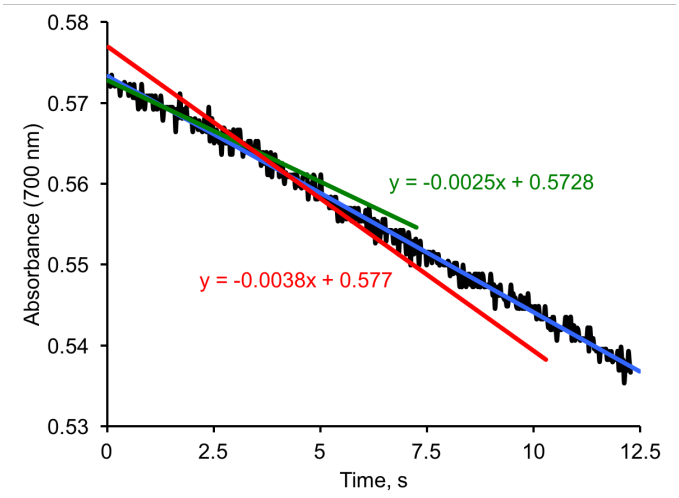

Figure 3.4. The shape of initial part of the kinetic curve of **PW12$_{red}$** oxidation by O_2 and dependence of initial rate ($-$d[**PW12$_{red}$**]/dt) on time intervals. Conditions: [**PW12$_{red}$**]$_0$ ~ 0.38 mM, [Cu(II)]$_0$ = 10 μM, [Fe(II)]$_0$ = 50 μM, [O_2]$_0$ = 0.12 mM, pH 1.8, 50 mM sulfate buffer, 0.1 M $NaNO_3$, 25 °C. Black line is experimental data. Red line is a trend line with a slope 0.0038 taken between 3 − 4 seconds. The slope measured in between 0.01 – 0.75 seconds is 0.0025 (green line). The blue curve is obtained from fitting using the parameter in the Table 3.2.

3.3.4 Thermodynamic Properties of Fe(III)/Fe(II) and Cu(II)/Cu(I) Complexes

First, we measured the reduction potential of Fe(III)/Fe(II) in sulfate buffer. The stock solutions of $Fe(NO_3)_3$ and $FeSO_4$ in 50 mM sodium sulfate buffer were mixed to obtain different ratios of [Fe(III)]/[Fe(II)], with the total iron concentration kept constant (Figure 3.5). The electrochemical solution potential measured by the redox electrode linearly increased with log([Fe(III)]/[Fe(II)]) with 0.051 V per decade slope, which is close

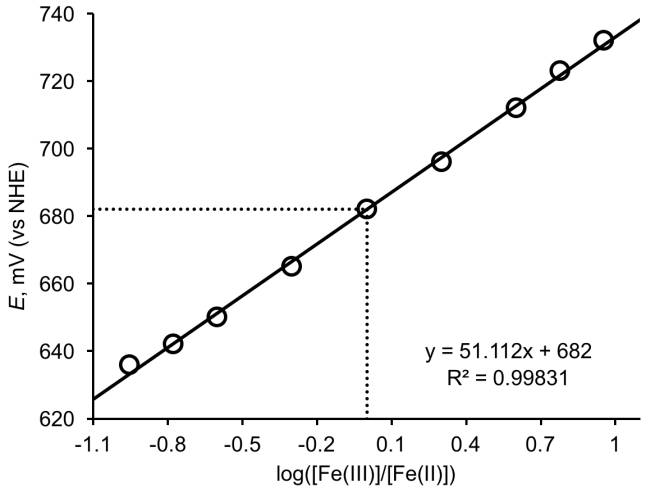

Figure 3.5. Dependence of a solution electrochemical potential on the ratio [Fe(III)]/[Fe(II)] in 50 mM sodium sulfate buffer containing 0.1 M $NaNO_3$ at pH 1.8.

to the theoretical value of 0.059 V. The potential at [Fe(III)]/[Fe(II)] = 1.0, E_s = 0.68 V (vs NHE), is the "standard" potential of this couple in 50 mM sulfate buffer (pH 1.8). This same procedure did not work in phosphate buffer due to a low solubility of Fe(III) complexes. Since Cu(I) is unstable in solution and is quickly oxidized by O_2, we did not use this procedure to evaluate the Cu(II)/Cu(I) couple.

Complex **SiVW11$_{red}$** has a characteristic absorbance in the range 450 – 650 nm, while **SiVW11$_{ox}$** only strongly absorbs at wavelengths < 450 nm (Figure 3.6). The reduction potential of the **SiVW11$_{ox}$**/**SiVW11$_{red}$** couple is 0.64 V (Figure 3.1) and is likely to be weakly dependent on the nature of the buffer. Therefore, the equilibrium in eq 3.2 can be used to determine spectrophotometrically the potential of Fe(III)/Fe(II) in sulfate and phosphate buffers. We mixed **SiVW11$_{ox}$** with Fe(II) at different ratios and recorded the UV-vis spectra (Figure 3.6).

$$\mathbf{SiVW11_{ox}} + \text{Fe(II)} \rightleftarrows \mathbf{SiVW11_{red}} + \text{Fe(III)} \qquad (3.2)$$

The extinction coefficients at 580 nm are 4.5×10^2 and 15 $M^{-1}cm^{-1}$ for $\mathbf{SiVW11_{red}}$ and $\mathbf{SiVW11_{ox}}$, respectively. Using COPASi software, we fitted the data from Figure 3.6 and obtained in phosphate buffer $\log K_{2(p)} = 1.2 \pm 0.2$ and in sulfate buffer $\log K_{2(s)} = -0.72 \pm 0.05$. From these values, the apparent reduction potentials E_{app} for the [Fe(III)]/[Fe(II)] couple are 0.57 and 0.68 V in phosphate and sulfate buffers, respectively. The latter value is the same as that determined using the redox electrode. The reaction rate constant $k_2 = (1.5 \pm 0.3) \times 10^4$ $M^{-1}s^{-1}$ was determined by stopped-flow techniques in phosphate buffer by mixing an excess of $\mathbf{SiVW11_{ox}}$ and Fe(II) and following the change of absorbance at 580 nm. These data were fitted using COPASi software to determine k_2. Since $K_{2(p)} > 10$, the equilibrium is shifted to the right, and it was impossible to quantify k_{-2}.

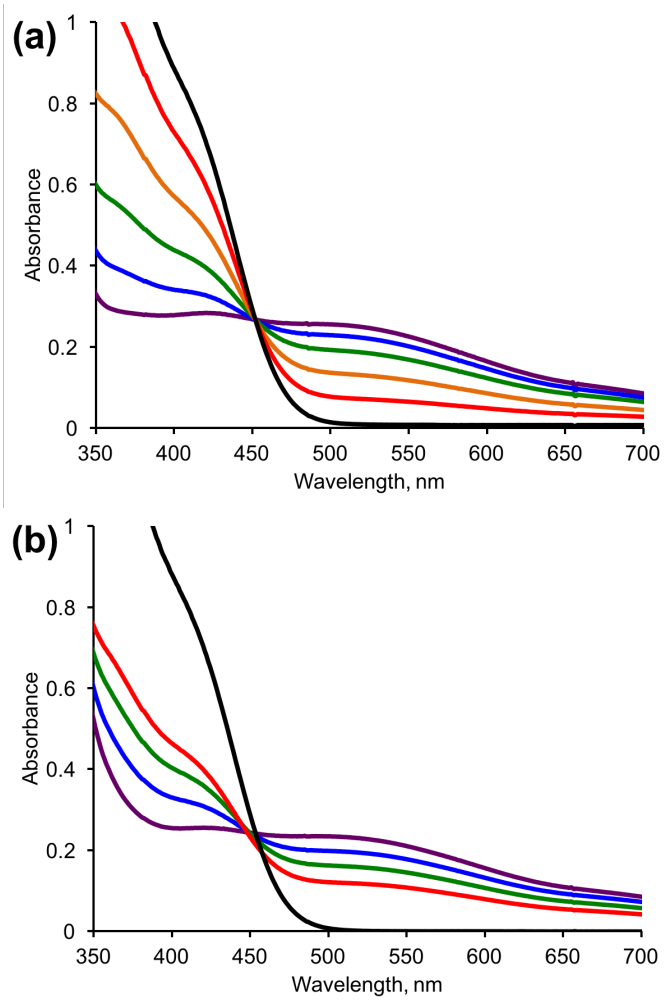

Figure 3.6. UV-Vis spectra of the mixture of **SiVW11$_{ox}$** and different concentrations of Fe(II) in (a) 50 mM phosphate and (b) 50 mM sulfate buffers at pH 1.8: [**SiVW11$_{ox}$**]$_0$ = 0.5 mM; (a) [Fe(II)] = 0 (black), 0.1 (red), 0.2 (orange), 0.3 (green), 0.4 (blue) and 0.5 mM (purple); (b) [Fe(II)] = 0 (black), 1 (red), 2 (green), 4 (blue) and 9 mM (purple).

In Chapter 2, the equilibrium constant for the reaction of **PW12$_{red}$** with Cu(II) was determined to be 4.4×10^{-4}, (50 mM sodium sulfate buffer, 100 mM $NaClO_4$, pH 2.0, 25 °C) which corresponds to E_{app} = 0.056 V for the Cu(II)/Cu(I) couple under these conditions.[39] The equilibrium constant for the reaction $Cu^{2+} + SO_4^{2-} \rightleftarrows CuSO_4$ at zero ionic strength is $K = 2.24 \times 10^2$.[48] If Cu^+ does not strongly bind sulfate anions, E_{app} for the Cu(II)/Cu(I) couple at hypothetically zero ionic strength in 50 mM sulfate buffer at pH 1.8 would be $E_{app} \approx 0.11$ V. The equilibrium constants for the reactions of Cu^+ and Cu^{2+} with $H_2PO_4^-$ are K = 0.090 and 0.072, respectively.[49] In 50 mM phosphate buffer at pH 1.8, the concentration of $H_2PO_4^-$ is 15 mM, the dominant species are Cu^{2+} and Cu^+, and therefore E_{app} is probably in the range 0.12 - 0.16 V. The reduction potentials used in fitting of kinetic data are summarized in Table 3.1.

Table 3.1. Range of reduction potentials used for fitting and values obtained from fitting (in parentheses) in phosphate and sulfate buffers.

	potentials, V	
species	phosphate buffer	sulfate buffer
PW12$_{ox}$/PW12$_{red}$	0.255	0.255
SiVW11$_{ox}$/SiVW11$_{red}$	0.64	0.64
Cu(II)/Cu(I)	0.12 - 0.16 (0.157)	0.05 - 0.11 (0.08)
Fe(III)/Fe(II)	0.57 - 0.63 (0.58)	0.64 - 0.70 (0.65)

3.3.5 Rate Constants of Fe(III) Reaction with $PW12_{red}$

The thermodynamically unfavorable reaction in eq 3.3 is the key process in the mechanism of Cu catalysis of Fe(II) oxidation by O_2[47]:

$$Cu(II) + Fe(II) \rightleftarrows Cu(I) + Fe(III) \quad (3.3)$$

$$Cu(II) + \mathbf{PW12_{red}} \rightleftarrows Cu(I) + \mathbf{PW12_{ox}} \quad (3.4)$$

$$\mathbf{PW12_{red}} + Fe(III) \rightarrow \mathbf{PW12_{ox}} + Fe(II) \quad (3.5)$$

The reaction in eq 3.5 is written for $\mathbf{PW12_{red}}$ as irreversible because the equilibrium is significantly shifted to the right. For efficient catalysis, the reactions of Cu(I) with O_2 and of Fe(III) with POM_{red} (eq 3.5) must be very fast. The high reactivity of Cu(I) toward O_2 is well-known and has been described in numerous publications.[50-52] The rate constant for the reaction of $\mathbf{PW12_{red}}$ and Fe(III) in 0.5 M $HClO_4$ was reported to be $k_5 = 6 \times 10^6$ $M^{-1}s^{-1}$.[53] Under our conditions, the kinetics of the reaction between $\mathbf{PW12_{red}}$ and Fe(III) in phosphate buffer is shown in Figure 3.7 (a). The fitting of experimental data gave $k_5 = (1.7 \pm 0.3) \times 10^4$ $M^{-1}s^{-1}$ and $k_{-5} < 1 \times 10^2$ $M^{-1}s^{-1}$. In sulfate buffer, the reaction is too fast and only the end of the reaction is observed and gives $k_5 \geq 1 \times 10^7$ $M^{-1}s^{-1}$ (Figure 3.7 (b)).

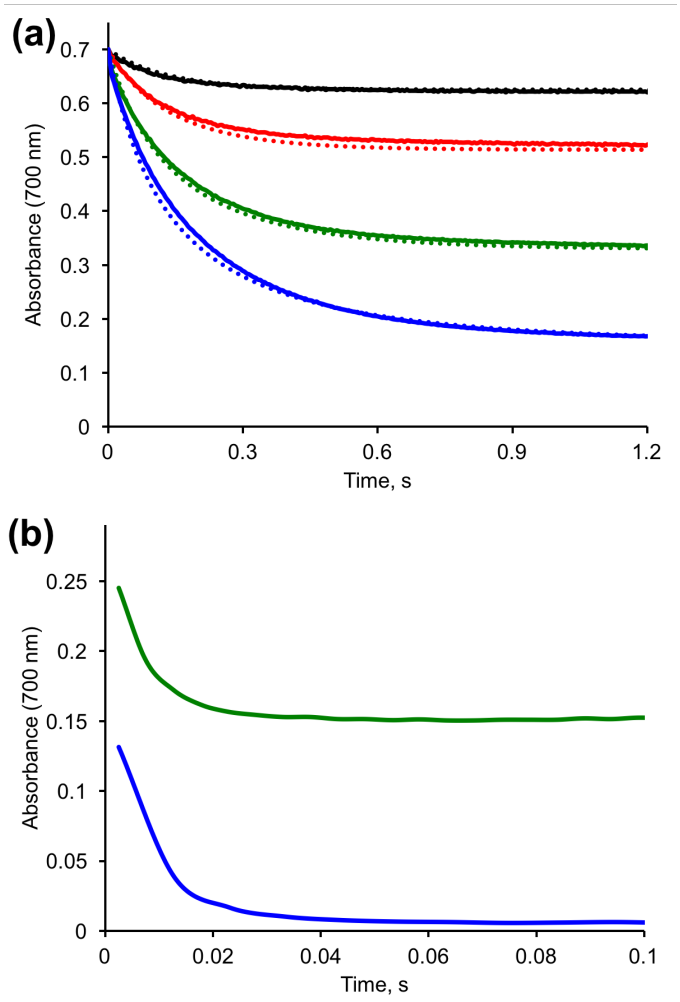

Figure 3.7. Kinetics of $\mathbf{PW12_{red}}$ oxidation by Fe(III) in (a) phosphate and (b) sulfate buffers. Conditions: $[\mathbf{PW12_{red}}]_0 \approx 0.44$ mM, [Fe(III)] = 50 (black), 125 (red), 250 (green), 375 (blue) μM, pH 1.8, 25 °C under Ar. Solid and dotted lines indicate the experimental and theoretical data, respectively.

3.3.6 Rate Constants of Fe(II) Reaction with H_2O_2

We thought that from the kinetics of this reaction we would be able to find the range of values for the reaction rate constants k_8. This reaction rate constant has been determined from the kinetics of **SiVW11$_{red}$** oxidation by H_2O_2 catalyzed by Fe(II). We have found that **SiVW11$_{red}$** oxidation by H_2O_2 is efficiently catalyzed by Fe(II), but that the addition of Cu(II) only slightly increases the reaction rate. Since the **SiVW11$_{red}$** oxidation by O_2 is very slow, only four reactions, eqs 3.2, 3.8, 3.9 and 3.13 (these reactions are given on the basis of the overall reaction mechanism shown below in section 3.4.7), were used to fit the experimental data.

$$\mathbf{SiVW11_{ox}} + \text{Fe(II)} \rightleftarrows \mathbf{SiVW11_{red}} + \text{Fe(III)} \qquad (3.2)$$

$$\text{Fe(II)} + H_2O_2 \rightarrow \text{Fe(III)} + HO^{\bullet} + HO^{-} \qquad (3.8)$$

$$POM_{red} + HO^{\bullet} \rightarrow POM_{ox} + HO^{-} \qquad (3.9)$$

$$\text{Fe(II)} + HO^{\bullet} \rightarrow \text{Fe(III)} + HO^{-} \qquad (3.13)$$

The equilibrium constants K_2 were varied ± 0.1 units from the values obtained from the thermodynamic analysis, k_{13} was taken to be 5×10^9 $M^{-1}s^{-1}$. The values of K_2 and k_8 were the variable parameters. The results of fitting are given in Figure 3.8. The equilibrium constant K_2 within experimental error is the same as estimated from the reaction thermodynamics. In the fitting of kinetics curves (Figure 3.8), k_2, was varied but over a narrow range of values, $(1.0 – 1.5) \times 10^4$ $M^{-1}s^{-1}$ in phosphate and 100 − 400 $M^{-1}s^{-1}$ in sulfate buffers.

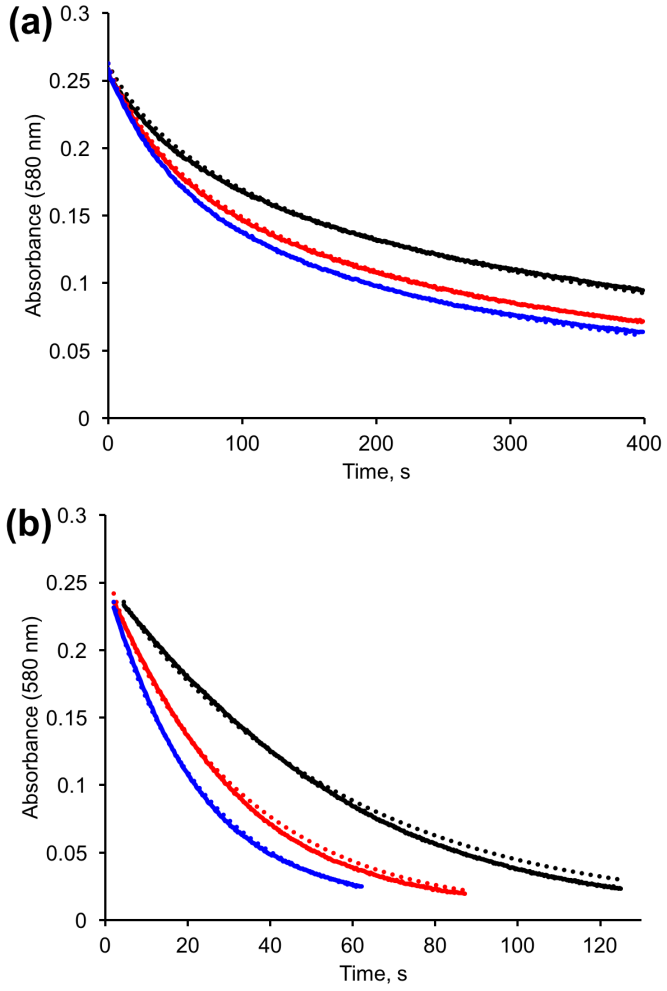

Figure 3.8. Absorbance changes during oxidation of 0.5 mM **SiVW11$_{red}$** by 0.5 mM H_2O_2 in 50 mM phosphate (a) and sulfate (b) buffers at pH = 1.8: [Cu(II)] = 10 μM, [Fe(II)] = 0.1 (black), 0.175 (red), and 0.25 (blue) mM. Solid and dotted lines are experimental data and calculated fits, respectively. The parameters: (a) k_8 = 106 $M^{-1}s^{-1}$, $k_4 = 1.2 \times 10^3$ $M^{-1}s^{-1}$, K_2 = 0.1; (b) k_8 = 350 $M^{-1}s^{-1}$, k_4 = 140 $M^{-1}s^{-1}$, K_2 = 17.

3.3.7 Reaction Mechanism and Kinetic Model

We comprehensively discussed the mechanism of the reaction between **SiW12$_{red}$** and **PW12$_{red}$** with O_2, catalyzed by Cu ions in our previous publication.[39] In the presence of both Fe and Cu, at least two additional reactions (eqs 3.3 and 3.5) should be considered. Since Fe(II) efficiently catalyzes POM_{red} oxidation by H_2O_2, the reactions in eqs 3.8 and 3.9 were added. The rate constant for the reaction of Cu(I) with H_2O_2 is quite high, ~ 4×10^3 $M^{-1}s^{-1}$.[54] Hypothetically, it can compete with the reaction in eq 3.8 ($k_8 \approx 65$ $M^{-1}s^{-1}$ for Fe^{2+}_{aq}).[55] However, it can be ignored because Cu(I) is quickly consumed by O_2. Thus, the oversimplified reaction mechanism of catalysis by copper and iron of the reaction between POM_{red} and O_2 can be written by eqs 3.3 – 3.10.

$$Cu(II) + Fe(II) \rightleftarrows Cu(I) + Fe(III) \quad (3.3)$$

$$POM_{red} + Cu(II) \rightleftarrows POM_{ox} + Cu(I) \quad (3.4)$$

$$POM_{red} + Fe(III) \rightarrow POM_{ox} + Fe(II) \quad (3.5)$$

$$Cu(I) + O_2 + H^+ \rightleftarrows Cu(II) + HO_2^{\bullet} \quad (3.6)$$

$$POM_{red} + HO_2^{\bullet} + H^+ \rightarrow POM_{ox} + H_2O_2 \quad (3.7)$$

$$Fe(II) + H_2O_2 \rightarrow Fe(III) + HO^{\bullet} + HO^- \quad (3.8)$$

$$POM_{red} + HO^{\bullet} \rightarrow POM_{ox} + HO^- \quad (3.9)$$

$$Cu(I) + HO_2^{\bullet} + H^+ \rightarrow Cu(II) + H_2O_2 \quad (3.10)$$

The reaction in eq 3.5 was studied independently. We used the rate constants $k_{5(p)} = 1.7 \times 10^4$ for phosphate, and $k_{5(s)}$ was varied in the range $(1 – 9) \times 10^7$ $M^{-1}s^{-1}$ for sulfate buffers, respectively. This rate constant, k_5, in 0.5 M $HClO_4$ and $\mu = 1.0$ was reported to be 6×10^6 $M^{-1}s^{-1}$, and $k_4 = 3.5 \times 10^2$ $M^{-1}s^{-1}$.[53] Since the ionic strength and buffers were different in our study, we assumed that $k_4 < 3.5 \times 10^3$ $M^{-1}s^{-1}$. The analysis of our kinetic

model shows that the reaction rate is independent of the value of the reverse reaction of eq 3.3 in the range of 1×10^6 to 1×10^{10} $M^{-1}s^{-1}$. For this reason, we also assumed that the reverse reaction in eq 3.3 and the reaction in eq 3.9 are close to diffusion controlled ~ 5×10^9 $M^{-1}s^{-1}$. The rate constant $k_7 = 5 \times 10^7$ $M^{-1}s^{-1}$ was estimated in our previous study,[33] and the value $k_{10} = 2 \times 10^9$ $M^{-1}s^{-1}$ was taken from the literature.[56] The equilibrium constants K_3 and K_4 were varied ± 0.2 log unit from the values obtained from the thermodynamic analysis.

However, despite all our efforts, we failed to achieve a good fitting of data collected under O_2 and air. A thorough analysis showed that the rate of the reaction in eq 3.6 is weakly dependent on $[O_2]$ but quadratically increases with [Cu(I)]. Therefore, we assumed that reaction 3.6 proceeds in two steps (eqs 3.11 and 3.12).[52,57]

$$Cu(I) + O_2 \rightleftarrows CuO_2 \qquad (3.11)$$

$$CuO_2 + Cu(I) + 2\,H^+ \rightarrow 2\,Cu(II) + H_2O_2 \qquad (3.12)$$

For simplicity, we assumed that reaction 3.12 is fast, $k_{12} = 1 \times 10^9$ $M^{-1}s^{-1}$. The results of fitting are summarized in Table 3.2, and the proposed model is in a good agreement with experimental data (Figure 3.9).

Table 3.2. Kinetic model and rate constants for catalytic **PW12$_{red}$** oxidation obtained from fitting.

eq	reaction	k [a]	
		phosphate buffer [b]	sulfate buffer [b]
(3.1)	$POM_{red} + O_2 \rightarrow POM_{ox} + O_2^{\bullet-}$	$k_{1(p)} = 1.4$	$k_{1(s)} = 1.4$
(3.3)	$Cu(II) + Fe(II) \rightleftarrows Cu(I) + Fe(III)$	$k_{3(p)} = 3.6 \times 10^2$ $k_{-3(p)} = 5 \times 10^9$ $\log K_{3(p)} = -7.1$	$k_{3(s)} = 1.5$ $k_{-3(s)} = 5 \times 10^9$ $\log K_{3(s)} = -9.7$
(3.4)	$POM_{red} + Cu(II) \rightleftarrows POM_{ox} + Cu(I)$	$k_{4(p)} = 1.3 \times 10^3$ $k_{-4(p)} = 5.6 \times 10^4$ $\log K_{4(p)} = -1.6$	$k_{4(s)} = 7.5 \times 10^2$ $k_{-4(s)} = 7.5 \times 10^5$ $\log K_{4(s)} = -3.0$
(3.5)	$POM_{red} + Fe(III) \rightarrow POM_{ox} + Fe(II)$	$k_{5(p)} = 1.7 \times 10^4$	$k_{5(s)} = 6.0 \times 10^7$
(3.7)	$POM_{red} + HO_2^{\bullet} + H^+ \rightarrow POM_{ox} + H_2O_2$ [c]	$k_{7(p)} = 5 \times 10^7$	$k_{7(s)} = 5 \times 10^7$
(3.8)	$Fe(II) + H_2O_2 \rightarrow Fe(III) + HO^{\bullet} + HO^-$	$k_{8(p)} = 1.1 \times 10^2$	$k_{8(s)} = 3.5 \times 10^2$
(3.9)	$POM_{red} + HO^{\bullet} \rightarrow POM_{ox} + HO^-$	$k_{9(p)} = 5 \times 10^9$	$k_{9(s)} = 5 \times 10^9$
(3.10)	$Cu(I) + HO_2^{\bullet} + H^+ \rightarrow Cu(II) + H_2O_2$ [c]	$k_{10(p)} = 2 \times 10^9$	$k_{10(s)} = 2 \times 10^9$
(3.11)	$Cu(I) + O_2 \rightleftarrows CuO_2$	$k_{11(p)} = 1 \times 10^7$ $k_{-11(p)} = 2.5 \times 10^4$	$k_{11(s)} = 4.6 \times 10^6$ $k_{-11(s)} = 80$
(3.12)	$CuO_2 + Cu(I) + 2H^+ \rightarrow 2Cu(II) + H_2O_2$	$k_{12(p)} = 1 \times 10^9$	$k_{12(s)} = 1 \times 10^9$

[a] Rate constants, $M^{-1}s^{-1}$; [b] subscripts (p) and (s) refer to 50 mM phosphate and 50 mM sulfate buffers at pH 1.8, respectively.; [c] $O_2^{\bullet-}$ is the primary product of the reaction, which quickly protonates to $HO_2^{\bullet}$ at low pH.

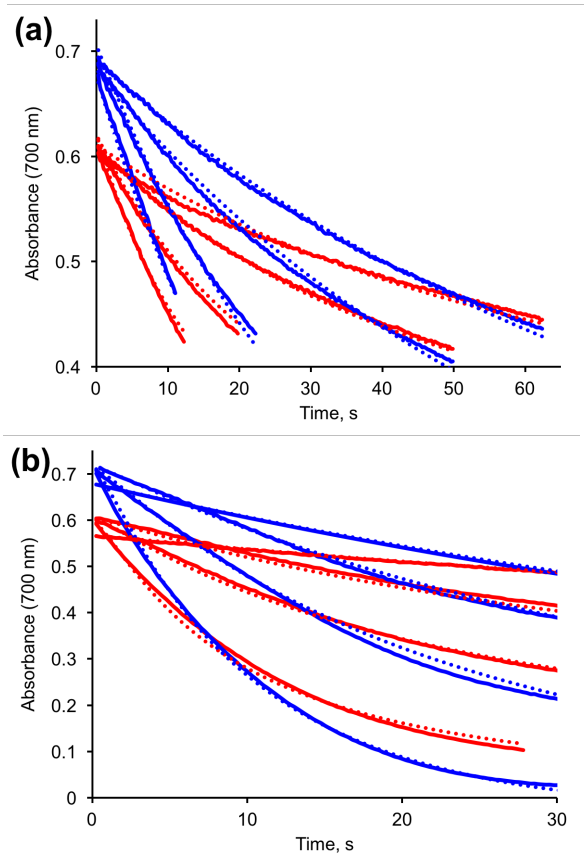

Figure 3.9. Kinetics of $\mathbf{PW12_{red}}$ oxidation by O_2 in (a) 50 mM phosphate buffer and (b) 50 mM sulfate buffer. Conditions: pH 1.8, 25 °C. Red and blue lines represent the kinetics performed under air and saturated O_2. Solid and dotted lines indicate the experimental and theoretical curves, respectively.

3.3.8 Catalytic Oxidation of $\mathbf{SiVW11_{red}}$ by $\mathbf{O_2}$

The standard reduction potential of $\mathbf{SiVW11_{ox}/SiVW11_{red}}$, 0.64 V, is higher than that of the $\mathbf{PW12_{ox}/PW12_{red}}$ couple (0.255 V). Therefore, $\mathbf{SiVW11_{ox}}$ is potentially able to oxidize organic compounds. However, the standard reduction potential of the O_2/H_2O_2

couple is close to the potential of the **SiVW11$_{ox}$**/**SiVW11$_{red}$** couple, making the regeneration of **SiVW11$_{ox}$** by noncatalyzed oxidation with O_2 prohibitively slow. For this reason, we looked at the activity of a Cu-Fe mixture as a catalyst for **SiVW11$_{red}$** oxidation by O_2. The representative data are given in Table 3.3. After all reagents were mixed, the readings of a redox electrode were unstable and typically lower than 0.55 V. Therefore, we placed the reactor in an oil bath thermostated at 100 °C for 5 – 7 min. The potentials were measured after cooling in water to room temperature. These potentials after 5 – 7 min were considered as the initial values, $E_{t=6min}$. In the absence of both Cu and Fe, the potential of **SiVW11$_{red}$** solution after 7 h at 100 °C did not exceed 0.56 V. The [**SiVW11$_{ox}$**]/[**SiVW11$_{red}$**] ratio was determined using Figure 3.1 as a calibration curve. Table 3.3 shows that addition of Fe(II) as a cocatalyst to Cu(II) increases the rate of

Table 3.3. O_2-based oxidation of **SiVW11$_{red}$** [a] catalyzed by Cu + Fe.[b]

[**SiVW11$_{red}$**], mM	[Fe(II)], mM	[Cu(II)], mM	$E_{t=7h}$, V	[**SiVW11$_{ox}$**]$_{t=7h}$, mM [c]	[Fe(III)]$_{t=7h}$, mM	ratio [d]	$E_{t=72h}$, V
10	5	0	0.60	1.5	0.12	0.11	0.64 (0.37) [d]
10	0	2.5	0.63	3.8	–	0.38	0.65 (0.59) [d]
10	0.5	2.5	0.64	4.8	0.066	0.46	0.67 (0.75) [d]
10	1.5	2.5	0.66	6.9	0.41	0.63	0.70 (0.89) [d]
10	2.5	2.5	0.67	7.7	0.92	0.69	0.70 (0.88) [d]

[a] $K_6SiVW_{11}O_{40}$; [b] Conditions: [H_2SO_4] = 50 mM (pH ~ 1.3), 1 atm air at room temperature, 100 °C.; [c] Determined after cooling to 25 °C on the basis of Figure 3.1; [d] The value of ([**SiVW11$_{ox}$**] + [Fe(III)]) / ([**SiVW11$_{red}$**]$_0$ + [Fe(II)]$_0$) determined after cooling to 25 °C.

SiVW11$_{red}$ oxidation by dioxygen. The experiment in the presence of Fe with higher concentration cannot be considered as Cu free, since the solutions are always contaminated by Cu.[39]

The reaction kinetics were also studied at 60 °C at lower concentrations of **SiVW11$_{red}$**, Cu(II), and Fe(II) by following the change in absorbance at 580 nm. The decrease in the 580 nm absorbance was assigned to the consumption of [**SiVW11$_{red}$**]. The amount of Fe(III) formed in the reaction was calculated using equilibrium constants for the reaction in eq 3.2. The equilibrium constant K_2 at 60 °C was determined experimentally

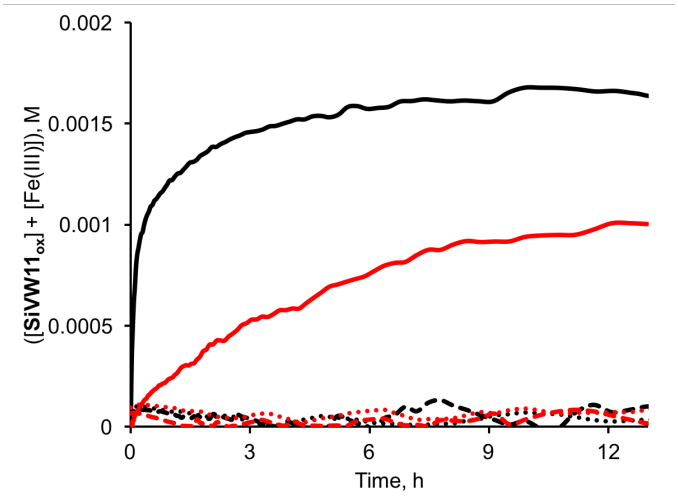

Figure 3.10. Kinetics of {[**SiVW11$_{ox}$**] + [Fe(III)]} accumulation in oxidation of {[**SiVW11$_{red}$**] + [Fe(II)]} by dioxygen in phosphate (black) and sulfate (red) buffers: [**SiVW11$_{red}$**] = 2.5 mM, 60 °C; solid lines [Fe(II)] = 2.0 mM and [Cu(II)] = 0.5 mM; dashed lines [Fe(II)] = 1.0 mM and [Cu(II)] = 0 mM; dotted lines [Fe(II)] = 0 mM and [Cu(II)] = 0.5 mM. The yields of **SiVW11$_{ox}$** and Fe(III) after 14 h are 0.67 and 1.28 mM in phosphate buffer, respectively, and those in sulfate buffer are 1.0 and 0.05 mM, respectively.

using the same protocol as described above: K_2 = 6 and 0.1 in phosphate and sulfate buffers, respectively. The exemplary kinetics of {[**SiVW11$_{ox}$**] + [Fe(III)]} accumulation is given in Figure 3.10. The initial rates and conversion are strongly dependent on the nature of the buffer. The reaction proceeds more efficiently in phosphate than in sulfate buffer. Since the reduction potentials are not known at elevated temperature, we did not fit the experimental data.

3.3.9 General Discussion

The reduction of Cu(II) by **AlW12$_{red}$** and **SiW12$_{red}$** is a thermodynamically favorable process, and the catalysis by Cu ions of O_2-based oxidation of **AlW12$_{red}$** and **SiW12$_{red}$** is very efficient;[39] there is no noticeable effect of adding only Fe ions. The standard reduction potential of $E°$(**PW12$_{ox}$**/**PW12$_{red}$**) = 0.255 V is higher than that for the Cu(II)/Cu(I) couple, and oxidation of **PW12$_{red}$** by O_2 is faster in the presence of Fe(II). We simulated the kinetics of 500 μM **PW12$_{red}$** oxidation by 115 μM O_2 catalyzed by 10 μM Cu(II) with 0 and 100 μM Fe(II) in both phosphate and sulfate buffers. The simulated kinetic curves of **PW12$_{red}$** consumption and H_2O_2 accumulation are presented in Figure 3.11.

Catalysis by Fe(II) of **PW12$_{red}$** oxidation by O_2 results in a change in the reaction stoichiometry. Hydrogen peroxide is the product of the reaction in the absence of Fe(II). The consumption of **PW12$_{red}$** does not proceed to completion because O_2 is the limiting reagent. Since Fe(II) efficiently catalyzes the **PW12$_{red}$** oxidation by H_2O_2, the reaction

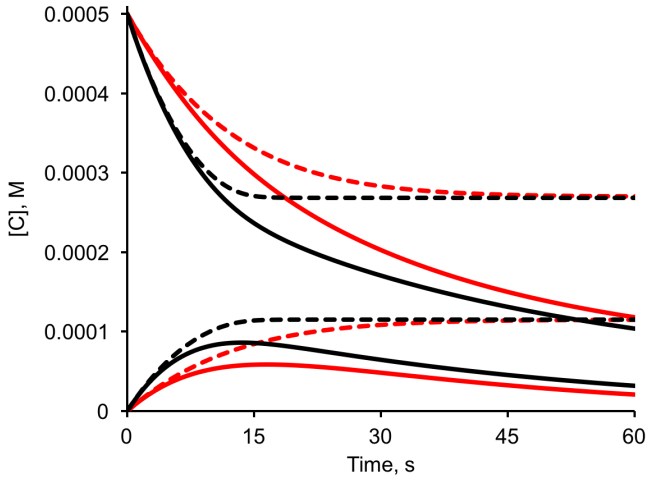

Figure 3.11. Simulated kinetics of $\mathbf{PW12_{red}}$ consumption and H_2O_2 accumulation in 50 mM phosphate (black lines) or sulfate (red lines) buffers: $[Cu(II)]_0$ = 10 μM, $[Fe(II)]_0$ = 0 (dashed lines) or 100 (solid lines) μM, $[O_2]$ = 0.12 mM, pH 1.8, 25 °C.

proceeds to a higher conversion in the presence of Fe(II). The contribution of this additional catalytic pathway starting from the reaction in eq 3.3 is small, and therefore the initial rates are independent of [Fe(II)]. In phosphate buffer, Cu(II) is a stronger oxidant in comparison to that in sulfate buffer by approximately 80 mV. Consequently, the reaction proceeds slightly faster in phosphate buffer. Thus, the main function of Fe(II) is the catalysis of $\mathbf{PW12_{red}}$ oxidation by H_2O_2.

The role of Fe(II) in catalysis of $\mathbf{SIVW11_{red}}$ oxidation is more complex, because the reaction in eq 3.2 is reversible. Assuming that the reaction of Cu(I) oxidation is fast, then the lowest thermodynamic barrier through the pathway starting from the reaction in eq 3.3 could not be lower than that of starting from the reaction in eq 3.4. However, the overall kinetics of $\mathbf{SiVW11_{red}}$ oxidation depends not only on thermodynamics but also on

rate constants, especially for the reactions in eqs 3.2 and 3.6. Using COPASi software, we optimized the conversion of **SiVW11$_{red}$** after 1 h in the oxidation of 1 mM **SiVW11$_{red}$** at constant concentration of O_2 (1.15 mM) by varying the concentrations of Cu(II), Fe(II), and their reduction potentials. The conversion increases with initial concentrations of Fe(II) and Cu(II) and with an increase in the Cu(II)/Cu(I) or a decrease in Fe(III)/Fe(II) reduction potentials. The theoretical kinetic curves of **SiVW11$_{ox}$** formation in the oxidation of 1 mM **SiVW11$_{red}$** at 0.1 mM Cu(II) and 0 or 0.2 mM Fe(II) and $E°$(Cu(II)/Cu(I)) = 0.2 V and $E°$(Fe(III)/Fe(II)) = 0.55 V, respectively, are given in Figure 3.12. The following rate constants were used for simulations: $k_1 = 0$ $M^{-1}s^{-1}$, $k_2 = 1 \times 10^4$ $M^{-1}s^{-1}$ (the experimental value of k_2 is 1.5×10^4 $M^{-1}s^{-1}$ in phosphate buffer as described in the thermodynamic analysis above), $k_{-3} = k_{-4} = 5 \times 10^9$ $M^{-1}s^{-1}$, $k_{11} = 1 \times 10^7$ $M^{-1}s^{-1}$, and

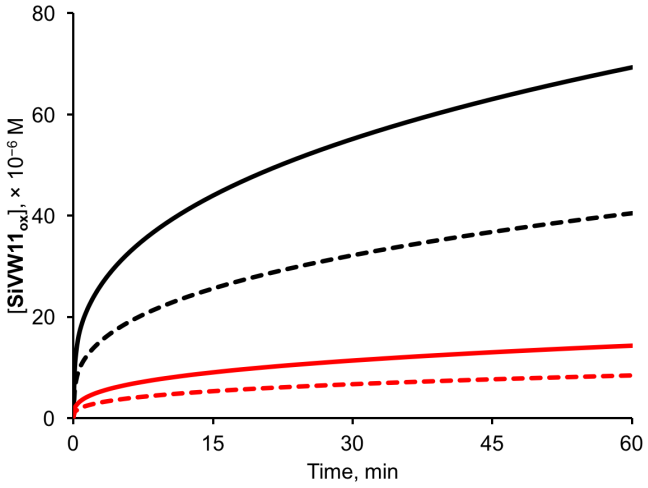

Figure 3.12. Theoretical kinetic curves of **SiVW11$_{ox}$** accumulation in the oxidation of 1.0 mM of **SiVW11$_{red}$** by 0.23 mM (dashed lines) or 1.15 mM (solid lines) O_2 in the presence of 0.1 mM Cu(II) and 0 (red curves) and 0.2 mM (black curves) Fe(II) at $E°$(Cu(II)/Cu(I)) = 0.2 V and $E°$(Fe(III)/Fe(II)) = 0.55 V.

$k_{-11} = 1 \times 10^3\ M^{-1}s^{-1}$. The reaction rate constants k_3, k_4, and k_{-2} were calculated from the difference in reduction potentials. Table 3.2 gives the rest of the rate constants.

Figure 3.12 clearly demonstrates a synergetic catalytic effect of Cu(II) and Fe(II): the reaction proceeds much more quickly in the presence of Fe(II) and does not take place in the absence of Cu(II), which is consistent with the data in Table 3.3. Importantly, the conversion is lower at lower $[O_2]$, indicating that the reaction in eq 3.11 also controls the conversion of **SiVW11$_{red}$**. The shape of the theoretical curves is similar to the experimental data obtained at 60 °C (Figure 3.10), confirming the reasonableness of the kinetic model.

3.4 Conclusions

We have studied the kinetics of POM_{red} oxidation by O_2 synergetically catalyzed by Cu and Fe together in phosphate and sulfate buffers and established the reaction mechanism, which quantitatively describes the experimental data. The main function of

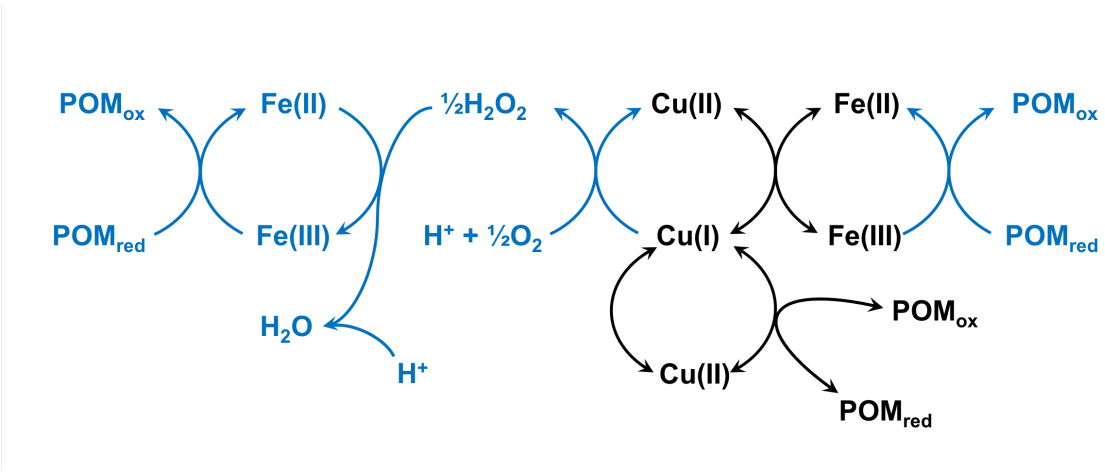

Scheme 3.1. Catalytic cycle of POM_{red} oxidation catalyzed by Cu(II) and Fe(II). The blue and black parts indicate the irreversible and reversible steps, respectively.

Fe(II) is as an efficient catalyst for POM_{red} oxidation by H_2O_2. The synergism of Cu(II) and Fe(II) is based on the reversible reaction of Cu(II) and Fe(II) to generate Cu(I) and Fe(III), followed by fast reactions of POM_{red} with Fe(III) and Cu(I) with O_2 (Scheme 3.1). Phosphate and sulfate buffers perturb the reduction potentials and speciation of copper and iron complexes, which result in different rate constants of the involved reactions.

3.5 References

(1) Baker, L. C. W.; Glick, D. C. *Chem. Rev.* **1998,** *98*, 3.

(2) Wang, H.; Hamanaka, S.; Nishimoto, Y.; Irle, S.; Yokoyama, T.; Yoshikawa, H.; Awaga, K. *J. Am. Chem. Soc.* **2012,** *134*, 4918.

(3) Weinstock, I. A.; Barbuzzi, E. M. G.; Wemple, M. W.; Cowan, J. J.; Reiner, R. S.; Sonnen, D. M.; Heintz, R. A.; Bond, J. S.; Hill, C. L. *Nature* **2001,** *414*, 191.

(4) Misono, M. *Stud. Surf. Sci. Catal.* **1993,** *75*, 1.

(5) Hill, C. L.; Prosser-McCartha, C. M. *Coord. Chem. Rev.* **1995,** *143*, 407.

(6) Okuhara, T.; Mizuno, N.; Misono, M. *Adv. Catal.* **1996,** *41*, 113.

(7) Kozhevnikov, I. V. *Chem. Rev.* **1998,** *98*, 171.

(8) Chambers, R. C.; Hill, C. L. *Inorg. Chem.* **1989,** *28*, 2509.

(9) Harrup, M. K.; Hill, C. L. *Inorg. Chem.* **1994,** *33*, 5448.

(10) Hill, C. L. *J. Mol. Catal. A: Chem.* **1996,** *114*, 1.

(11) Neumann, R.; Dahan, M. *Nature* **1997,** *388*, 353.

(12) Hill, C. L.; Weinstock, I. A. *Nature (London)* **1997,** *388*, 332.

(13) Hill, C. L. *J. Mol. Catal. A: Chem.* **2007 Special Issue,** *262*, 1.

(14) Snir, O.; Wang, Y.; Weinstock, I. A. *Isr. J. Chem.* **2011,** *51*, 247.

(15) Wang, S.-S.; Yang, G.-Y. *Chem. Rev.* **2015,** *115*, 4893.

(16) Mizuno, N.; Misono, M. *J. Mol. Catal.* **1994,** *86*, 319.

(17) Punniyamurthy, T.; Velusamy, S.; Iqbal, J. *Chem. Rev.* **2005,** *105*, 2329.

(18) Piera, J.; Bäckvall, J.-E. B. *Angew. Chem. Int. Ed.* **2008,** *47*, 3506.

(19) Gligorich, K. M.; Sigman, M. S. *Chem. Commun.* **2009**, 3854.

(20) Shi, Z.; Zhang, C.; Tang, C.; Jiao, N. *Chem. Soc. Rev.* **2012,** *41*, 3381.

(21) Liu, W.; Mu, W.; Liu, M.; Zhang, X.; Cai, H.; Deng, Y. *Nat. Commun.* **2014,** *5*, 3208.

(22) Liu, W.; Cui, Y.; Du, X.; Zhang, Z.; Chao, Z.; Deng, Y. *Energy Environ. Sci* **2016,** *9*, 467.

(23) Bonchio, M.; Carraro, M.; Sartorel, A.; Scorrano, G.; Kortz, U. *J. Mol. Catal. A: Chem.* **2006,** *251*, 93.

(24) Neumann, R.; Khenkin, A. M. *Chem. Commun.* **2006**, 2529.

(25) Neumann, R. *Inorg. Chem.* **2010,** *49*, 3594.

(26) Berardi, S.; Carraro, M.; Sartorel, A.; Modugno, G.; Bonchio, M. *Isr. J. Chem.* **2011,** *51*, 259.

(27) Hill, C. L. In *Comprehensive Coordination Chemistry-II: From Biology to Nanotechnology*; Wedd, A. G., Ed.; Elsevier: Oxford, U.K., 2004; Vol. 4, 679.

(28) Duncan, D. C.; Hill, C. L. *J. Am. Chem. Soc.* **1997,** *119*, 243.

(29) Khenkin, A. M.; Neumann, R. *Angew. Chem. Int. Ed.* **2000,** *39*, 4088.

(30) Khenkin, A. M.; Weiner, L.; Wang, Y.; Neumann, R. *J. Am. Chem. Soc.* **2001,** *123*, 8531.

(31) Hill, C. L.; Gall, R. D. *J. Mol. Catal. A: Chem.* **1996,** *114*, 103.

(32) Neumann, R. *Mod. Oxidation Methods* **2005**, 223.

(33) Geletii, Y. V.; Hill, C. L.; Atalla, R. H.; Weinstock, I. A. *J. Am. Chem. Soc.* **2006,** *128*, 17033.

(34) Rorabacher, D. B. *Chem. Rev.* **2004,** *104*, 651.

(35) Wang, X.; Stanbury, D. M. *J. Phys. Chem. A* **2004,** *108*, 7637.

(36) Saha, B.; Hung, M.; Stanbury, D. M. *Inorg. Chem.* **2002,** *41*, 5538.

(37) Bridgart, G. J.; Fuller, M. W.; Wilson, I. R. *J. Chem. Soc., Dalton Trans.* **1973**, 1274.

(38) Bagiyan, G. A.; Koroleva, I. K.; Soroka, N. V.; Ufimtsev, A. V. *Russ. Chem. Bull.* **2003,** *52*, 1135.

(39) Kim, M.; Weinstock, I. A.; Geletii, Y. V.; Hill, C. L. *ACS Catal.* **2015,** *5*, 7048.

(40) Cowan, J. J.; Bailey, A. J.; Heintz, R. A.; Do, B. T.; Hardcastle, K. I.; Hill, C. L.; Weinstock, I. A. *Inorg. Chem.* **2001,** *40*, 6666.

(41) Yang, B.; Pignatello, J. J.; Qu, D.; Xing, B. *J. Phys. Chem. A* **2015,** *119*, 1055.

(42) Ermakov, A. N.; Kozlov, Y. N.; Purmal', A. P. *Kinet. Catal.* **1999,** *40*, 598.

(43) Geletii, Y. V.; Hill, C. L.; Bailey, A. J.; Hardcastle, K. I.; Atalla, R. H.; Weinstock, I. A. *Inorg. Chem.* **2005,** *44*, 8955.

(44) Geletii, Y. V.; Weinstock, I. A. *J. Mol. Catal. A: Chem.* **2006,** *251*, 255.

(45) Domaille, P. J. *J. Am. Chem. Soc.* **1984,** *106*, 7677.

(46) Müller, A.; Dloczik, L.; Diemann, E.; Pope, M. T. *Inorg. Chim. Acta* **1997,** *257*, 231.

(47) Cher, M.; Davidson, N. *J. Am. Chem. Soc.* **1955,** *77*, 793.

(48) Powell, K. J.; Brown, P. L.; Byrne, R. H.; Gajda, T.; Hefter, G.; Sjöberg, S.; Wanner, H. *Pure Appl. Chem.* **2007,** *79*, 895.

(49) Aksu, S. *J. Electrochem. Soc.* **2009,** *156*, C387.

(50) Gray, R. D. *J. Am. Chem. Soc* **1969,** *91*, 56.

(51) Mi, L.; Zuberbühler, A. D. *Helv. Chim. Acta* **1991,** *74*, 1679.

(52) Elwell, C. E.; Gagnon, N. L.; Neisen, B. D.; Dhar, D.; Spaeth, A. D.; Yee, G. M.; Tolman, W. B. *Chem. Rev.* **2017,** *117*, 2059.

(53) Kozhevnikov, L. V.; Kholdeeva, O. A. *Izv. Akad. Nauk SSSR, Ser. Khim.* **1987**, 528.

(54) Masarwa, M.; Cohen, H.; Meyerstein, D.; Hickman, D. L.; Bakac, A.; Espenson, J. H. *J. Am. Chem. Soc* **1988,** *110*, 4293.

(55) Conocchioli, T. J.; Hamilton, E. J.; Sutin, N. *J. Am. Chem. Soc* **1965,** *87*, 926.

(56) Dribinskii, V. L.; Kozlov, Y. N. *Russ. J. Phys. Chem.* **2001,** *75*, 551.

(57) Gorbunova, N. V.; Purmal, A. P.; Skurlatov, Y. I.; Travin, A. O. *Int. J. Chem. Kinet.* **1977,** *9*, 983.

(58) Weinstock, I. A.; Schreiber, R. E.; Neumann, R. *Chem. Rev*. **2018**, *118*, 2680.

Chapter 4

Oxidation of Reduced Keggin Heteropolytungstates by Dioxygen Catalyzed by Nitrous Acid

With Yurii V. Geletii and Craig L. Hill

4.1 Introduction

As mentioned in **Chapter 1**, O_2-based polyoxometalate (POM) catalysis is based on oxidation of substrates by POMs in high oxidation states (POM_{ox}) followed by reoxidation of reduced POMs (POM_{red}) by O_2, which is commonly too slow to achieve an efficient catalysis.[1-9] The well characterized one-electron-reduced α-Keggin anions, α-$X^{n+}W_{12}O_{40}^{(9-n)-}$ (X = Al^{3+}, Si^{4+}, and P^{5+}), which are quite stable under the experimental conditions,[10-12] were used to study the catalytic reoxidation process. **Chapter 2** demonstrated that submicromolar concentrations of Cu efficiently catalyze POM_{red} reoxidation by O_2.[13] Dioxygen directly oxidizes POM_{red} through a very slow outer-sphere electron transfer (ET) step.[14,15,11,16] In the presence of Cu-complexes, dioxygen is involved in the overall catalytic process through a fast reaction with Cu(I), formed by Cu(II) reduction with POM_{red}. Such a switch in reaction mechanism of O_2 reduction results in a significant increase in rates. However, the reduction of Cu(II) by POM_{red} is generally thermodynamically unfavorable and might be a rate-limiting step. A combination of Cu and Fe compounds additionally increases the catalytic activity, but does not change the thermodynamics of Cu(II) reduction by POM_{red}.[17] Therefore, we thought that the replacement of Cu/Fe with a catalyst with a higher oxidation potential and faster regeneration by O_2 would create a significantly more active catalytic system. A thorough analysis of fast O_2 reactions with different compounds revealed that nitrogen oxide, NO, quickly reacts with O_2 and produces NO_2 radical with a relatively high reduction potential (NO_2/NO_2^- couple is 1.04 V vs NHE).[18,19] Under acidic conditions, NO_2^- is protonated (pK_a = 3.3) and HNO_2 is known to react with several reductants regenerating NO, such as oxidation of hexachloroiridate(IV)[18] and trivalent plutonium.[20]

This Chapter discloses that vanadium(IV)-substituted Keggin anions with relatively positive reduction potentials, α-$X^{n+}V^{IV}W_{11}O_{40}^{(10-n)-}$ (X = Al^{3+}, and Si^{4+}, for **AlVW11$_{red}$**, and **SiVW11$_{red}$**, respectively), are efficiently oxidized by O_2 in acidic aqueous solution in the presence of nitrous acid. The kinetic curves of POM_{red} consumption have a characteristic shape: the reactions quickly proceed in the beginning and then much more slowly. The reaction rate laws are different in each phase. Interestingly, the oxidation rates of **AlVW11$_{red}$**, and **SiVW11$_{red}$**, are very similar despite a large difference in redox potentials of these POMs. The proposed reaction mechanism quantitatively describes the experimental data.

4.2 Experimental

4.2.1 Materials

One-electron-reduced α-Keggin POMs, α-$K_6SiV^{IV}W_{11}O_{40}$ and α-$K_7AlV^{IV}W_{11}O_{40}$ were prepared as described in published methods.[21,22] $NaNO_2$ (≥99 %), $NaNO_3$ (98+ %), NaOH (99.99 %), and H_2SO_4 (ACS Grade) were purchased from EMD Millipore, Alfa Aesar, Sigma-Aldrich, and Macron Fine Chemicals, respectively. We used 50 mM sulfuric acid (pH 1.25) in water as the solvent in this study. All chemicals were commercial quality unless specified otherwise and all solutions were prepared from a Barnstead Nanopure® quality water for the highest purity.

4.2.2 Electrochemistry

All electrochemical experiments were conducted by using a BAS CV-50W electrochemical analyzer. Cyclic voltammograms (CVs) were obtained at room

temperature (24 ± 2 °C) as previously described[14,23,13,17] using glassy carbon, an Ag/AgCl (1 M KCl) BAS (+ 235 mV difference vs NHE), and Pt wire as the working, reference and counter electrodes, respectively.

4.2.3 Kinetic Measurements

General experimental procedure was described in the previous Chapters and our publications.[13,17] The UV-vis spectra of fully oxidized and $1e^-$-reduced α-Keggin anions (Figure 4.1) were collected on an Agilent 8453 diode-array spectrophotometer equipped with an Agilent 8909A Peltier temperature-control unit. The extinction coefficients of $\mathbf{AlVW11_{ox}}$ and $\mathbf{AlVW11_{red}}$ are 12 and 4.2×10^2 $M^{-1}cm^{-1}$, respectively ($\varepsilon_{560}(\mathbf{SiVW11_{ox}})$ = 10 $M^{-1}cm^{-1}$, $\varepsilon_{560}(\mathbf{SiVW11_{red}}) = 5.0 \times 10^2$ $M^{-1}cm^{-1}$).

All stopped-flow studies and the reaction kinetics were monitored by the absorbance changes with time at the desired wavelength using a SF-61 stopped-flow instrument (Hi-Tech Scientific, UK). The kinetic curve fitting, simulation of reaction kinetics, and optimization of conditions were performed using COPASI 4.13 (Build 87) software (www.copasi.org). The solubility of O_2 at 25 °C and 1 atm was taken to be 1.15 mM.

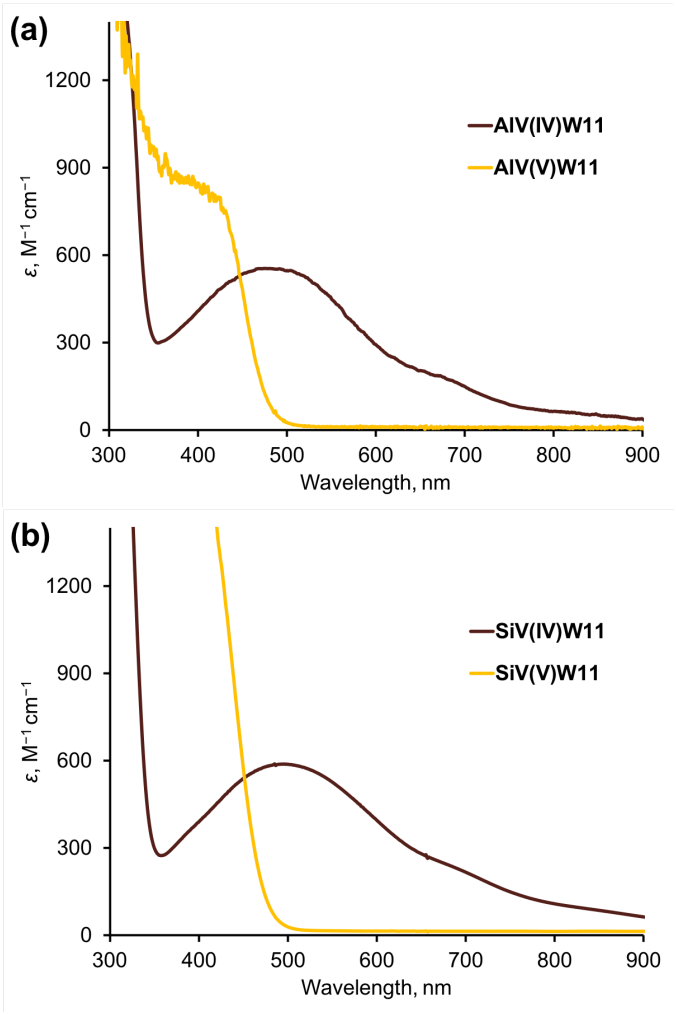

Figure 4.1. UV-vis spectra of (a) **AlVW11$_{ox}$** (yellow), **AlVW11$_{red}$** (brown), (b) **SiVW11$_{ox}$** (yellow), **SiVW11$_{red}$** (brown).

4.3 Results and Discussion

4.3.1 Catalytic Effect of HNO_2

We used $NaNO_2$ as a source of nitrous acid ($pK_a = 3.3$). The addition of $NaNO_2$ to aerated solution of **SiVW11$_{red}$** in 50 mM sulfuric acid significantly increases the rate of **SiVW11$_{red}$** oxidation by O_2 as shown in Figure 4.2. For comparison, the same reaction of **SiVW11$_{red}$** in the presence of Cu(II)/Fe(II) is *3-orders* of magnitude slower,[17] indicating significant improvement in the catalytic performance. The use of this catalyst is a breakthrough in POM chemistry since the POMs with higher reduction potentials, to be potentially practical, cannot be oxidized by O_2 or can only be oxidized extremely slowly.

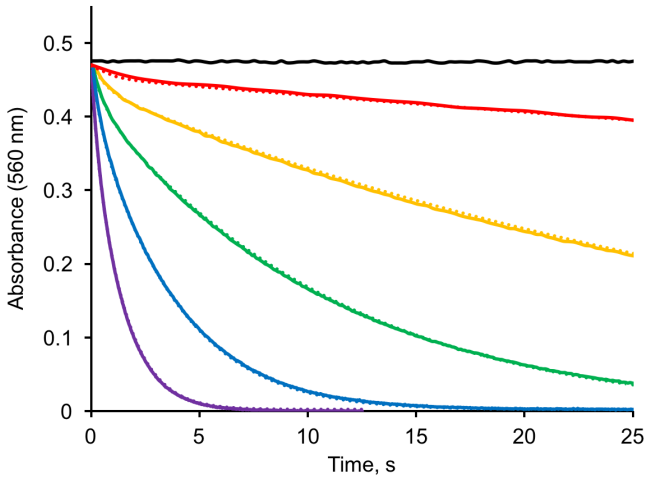

Figure 4.2. Effect of NO_2^- concentration on the kinetics of O_2-based oxidation of **SiVW11$_{red}$** in 50mM sulfuric acid, followed by the decrease of absorbance at 560 nm: [**SiVW11$_{red}$**]$_0$ ≈ 0.95 mM, $[O_2]_0$ = 0.23 mM in all cases, $[NO_2^-]_0$ = 0 (black), 50 (red), 125 (dark gold), 250 (green), 500 (blue), 1000 (purple) μM, 25 °C. Solid and dotted lines represent experimental and fitted curves, respectively.

4.3.2 Kinetics of Catalytic POM_{red} Oxidation by O_2

The catalytic oxidation of **SiVW11$_{red}$** by O_2 proceeds very quickly in the beginning (red solid line) and then significantly slower (blue dashed line) as displayed in Figure 4.3. Therefore, the initial-rate method is not applicable to study the overall reaction. However, we did thoroughly study the dependence of initial rates on concentrations of each reagents and used these data to analyze the initial parts of kinetic curves.

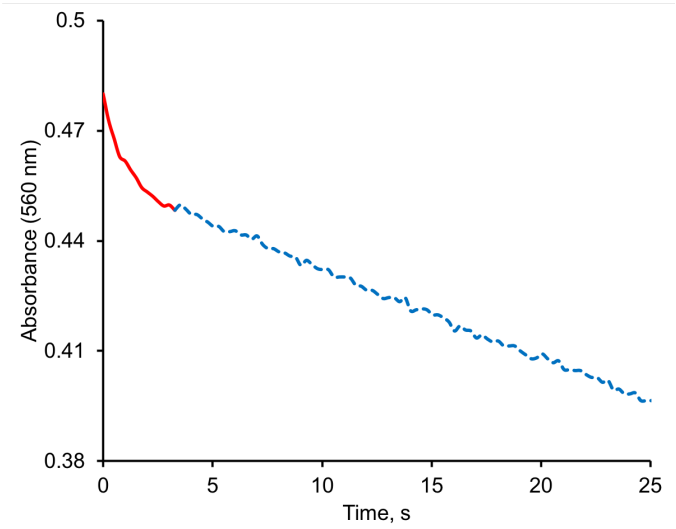

Figure 4.3. Two phase kinetics of O_2-based oxidation of **SiVW11$_{red}$** in 50mM sulfuric acid followed by the decrease of absorbance at 560 nm: [**SiVW11$_{red}$**]$_0$ ≈ 0.95 mM, [O_2]$_0$ = 0.23 mM in all cases, [NO_2^-]$_0$ = 50 μM, 25 °C. Red solid and blue dashed lines represent the first fast initial kinetics and following slow kinetics, respectively.

4.3.3 Initial Reaction Rates

The initial reaction rates are linearly dependent on $[NO_2^-]_0$ (Figure 4.4 (a)) and $[\mathbf{SiVW11_{red}}]_0$ (Figure 4.4 (b)), but independent of O_2 concentration, $[O_2]_0$ (Figure 4.5). This implies that the beginning of the reaction is a stoichiometric oxidation of POM_{red} by nitrous acid ($pK_a = 3.3$), eqs 4.1 – 4.2, and obeys the reaction rate law in eq 4.2a with an apparent rate constant $k_{app} = 9.2 \times 10^2\ M^{-1}s^{-1}$. The other reasonable reactions are eqs 4.3 – 4.7, and these will be discussed systematically culminating in the overall proposed reaction mechanism.

$$NO_2^- + H^+ \rightleftarrows HNO_2 \tag{4.1}$$

$$\mathbf{SiVW11_{red}} + HNO_2 + H^+ \rightarrow \mathbf{SiVW11_{ox}} + NO + H_2O \tag{4.2}$$

$$-d[\mathbf{SiVW11_{red}}]/dt = k_{app}[NO_2^-]_0[\mathbf{SiVW11_{red}}]_0 \tag{4.2a}$$

$$2\ NO + O_2 \rightarrow 2\ NO_2 \tag{4.3}$$

$$\mathbf{SiVW11_{red}} + NO_2 + H^+ \rightleftarrows \mathbf{SiVW11_{ox}} + HNO_2 \tag{4.4}$$

$$NO + NO_2 + H_2O \rightleftarrows 2\ HNO_2 \tag{4.5}$$

$$2\ NO_2 \rightleftarrows N_2O_4 \tag{4.6}$$

$$N_2O_4 + H_2O \rightarrow HNO_2 + NO_3^- + H^+ \tag{4.7}$$

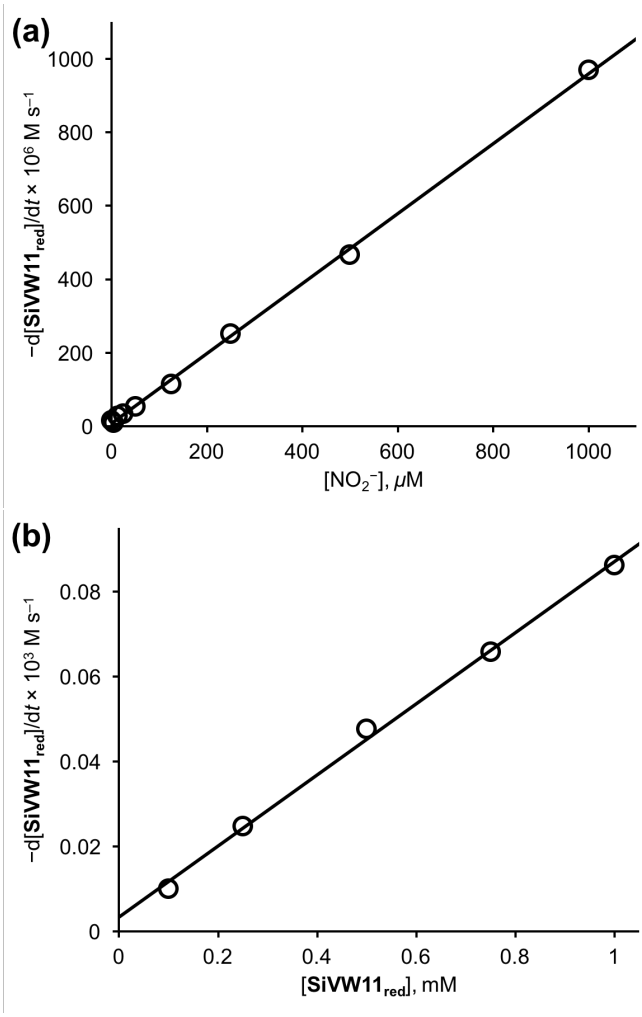

Figure 4.4. (a) Dependence of the initial rate ($-d[\mathbf{SiVW11_{red}}]_0/dt$) on $[NO_2^-]_0$: $[\mathbf{SiVW11_{red}}]_0 \approx 1.0$ mM, $[O_2]_0 = 0.23$ mM, 50 mM sulfuric acid, 25 °C. (b) Dependence of initial rate ($-d[\mathbf{SiVW11_{red}}]_0/dt$) on $[\mathbf{SiVW11_{red}}]_0$: $[NO_2^-]_0 = 100$ μM, $[O_2]_0 = 0.23$ mM, 50 mM sulfuric acid, 25 °C.

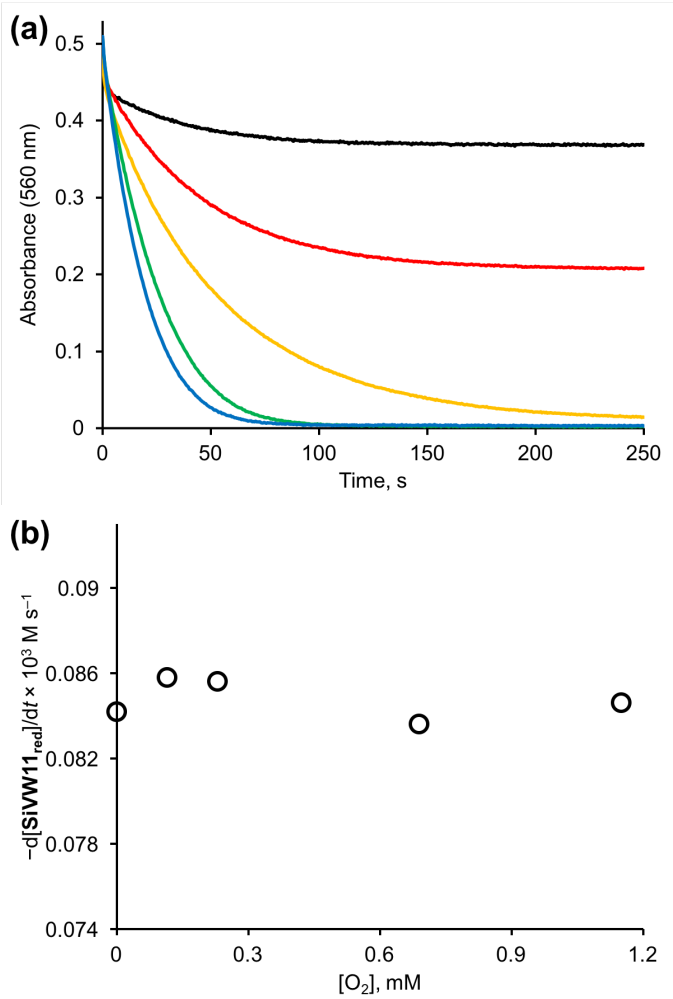

Figure 4.5. (a) Effect of O_2 concentration on the kinetics of O_2-based oxidation of **SiVW11$_{red}$** in 50 mM sulfuric acid followed by the decrease of absorbance at 560 nm: [**SiVW11$_{red}$**]$_0$ ≈ 1.0 mM, [O_2]$_0$ = 0 (black), 0.12 (red), 0.23 (yellow), 0.69 (green), 1.15 (blue) mM, [NO_2^-]$_0$ = 100 μM in all cases, 25 °C. (b) Dependence of initial rate ($-$d[**SiVW11$_{red}$**]$_0$/dt) on [O_2]$_0$ at 0.1 mM [NO_2^-]$_0$: [**SiVW11$_{red}$**]$_0$ ≈ 1.0 mM, 50 mM sulfuric acid, 25 °C.

4.3.4 Reaction Thermodynamics, Mechanism and Kinetic Model

The ionic strength, I, of 50 mM H_2SO_4 solution is about 0.12 M, and the activity coefficients of proton and NO_2^- are about 0.85 and 0.8, respectively.[24,25] The pK_a of HNO_2 at zero ionic strength is 3.3 and decreases to pK_a' = 3.1 at I = 0.12 M (calculated based on activity coefficients). Therefore, under our conditions > 98% of total nitrite is present in the protonated form HNO_2, and the equilibrium in eq 4.1 was significantly shifted to the right.

The oxidation of $\mathbf{SiVW11_{red}}$ by HNO_2 is written for simplicity as eq 4.2 with the reaction rate law $r_2 = k_2[\mathbf{SiVW11_{red}}][HNO_2]$ (eq 4.2a). The rate constant k_2 was estimated from the initial reaction rates, 9.2×10^2 $M^{-1}s^{-1}$, and was varied in the narrow range $(6 – 12) \times 10^2$ $M^{-1}s^{-1}$ in fitting. Dioxygen is involved in the overall process especially via eq 4.3, and the rate constant is well documented in the literatures to be $k_3 \approx 2.2 \times 10^6$ $M^{-2}s^{-1}$.[26-28] In our fitting, k_3 was varied in the range of $(1.5 – 3.0) \times 10^6$ $M^{-2}s^{-1}$ and was found to be 2.6×10^6 $M^{-2}s^{-1}$.

In acidic aqueous solutions nitrous acid is in equilibrium with NO and NO_2 (eq 4.5). The reaction rate constants k_5 and k_{-5} are reported in numerous studies to be in the range of $(0.3 – 1.75) \times 10^8$ and $(5.6 – 25)$ $M^{-1}s^{-1}$, respectively.[29,18,30-32] The mean values $k_5 = 1 \times 10^8$ $M^{-1}s^{-1}$ and $k_{-5} = 15$ $M^{-1}s^{-1}$ were used in fitting. Nitrogen dioxide reversibly dimerizes to N_2O_4 with $k_6 = 4.5 \times 10^8$ $M^{-1}s^{-1}$ and $k_{-6} = 1.4 \times 10^4$ s^{-1}, and the dimer N_2O_4 undergoes hydrolysis to form NO_2^- and NO_3^- with a rate constant $k_7 = 1.0 \times 10^3$ s^{-1}.[33]

The standard reduction potential of the NO_2/NO_2^- is relatively high 1.04 V[18,19] and eq 4.4 is thermodynamically favorable. The reaction rate constant k_4 was set as a variable

parameter in our fitting. The value of the rate constant k_{-4} was calculated as $k_{-4} = k_4/K_4$, where $\log K_4 = \Delta E_4 / 0.059$, and $\Delta E_4 \sim 0.5$ V.

The results of fitting appeared to be independent on the reaction rate constant k_4. The Marcus cross relation (MCR) was employed to estimate the value k_4 for **SiVW11$_{red}$**, and the resulting theoretical value was $\approx 2.5 \times 10^4$ $M^{-1}s^{-1}$ (see the section 4.3.5 for detailed

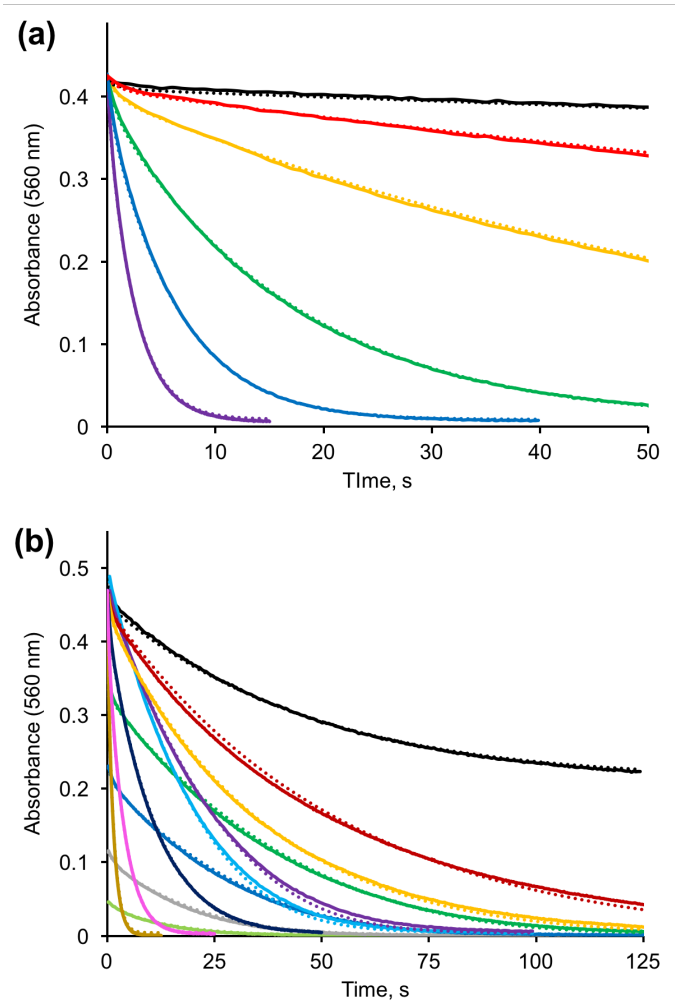

Figure 4.6. Global curve fittings on the kinetics of O_2-based oxidation of (a) **AlVW11$_{red}$** and (b) **SiVW11$_{red}$** in 50 mM sulfuric acid, 25 °C. Solid and dotted lines indicate the experimental and simulated curves, respectively.

calculations). This value was used in fitting. The simulation of the reaction kinetics confirmed that the contribution of the reaction in eq 4.4 is negligible under our experimental conditions relative to eq 4.2. For this reason the reaction in eq 4.4 is not included in the catalytic cycle (Scheme 4.1). The best fit was achieved at $k_2 = (1.1 \pm 0.1) \times 10^3$ and $(6.2 \pm 0.3) \times 10^2$ $M^{-1}s^{-1}$ for **SiVW11$_{red}$** and **AlVW11$_{red}$**, respectively, and at $k_3 = 2.6 \times 10^6$ $M^{-1}s^{-1}$ for both POMs. Several experimental and theoretical kinetic curves are given in Figure 4.2 (partial fit) and Figure 4.6 (global fit).

4.3.5 Calculation of the Rate Constants for the Reaction of SiVW11$_{red}$ with NO_2 and NO^+

The kinetic model, eqs 4.1 – 4.7, quantitatively describes the experimental data despite oversimplifying the reaction mechanism. The reaction in eq 4.4 appears to be unimportant in the catalytic cycle from our fitting analysis. Accordingly, the excellent fitting was achieved by varying only a single parameter k_2.

Calculation of the rate constant for the cross reaction in the eq 4.1.2 is based on data for the reactions of electron self-exchange in eqs 4.1.1 and 4.2.2 using the Marcus Cross Relationship (MCR),[34,11] eq 4.8:

$$NO_2 + NO_2^{-}* \rightleftarrows NO_2^{-} + NO_2* \qquad k_{11} \qquad (4.1.1)$$

$$\mathbf{SiVW11_{red}} + \mathbf{SiVW11_{ox}}* \rightleftarrows \mathbf{SiVW11_{ox}} + \mathbf{SiVW11_{red}}* \qquad k_{22} \qquad (4.2.2)$$

$$NO_2 + \mathbf{SiVW11_{red}} \rightleftarrows NO_2^{-} + \mathbf{SiVW11_{ox}} \qquad k_{12} \qquad (4.1.2)$$

where

$$k_{12} = (k_{11}k_{22}K_{12}f_{12})^{1/2}C_{12} \qquad (4.8)$$

$$\ln f_{12} = 1/4\ [(\ln K_{12} + (W_{12} - W_{21}) / RT)^2 / (\ln (k_{11}k_{22} / Z^2) + (W_{11} - W_{22}) / RT)] \qquad (4.9)$$

$$C_{12} = \exp\,[\,-(W_{12} + W_{21} - W_{11} - W_{22}) / 2RT\,] \quad (4.10)$$

$$k_{11} = \mathrm{Z}\exp\,[\,-(W_{11} + \lambda_1 / 4) / RT\,] \quad (4.11)$$

$$k_{22} = \mathrm{Z}\exp\,[\,-(W_{22} + \lambda_2 / 4) / RT\,] \quad (4.12)$$

The Debye-Hückel equation is applied for the ionic strength correction, where k_0 is a rate constant at $\mu = 0$ (μ = ionic strength),

$$\log k = \log k_0 + [2z_1z_2\alpha\mu^{1/2} / (1 + \beta r_{12}\mu^{1/2})] \quad (4.13)$$

where α = 0.509, β = 0.329 Å^{-1}, and r is an intermolecular distance in the collision complexes. The collision factor Z is commonly taken to be 6×10^{11} $\text{M}^{-1}\text{s}^{-1}$ for a spherical particle. Here, we used the collision frequency, $\mathrm{Z} = 1 \times 10^{11}$ $\text{M}^{-1}\text{s}^{-1}$ for reactants with localized reactive centers. The charges are 0 for NO_2, –1 for NO_2^-, 0 for NO, +1 for NO^+, –6 for **SiVW11$_{red}$** and –5 for **SiVW11$_{ox}$**. The radii of POM and NO_2 are taken as ≈ 5.6 Å and ≈ 1.5 Å, respectively. The λ_1 and λ_2 are the reorganization energies for the electron self-exchange reactions. The reorganization energy of **SiVW11$_{red}$**/**SiVW11$_{ox}$** is λ_2 ≈ 75 kcal/mol,[35] and that for NO_2/NO_2 is λ_1 = 31 kcal/mol.[36] The Coulombic work terms, W_{12}, W_{21}, W_{11}, and W_{22}, are associated with all four combinations of the reacting species,

$$W = z_1z_2e^2 / Dr = z_1z_2e^2N_\mathrm{A} / 4\pi\varepsilon_0 Dr \quad (4.14)$$

where z_n is the charge of each species, e is the elementary charge, N_A is the Avogadro constant, ε_0 is the vacuum permittivity constant, D is the dielectric constant of the reaction medium (water in this study, 80.4), and r is the distance between the collision species. The equilibrium constant K_{12} is calculated on the basis of reduction potentials, $E^o(NO_2/NO_2^-)$ = 1.04 V[18,19] and E^o(**SiVW11$_{ox}$**/**SiVW11$_{red}$**) = 0.62 V. The calculated rate constant for the reaction of **SiVW11$_{red}$** with NO_2, k_{12} is 2.48×10^4 $\text{M}^{-1}\text{s}^{-1}$.

The calculation of k_{12} for the reaction in eq 4.1.2' was performed similarly as described above.

$$NO^+ + NO^* \rightleftarrows NO + NO^+ * \qquad k_{11'} \qquad (4.1.1')$$

$$NO^+ + \mathbf{SiVW11_{red}} \rightleftarrows NO + \mathbf{SiVW11_{ox}} \qquad k_{12'} \qquad (4.1.2')$$

In calculations the following numbers were used; λ_1 = 102 kJ/mol = 24.4 kcal/mol,[36] r_1 = 1.5 Å, and $E^o(NO^+/NO)$ = 1.21 V.[18,19] The calculated rate constant for the reaction of $\mathbf{SiVW11_{red}}$ with NO^+, $k_{12'}$ is 7.34×10^7 $M^{-1}s^{-1}$.

4.3.6. General Discussion

The kinetic model, eqs 4.1 – 4.3, 4.5 – 4.7, quantitatively describes experimental data despite oversimplifying the reaction mechanism. Significantly, the excellent fitting was achieved by varying a single parameter k_2.

Surprisingly, k_2 for $\mathbf{AlVW11_{red}}$ is about half that for $\mathbf{SiVW11_{red}}$ despite the more negative standard reduction potential of $\mathbf{AlVW11_{red}}$. For a visual comparison of $\mathbf{AlVW11_{red}}$ and $\mathbf{SiVW11_{red}}$ oxidation kinetics under the same conditions, we converted a decrease in absorbance at 560 nm to a decrease of [$\mathbf{POM_{red}}$] as presented in Figure 4.7. The shapes of these curves are only slightly different, and that for $\mathbf{AlVW11_{red}}$ can be considered roughly similar to that for $\mathbf{SiVW11_{red}}$. Therefore, we used the cyclic voltammetry to look at the reduction potentials of $\mathbf{AlVW11_{ox}}$/$\mathbf{AlVW11_{red}}$ and $\mathbf{SiVW11_{ox}}$/$\mathbf{SiVW11_{red}}$ couples under our experimental conditions. The potential of the $\mathbf{SiVW11_{ox}}$/$\mathbf{SiVW11_{red}}$ couple was constant ≈ 0.62 V (vs NHE) in the between pH 1 and 2 indicating that neither $\mathbf{SiVW11_{ox}}$ nor $\mathbf{SiVW11_{red}}$ are protonated. In contrast, the potential of the $\mathbf{AlVW11_{ox}}$/$\mathbf{AlVW11_{red}}$ couple decreases linearly with pH with a slope close to 60

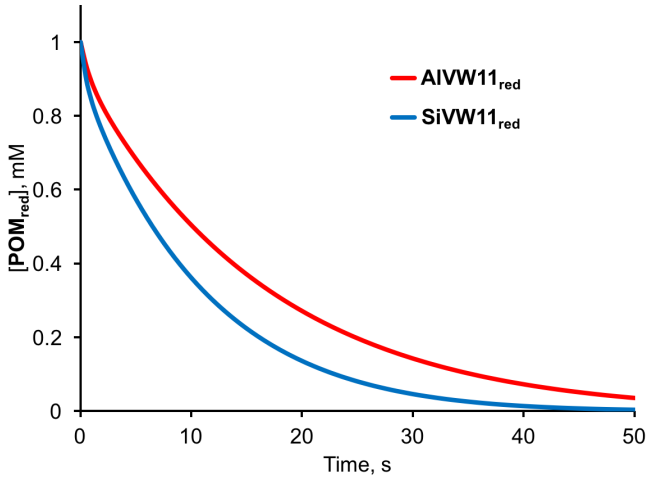

Figure 4.7. Kinetics of NO_2-catalyzed O_2-based oxidation of **AlVW11$_{red}$** (red) and **SiVW11$_{red}$** (blue) in 50 mM sulfuric acid. Conditions: [**AlVW11$_{red}$**]$_0$ = [**SiVW11$_{red}$**]$_0$ = 1 mM, $[O_2]_0$ = 0.23 mM, $[NO_2^-]_0$ = 250 μM, 25 °C.

mV/pH and is equal to 0.63 V (vs NHE) at pH 1.25 (Figure 4.8). This indicates that **AlVW11$_{red}$** is significantly protonated under our conditions and the charge is close to that of **SiVW11$_{red}$**.

The oxidation of **SiVW11$_{red}$** by HNO_2 might proceed via intermediate formation of nitrosonium cation, NO^+, with E^o = 1.21 V,[18,19] for NO^+/NO couple (eq 4.15). The equilibrium constant of NO^+ formation K_{15} is approximately 1×10^{-8} M^{-1}.[37-39]

$$HNO_2 + H^+ \rightleftarrows NO^+ + H_2O \qquad (4.15)$$

$$\textbf{SiVW11}_{red} + NO^+ \rightarrow \textbf{SiVW11}_{ox} + NO \qquad (4.16)$$

The theoretical value k_{16} is about 1×10^8 $M^{-1}s^{-1}$ for **SiVW11$_{red}$** (see the section 4.3.5 for detailed calculations). Therefore, the expected value of k_2 is $K_{15}k_{16}[H^+] \approx 0.065$ $M^{-1}s^{-1}$, which is *4 orders* of magnitude lower than the fitting value. As a consequence, NO^+ is not likely to be involved in the catalytic cycle.

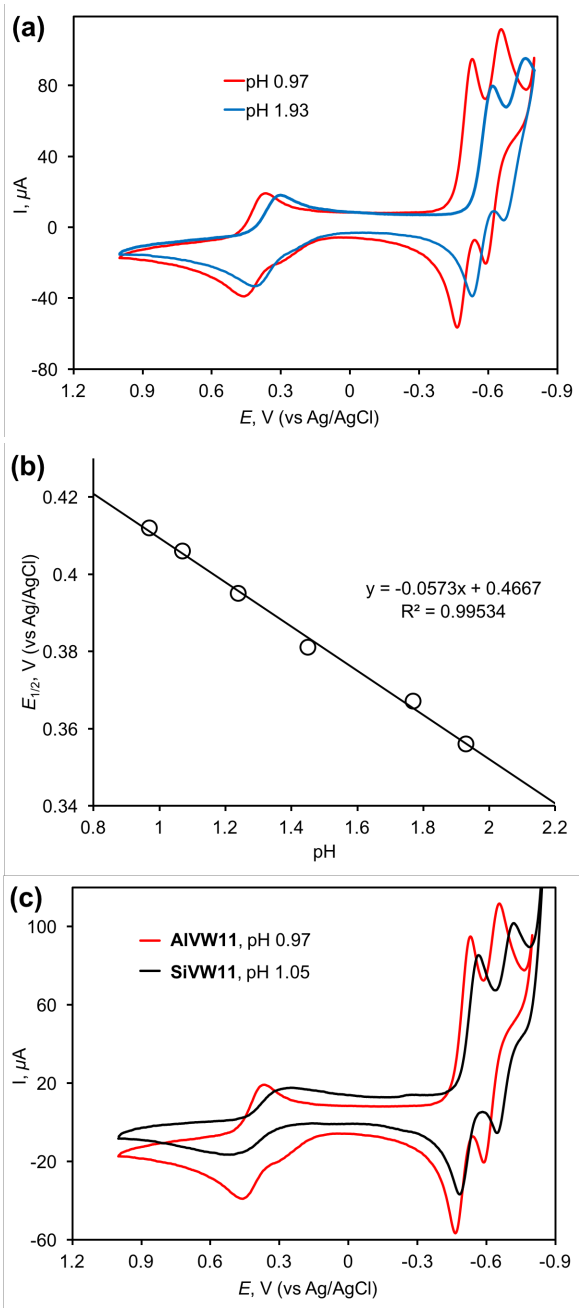

Figure 4.8. (a) Cyclic voltammograms of 2.0 mM **AlVW11** in 100 mM sulfuric acid at different pH values adjusted by NaOH. (b) pH dependence of potential of **AlVW11** between pH 1 and 2. (c) Cyclic voltammograms of 2.0 mM **AlVW11** and **SiVW11** in 100 mM sulfuric acid (100 mV/s scan rate). The pH was adjusted by addition of concentrated NaOH solution.

The NO and NO_2 reversibly form N_2O_3 with forward and reversed rate constants 1.1×10^9 $M^{-1}s^{-1}$ and 3.7×10^4 s^{-1}.[28] The reaction of N_2O_3 with water with the rate constant 1.1×10^3 s^{-1},[28] in acid produces two molecules of nitrous acid. For simplicity, these two reactions are written as in eq (5) and are not included in reaction mechanism.

The catalytic cycle of POM_{red} oxidation is presented in Scheme 4.1. Four nitrous acid molecules are reduced by four POM_{red}, accumulating four NO, and two of these are oxidized by O_2 to produce two NO_2. Two remaining NO, then, react with two newly formed NO_2 to regenerate total four nitrous acid molecules. The recombination of two NO_2 produces N_2O_4, which is an equilibrium with nitrous acid and nitrate anion. Since this reaction is reversible, it affects only the steady state concentrations of NO_x. If the reaction proceeds in a reactor with headspace, some NO and NO_2 will be in the gas phase. This system is thoroughly discussed in the literature.[29]

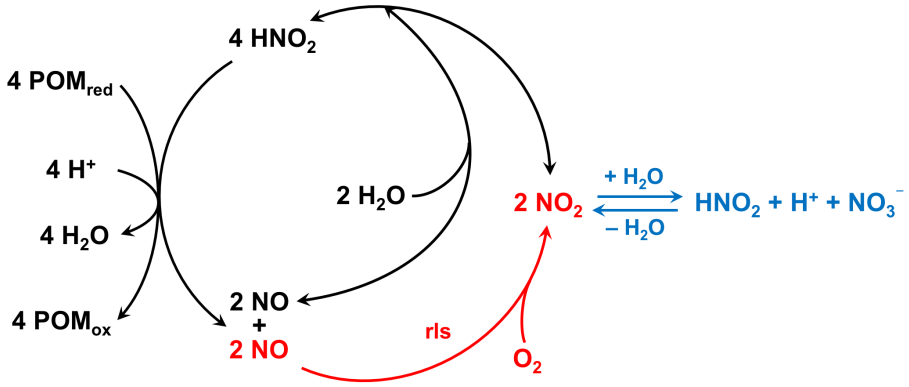

Scheme 4.1. Catalytic cycle of POM_{red} oxidation catalyzed by nitrous acid. The red part indicates the rate-limiting step (rls) and the blue part represents the possible pathway of nitrous acid loss.

In stopped-flow experiments, the initial concentration of O_2 is limited by O_2 solubility in water, which does not allow to use the higher concentrations of POM_{red}. Therefore, we simulated the kinetics of formation/consumption of all intermediates at 10 mM [**SiVW11$_{red}$**], 50 μM HNO_2 and constant [O_2], under O_2- and air-saturated conditions (Figure 4.9). A 50 % conversion of **SiVW11$_{red}$** is achieved at 202 and 850 seconds (ratio $\approx$ 0.24) under O_2 and air, respectively (Figure 4.9 (a)). This indicates that the reaction rate order with respect to [O_2] is close to 1. The rate of **SiVW11$_{red}$** consumption is constant up to very high conversion, consistent with the zero order with respect to [**SiVW11$_{red}$**]. The dominant intermediate in the course of the reaction is NO (Figure 4.9 (b)). When the reaction is complete, NO is oxidized to HNO_2. These data indicate that oxidation of NO by O_2 (eq 4.3) is the rate-limiting step (rls).

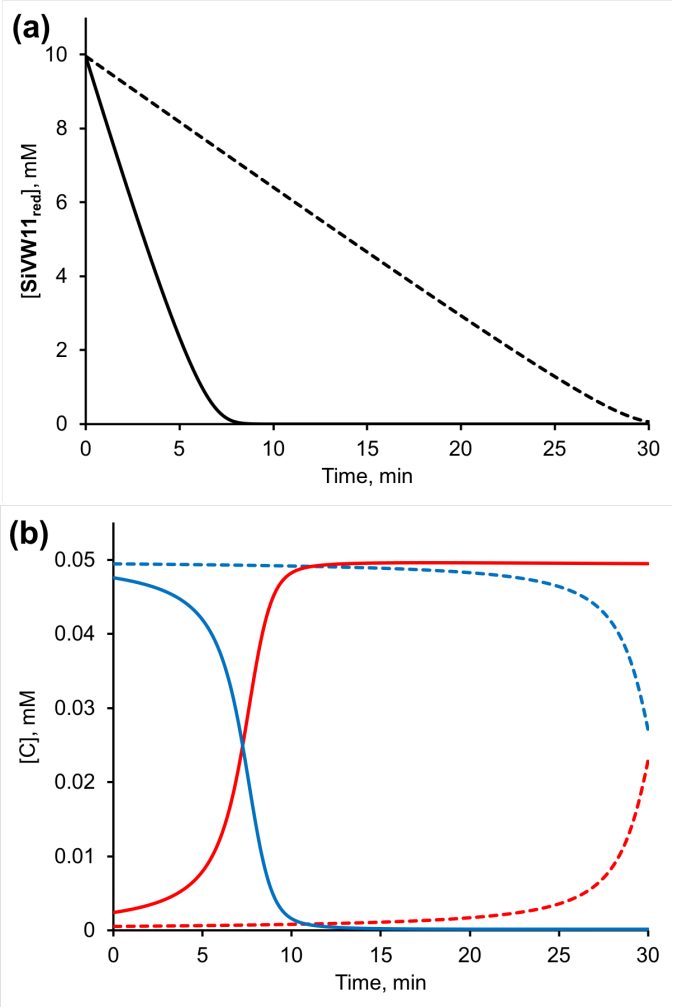

Figure 4.9. Simulated kinetics of oxidation of **SiVW11$_{red}$** by air and O_2. (a) [**SiVW11$_{red}$**], (b) [HNO_2] (red) and [NO] (blue). Conditions: [**SiVW11$_{red}$**]$_0$ = 10 mM, [NO_2^-]$_0$ = 50 μM. Solid and dashed lines represent the O_2- and air-saturated conditions, respectively.

The formation of nitrate results in termination of the catalytic cycle and is directly related to the stability of the catalyst. The simulation of kinetics at 10 mM **SiVW11$_{red}$**, and 0.05 mM HNO_2 shows that $[NO_3^-]$ increases very slowly during the reaction and the results in final yield of 0.12 % and 0.18% based on $[NO_2^-]_0$, under air and O_2 respectively. We looked at the effect of NO_3^- on the reaction rates (Figure 4.10) and observed no effect on the reaction kinetics. This indicates that possible reduction of nitrate to nitrite is very slow. The turnover number, TON = $[\mathbf{SiVW11_{red}}]_0/[HNO_2]_0$, calculated under conditions in Figure 4.9 is 2×10^2, confirming a rather high stability of the catalyst.

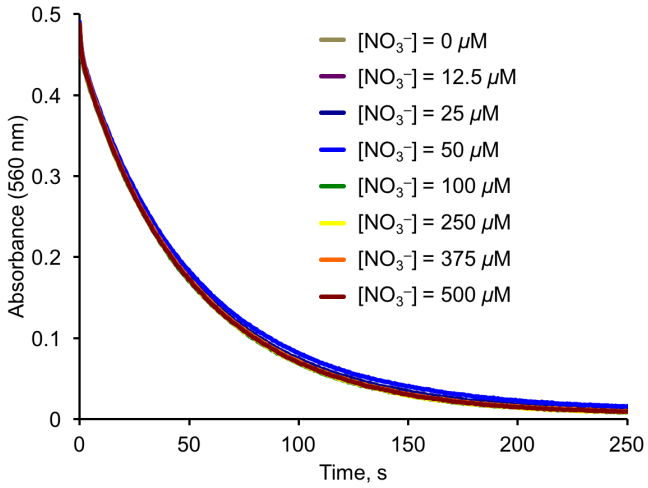

Figure 4.10. Effect of NO_3^- concentration on the kinetics of O_2-based oxidation of **SiVW11$_{red}$** in 50 mM sulfuric acid followed by the decrease of absorbance at 560 nm: $[\mathbf{SiVW11_{red}}]_0 \approx 1.0$ mM, $[O_2]_0 = 0.23$ mM, $[NO_2^-]_0 = 100$ μM in all cases, 25 °C.

4.4 Conclusions

We have found that under acidic conditions, that nitrous acid is a very efficient catalyst for the oxidation of reduced polyoxometalates, POM_{red}, $[AlV^{IV}W_{11}O_{40}]^{7-}$ and $[SiV^{IV}W_{11}O_{40}]^{6-}$ by O_2. The catalytic cycle involves the oxidation of POM_{red} by HNO_2, and oxidation of intermediate NO by O_2. The latter reaction is the rate limiting. The kinetic curves were quantitatively fitted using the value of rate constant for the reaction POM_{red} with HNO_2 as a single variable parameter. Under turnover conditions, the accumulation of nitrate is very slow, which makes the catalytic system fairly stable. This work has potential applications in several O_2- or air-based oxidations of importance.

4.5 References

(1) Harrup, M. K.; Hill, C. L. *Inorg. Chem.* **1994,** *33*, 5448.

(2) Hill, C. L. *J. Mol. Catal. A: Chem.* **1996,** *114*, 1.

(3) Hill, C. L.; Gall, R. D. *J. Mol. Catal. A: Chem.* **1996,** *114*, 103.

(4) Duncan, D. C.; Hill, C. L. *J. Am. Chem. Soc.* **1997,** *119*, 243.

(5) Khenkin, A. M.; Neumann, R. *Angew. Chem. Int. Ed.* **2000,** *39*, 4088.

(6) Khenkin, A. M.; Weiner, L.; Wang, Y.; Neumann, R. *J. Am. Chem. Soc.* **2001,** *123*, 8531.

(7) Hill, C. L. In *Comprehensive Coordination Chemistry-II: From Biology to Nanotechnology*; Wedd, A. G., Ed.; Elsevier Ltd.: Oxford, UK, 2004; Vol. 4.

(8) Neumann, R. *Mod. Oxidation Methods* **2004**, 223.

(9) Hill, C. L. *J. Mol. Catal. A: Chem.* **2007 Special Issue,** *262*, 1.

(10) Cowan, J. J.; Bailey, A. J.; Heintz, R. A.; Do, B. T.; Hardcastle, K. I.; Hill, C. L.; Weinstock, I. A. *Inorg. Chem.* **2001,** *40*, 6666.

(11) Snir, O.; Wang, Y.; Weinstock, I. A. *Isr. J. Chem.* **2011,** *51*, 247.

(12) Yang, B.; Pignatello, J. J.; Qu, D.; Xing, B. *J. Phys. Chem. A* **2015,** *119*, 1055.

(13) Kim, M.; Weinstock, I. A.; Geletii, Y. V.; Hill, C. L. *ACS Catal.* **2015,** *5*, 7048.

(14) Geletii, Y. V.; Hill, C. L.; Atalla, R. H.; Weinstock, I. A. *J. Am. Chem. Soc.* **2006,** *128*, 17033.

(15) Snir, O.; Wang, Y.; Tuckerman, M. E.; Geletii, Y. V.; Weinstock, I. A. *J. Am. Chem. Soc.* **2010,** *132*, 11678.

(16) Weinstock, I. A.; Schreiber, R. E.; Neumann, R. *Chem. Rev.* **2018**, *118*, 2680.

(17) Kim, M.; Chamack, M.; Geletii, Y. V.; Hill, C. L. *Inorg. Chem.* **2018,** *57*, 311.

(18) Ram, M. S.; Stanbury, D. M. *Inorg. Chem.* **1985,** *24*, 2954.

(19) Stanbury, D. M. In *Adv. Inorg. Chem.*; Sykes, A. G., Ed.; Academic Press, Inc, 1989; Vol. 33.

(20) Dukes, E. K. *J. Am. Chem. Soc.* **1960,** *82*, 9.

(21) Müller, A.; Dloczik, L.; Diemann, E.; Pope, M. T. *Inorg. Chim. Acta* **1997,** *257*, 231.

(22) Cowan, J. J.; Hill, C. L.; Reiner, R. S.; Weinstock, I. A. In *Inorg. Synth.*; Coucouvanis, D., Ed.; John Wiley& Sons, Inc.: New York, 2002; Vol. 33.

(23) Geletii, Y. V.; Weinstock, I. A. *J. Mol. Catal. A: Chem.* **2006,** *251*, 255.

(24) Kielland, J. *J. Am. Chem. Soc.* **1937,** *59*, 1675.

(25) Staples, B. R. *J. Phys. Chem. Ref. Data* **1981,** *10*, 765.

(26) Awad, H. H.; Stanbury, D. M. *Int. J. Chem. Kinet.* **1993,** *25*, 375.

(27) Wink, D. A.; Darbyshire, J. F.; Nims, R. W.; Saavedra, J. E.; Ford, P. C. *Chem. Res. Toxicol.* **1993,** *6*, 23.

(28) Lewis, R. S.; Deen, W. M. *Chem. Res. Toxicol.* **1994,** *7*, 568.

(29) Schwartz, S. E.; White, W. H. In *Trace Atmospheric Constituents: Properties, Transformations, & Fates*; John Wiley & Sons, Inc., 1983.

(30) Park, J.-Y.; Lee, Y.-N. *J. Phys. Chem.* **1988,** *92*, 6294.

(31) Beake, B. D.; Moodie, R. B. *J. Chem. Soc. Perkin Trans. 2* **1995,** *0*, 1045.

(32) Rayson, M. S.; Mackie, J. C.; Kennedy, E. M.; Dlugogorski, B. Z. *Inorg. Chem.* **2012,** *51*, 2178.

(33) Grätzel, M.; Henglein, A.; Lilie, J.; Beck, G. *Ber. Bunsenges. phys. Chem.* **1969,** *73*, 646.

(34) Weinstock, I. A. *Chem. Rev.* **1998,** *98*, 113.

(35) Galli, C.; Gentili, P.; Nunes Pontes, A. S.; Gamelas, J. A. F.; Evtuguin, D. V. *New J. Chem.* **2007,** *31*, 1461.

(36) Stanbury, D. M. In *Electron Transfer Reactions*; American Chemical Society, 1997; Vol. 253.

(37) Seel, F.; Winkler, R. *Z. Phys. Chem.* **1960,** *25*, 217.

(38) Becker, K. H.; Kleffmann, J.; Kurtenbach, R.; Wiesen, P. *J. Phys. Chem.* **1996,** *100*, 14984.

(39) Williams, D. L. H. *Nitrosation Reactions and the Chemistry of Nitric Oxide*; Elsevier: Amsterdam, 2004.

Chapter 5

Water Oxidation Catalyzed by $[Co_4(H_2O)_2(VW_9O_{34})_2]^{10-}$ and Co^{2+}_{aq}: Identification of the True Catalysts

With Daniel Ouedraogo, Marika Wieliczko, Giovanni Gadda, Yurii V. Geletii, Petro F. Zhuk, and Craig L. Hill

5.1 Introduction

The development of water oxidation catalysts (WOCs) continues to be a central focus of attention in solar fuel production.[1-7] The use of earth-abundant cobalt in molecular WOCs with excellent catalytic performance has led to considerable research in this area involving assessment of catalytic water oxidation performance by multiple approaches.[8-37] The first Co-based WOC was $Co(II)_{aq}$ in studies of water oxidation using $[Ru(bpy)_3]^{3+}$ as the terminal oxidant.[8] Detailed mechanistic study of aquocobalt(II)-catalyzed water oxidation followed.[9] In part on the basis of these studies, the Nocera group reported improved Co-based WOCs.[10,38,39] The heterogeneous cobalt oxy-hydroxide WOC which forms in situ from $Co(II)_{aq}$/phosphate buffer exhibits reasonable catalytic water oxidation activity at a moderate overpotential near neutral pH. Further studies confirmed that Co(IV) sites oxidizes water.[40,41]

A breakthrough in homogeneous Co-containing WOCs was achieved by the Hill group with publication of the molecular Co-containing POM, $[Co_4(H_2O)_2(PW_9O_{34})_2]^{10-}$ (**Co_4P_2**).[12] The catalytic performance of this carbon-free, earth-abundant metal-containing, all-inorganic compound, **Co_4P_2**, was thoroughly demonstrated under dark and light-driven conditions.[12,16,42] The catalytic efficiency of this Co-containing POM was significantly improved by substituting P(V) by V(V), in the complex, $[Co_4(H_2O)_2(VW_9O_{34})_2]^{10-}$ (**Co_4V_2**).[27] Under dark conditions, **Co_4V_2** exhibits exceptionally fast catalytic water oxidation (TOF ~ 1×10^3 s^{-1}) at pH 9.0. Folkman and Finke, however, called into question the stability of the **Co_4V_2**, noting **Co_4V_2** decomposes into $Co(II)_{aq}$.[43] Their report argued that the catalytic activity of **Co_4V_2**, really originates from $Co(II)_{aq}$, which leads to formation of the Nocera-type heterogeneous WOC, cobalt-oxide-phosphate via reaction of $Co(II)_{aq}$,

generated from **Co_4V_2**, under electrochemical conditions. Consequently, it was essential to further examine and identify the active WOCs in solution of **Co_4V_2**.

In this Chapter, we first examine the early-time kinetics of **Co_4V_2** and $Co(II)_{aq}$ which demonstrate that the observed catalytic activity *cannot* be explained simply by $Co(II)_{aq}$, and confirming that **Co_4V_2** is the most active WOC in this system. Subsequently, we provide an account of the characteristic water oxidation kinetics by $Co(II)_{aq}$ associated with the possible formation of true active cobalt-containing species. The goal is to identify these $Co(II)_{aq}$-derived WOCs and better understand the overall catalytic behavior of these complex systems. To this end, a double mixing stopped-flow technique is used to obtain water oxidation kinetics depending on aging times, which are defined as a time interval between first and subsequent mixing events. After the first mixing of $Co(II)_{aq}$ with $[Ru(bpy)_3]^{3+}$ in 1:1 ratio, the following points are considered: (1) $Co(II)_{aq}$ is oxidized by $[Ru(bpy)_3]^{3+}$, resulting in accumulation of $Co(III)_{aq}$, (2) the generated $Co(III)_{aq}$ with remaining $Co(II)_{aq}$ (or $Co(III)_{aq}$) aggregates into mixed-valence Co_n complexes, where n is the total number of Co-atoms in each complex, and (3) the distribution of complexes depends on the aging time and concentration of $Co(II)_{aq}$ and $[Ru(bpy)_3]^{3+}$, and this distribution reveals that different aggregates have different catalytic water oxidation activities.

5.2 Experimental

5.2.1 Materials

Materials, reagents and solvents were purchased from commercial sources in the highest purity available and used without further purification unless otherwise noted. $Ru(bpy)_3(ClO_4)_3$ was prepared by the literature procedure.[27]

Synthesis of $Na_{10}[Co_4(H_2O)_2(VW_9O_{34})_2]\bullet 13H_2O$. The sodium salt of $\mathbf{Co_4V_2}$ was prepared by modifications of the literature procedure.[44] In a 150 mL beaker, $Na_2WO_4\bullet 2H_2O$ (2.97g, 9 mmol) and V_2O_5 (91 mg, 0.5 mmol) were stirred in 50 mL of NaOAc buffer (1.0 M, pH 4.8) at 70 – 80 °C to yield a slightly turbid yellow-brown solution. The solution may be filtered at this point, however we found that filtration did not significantly affect the yield. To the stirred, heated solution was added $Co(OAc)_2\bullet 4H_2O$ (498 mg, 2 mmol) and the solution immediately became deep brown. The stirred solution was maintained at 70 – 80 °C for 40 – 60 minutes, then uncovered until the solution was concentrated to approximately half the original volume. The solution was filtered while hot through a medium-porosity fritted glass filter. We observed that the use of a coarse-porosity funnel did not sufficiently trap the fine precipitate that is likely some insoluble vanadium-based impurities. Within minutes upon cooling to room temperature, dark brown crystals began to form. The solution was allowed to cool completely before ~ 5mL EtOH was slowly added. This avoids the crystals turning a fine powder that is difficult to collect. The crystals were grown for 24 – 72 hours, collected on a coarse-porosity fritted glass filter with aspiration, and the resulting brown crystals were washed gently with EtOH. The material was dried with aspiration for ~30 minutes until it could

be transferred to dry overnight on a piece of filter paper to afford the compound in 46 – 58% yield based on W.

5.2.2 Kinetic Measurements

For the reaction catalyzed by **Co_4V_2** or $Co(II)_{aq}$ with $[Ru(bpy)_3](ClO_4)_3$ as an oxidant, kinetic curves were acquired by monitoring spectral changes using a Hi-Tech Scientific KinetAsyst SF-61SX2 sample-handling unit with a diode array spectrophotometer. One syringe was filled with **Co_4V_2** or $Co(NO_3)_2$ (as the source of $Co(II)_{aq}$) in sodium borate buffer solution (NaB_i) and the second syringe was filled with $[Ru(bpy)_3](ClO_4)_3$ in water. The **Co_4V_2** solution, especially, was freshly prepared (within ~ 3 min) to avoid the challenge in hydrolytic stability of **Co_4V_2** questioned by Folkman and Finke. The kinetics of consumption of $[Ru(bpy)_3]^{3+}$ under catalytic conditions, where $[[Ru(bpy)_3]^{3+}] >> [\mathbf{Co_4V_2}]$ or $[Co(II)_{aq}]$, were measured by the decrease in absorbance at 670 nm with time ($\varepsilon_{670} = 4.2 \times 10^2\ M^{-1}cm^{-1}$).

The double-mixing stopped-flow experiment was performed using an SF-61DX2 Hi-Tech KinetAsyst high-performance stopped-flow spectrophotometer with a photo diode array detector. The first mixing in the stopped-flow spectrophotometer was between the $Co(II)_{aq}$ in NaB_i in low concentrations (4 – 40 μM) and $[Ru(bpy)_3]^{3+}$ in water, thus potentially enabling the formation of Co-multimers. The $[Ru(bpy)_3]^{3+}$ solution at higher concentration prepared in the third syringe (~ 1.0 mM) was combined with the solution from the first mixing event after the desired aging times (0.01 – 5 s). The time-resolved kinetics were measured by the absorbance change at 670 nm in the same manner.

The kinetic curve fitting, simulation of reaction kinetics, and optimization of conditions were performed using COPASI 4.13 (Build 87) software (www.copasi.org).

5.3 Results and Discussion

5.3.1 Differentiating Water Oxidation Catalytic Activities of Co_4V_2 and $Co(II)_{aq}$ by Early-Time Kinetic Studies

Folkman and Finke,[43] raised a question whether observed WOC activity is due to **Co_4V_2** or to a decomposition product such as $Co(II)_{aq}$. Kinetics of catalytic $[Ru(bpy)_3]^{3+}$ reduction were compared for $Co(II)_{aq}$ and **Co_4V_2** by tracking early-time kinetic curves

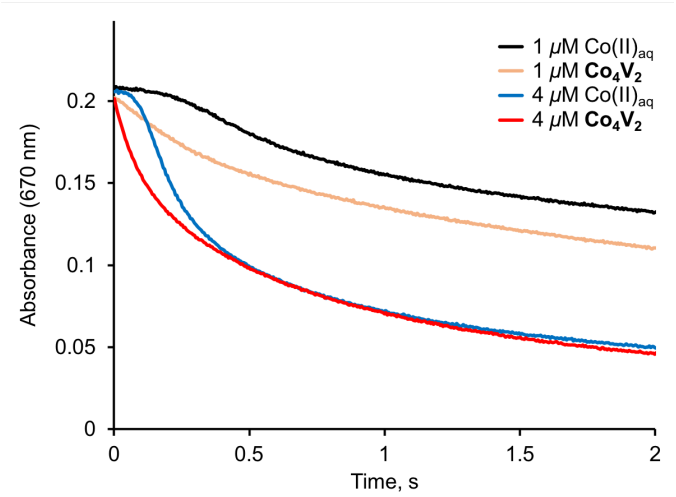

Figure 5.1. Kinetics of $[Ru(bpy)_3]^{3+}$ reduction (measured at 670 nm) catalyzed by solutions of $Co(NO_3)_2$ and **Co_4V_2** in 80 mM NaB_i at pH 8.3. All stock solutions of the catalysts were freshly prepared in 160 mM of NaB_i at pH 8.5 and then the solution was mixed by adding 1.0 mM $[Ru(bpy)_3]^{3+}$ in nitric acid solution (pH ~ 3) to bring the final pH to 8.3. The concentrations in the inset show the final concentrations after mixing.

using stopped-flow UV-vis techniques (Figure 5.1). For **Co_4V_2**, the maximum rates are achieved at the very beginning of the reaction with no observed induction period. For $Co(II)_{aq}$, however, the reaction begins only after an induction period, which is typically 0.04 – 0.1 s long. This strongly suggests that the activity of **Co_4V_2** is not simply due to the release of $Co(II)_{aq}$, as the additional time necessary for decomposition of the POM into $Co(II)_{aq}$ would require a longer induction period than what is observed for $Co(II)_{aq}$ alone.

These early-time kinetics make the case that **Co_4V_2** is an active WOC in this system, confirming the conclusions of our initial study.[27] Significantly however, the kinetics of this system become quite complex at later times. For example, slight induction periods for the **Co_4V_2**-catalyzed reduction of $[Ru(bpy)_3]^{3+}$ are observed after incubation periods of 20 minutes. Thus at very early time points, **Co_4V_2** is the most likely dominant catalyst, but at longer time points complex mixtures composed of **Co_4V_2**, $Co(II)_{aq}$, and other potential WOCs are likely responsible for the observed activity. A more complete study of the stability of **Co_4V_2** is beyond the scope of this work.

5.3.2 Background of Cobalt Speciation and Distribution of Co-Multimers

Understanding of cobalt speciation is essential prior to the thorough analysis of the induction period in water oxidation kinetics by $Co(II)_{aq}$. The reduction potential of $Co^{3+}{}_{aq}/Co^{2+}{}_{aq}$ couple is very high with the value of 1.82 V (vs NHE), resulting in spontaneous water oxidation even under acidic conditions. The $Co(II)_{aq}$ is known to be a very active catalyst in water oxidation mediated by $[Ru(bpy)_3]^{3+}$ as an oxidant (E^o = 1.26 V) or electrochemically at pH > 8. In this pH range, both $Co^{2+}{}_{aq}$ and $Co^{3+}{}_{aq}$ undergo hydrolysis as described in eqs 5.1 – 5.4.

$$Co^{2+}_{aq} \rightleftarrows Co(OH)^{+} + H^{+} \qquad pK_1 \qquad (5.1)$$

$$Co(OH)^{+} \rightleftarrows Co(OH)_2 + H^{+} \qquad pK_2 \qquad (5.2)$$

Co(II)-species are composed of 72% Co^{2+}_{aq}, 18% $Co(OH)^{+}$ and 10% $Co(OH)_2$ at pH 9.0.

$$Co^{3+}_{aq} \rightleftarrows Co(OH)^{2+} + H^{+} \qquad pK_3 \qquad (5.3)$$

$$Co(OH)^{2+} \rightleftarrows Co(OH)_2^{+} + H^{+} \qquad pK_4 \qquad (5.4)$$

The formation constants for Co^{2+}_{aq} are $pK_1 = 9.65$ and $pK_2 = 9.15$,[45-47], however, for Co^{3+}_{aq}, pK_3 is reported with the upper limit, $pK_3 < 2$,[47] and pK_4 has been reported with different values and thus remains uncertain. For the details, a ladder scheme for 1 e^- ET processes for 2-protic Co^{3+}_{aq} reagents and 2-protic Co^{2+}_{aq} products is given in Scheme 5.1.

From this Scheme, the standard potential of $Co(OH)^{2+}/Co(OH)^{+}$ is calculated by $E^o_2 = E^o_1 - 0.059 \times (pK_1 - pK_3) = 1.82 - 0.059 \times (9.65 - 2) = 1.37$ V. The standard potential of $Co(OH)_2^{+}/Co(OH)_2$ is $E^o_3 = E^o_2 - (pK_2 - pK_4) = 1.37 - 0.05916 \times (9.15 - pK_4) = 0.83 + (0.05916 \times pK_4)$ V. Thus, the oxidation of $Co(OH)_2$ to $Co(OH)_2^{+}$ by $[Ru(bpy)_3]^{3+}$ becomes

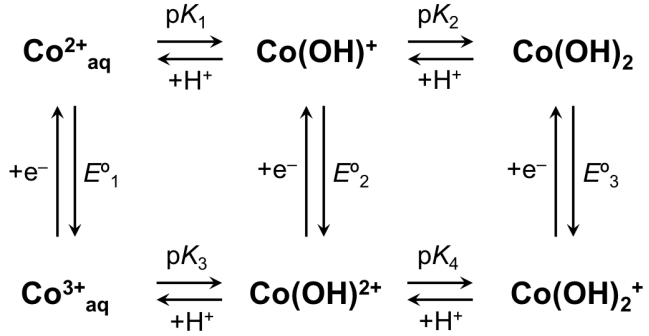

Scheme 5.1. Ladder scheme for one electron transfer processes with respect to 2-protic Co^{3+}_{aq} reactants and 2-protic Co^{2+}_{aq} products.

thermodynamically favorable at $pK_4 < (1.26 - 0.83) / 0.059 = 7.3$. Therefore, $Co(OH)_2$ is the most likely the species reacting with $[Ru(bpy)_3]^{3+}$. However, the deprotonated form of Co^{3+}_{aq}, namely $Co(OH)_2^+$ is unstable in water and forms polynuclear species. The kinetics of such aggregation and the catalytic activity of these species are not well understood.

Prior to conducting experimental work, we performed simulations of the aggregation kinetics assuming that the species with more than n = 10 Co atoms, Co_n, are not formed on this reaction timescale. We considered the most rapid scenario, namely the reversible oxidation of Co(II) by $[Ru(bpy)_3]^{3+}$ to Co(III) proceeds with a rate constant of 1.0×10^9 $M^{-1}s^{-1}$, with a rate constant for the reverse reaction of 1.0×10^7 $M^{-1}s^{-1}$ (corresponding to $pK_4 \approx 5.3$ based on the potentials). Co(III) complexes commonly have very slow water exchange rates, resulting in significantly decreased rates of aggregation. Therefore, we considered the aggregation of Co(III) for several cases with different association rate constants for the reaction $Co_{n-1} + Co(III) \rightarrow Co_n$ to examine the distribution of Co-multimers. The simulation with 5 μM $Co(II)_{aq}$ proceeds with the apparent rate constant of 1.0×10^6 $M^{-1}s^{-1}$, are shown in Figure 5.2(a), clearly demonstrating that in the timescale of induction period under turnover conditions, the dimer is the dominant species with minor concentrations of trimer and tetramer even at high association rate constants ($1.0 \times 10^5 - 1.0 \times 10^9$ $M^{-1}s^{-1}$) as shown in Figure 5.2(b). The dimer of Co(III)is likely to be either $[Co(\mu\text{-}O)Co]^{4+}(aq)$ or $[Co(\mu\text{-}OH)_2Co]^{4+}$.[47]

Experimentally, it is very challenging to get an aqueous Co(III) stock solution since Co(III) is unstable. In order to trigger the polymerization of Co^{3+}_{aq} as described earlier, we mixed Co^{2+}_{aq} with $[Ru(bpy)_3]^{3+}$ in 1:1 ratio, and after desired times we added an excess of

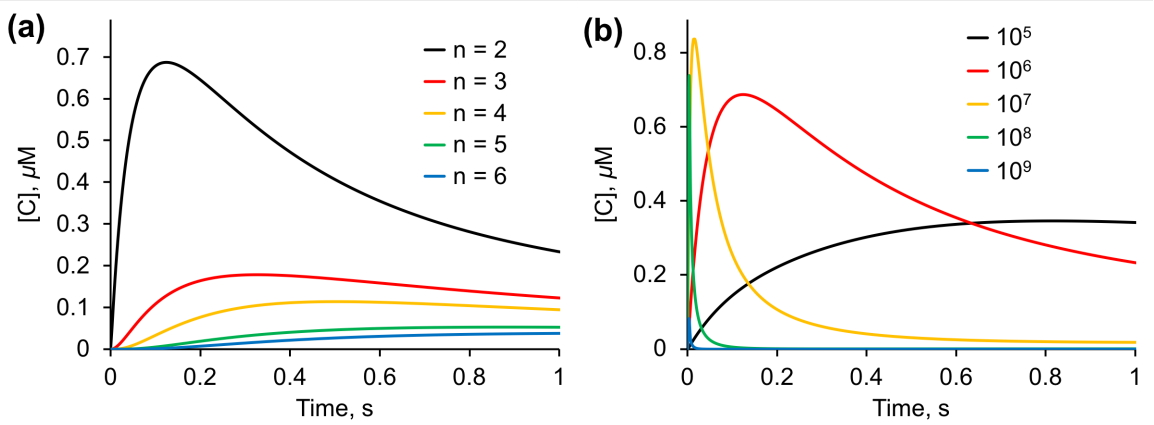

Figure 5.2. (a) Representative simulated distribution of polynuclear Co-species as a function of time with the rate constant 1.0×10^6 $M^{-1}s^{-1}$ for the reaction Co_{n-1} + Co(III) → Co_n. The numbers in the label are the number of aggregated cobalt atoms. (b) Simulated distribution of Co-dimers as a function of time with varying rate constants. The numbers in the label are the rate constants. $[Co^{2+}_{aq}] = 5$ μM in all cases.

$[Ru(bpy)_3]^{3+}$ and checked for catalytic activity as a function of aging time using a double-mixing stooped-flow method that is discussed below.

5.3.3 Dependence on $[[Ru(bpy)_3]^{3+}]_0$ and $[Co^{2+}_{aq}]_0$ in Kinetics of Water Oxidation Catalysis and the Reaction Mechanism

The length of the characteristic induction periods in the oxidation of $Co(II)_{aq}$ by $[Ru(bpy)_3]^{3+}$ (Figure 5.1) depends on the concentrations of $[Ru(bpy)_3]^{3+}$ and $Co(II)_{aq}$. Figure 5.3(a) shows the kinetics of water oxidation catalyzed by $Co(II)_{aq}$ depending on $[[Ru(bpy)_3]^{3+}]_0$.

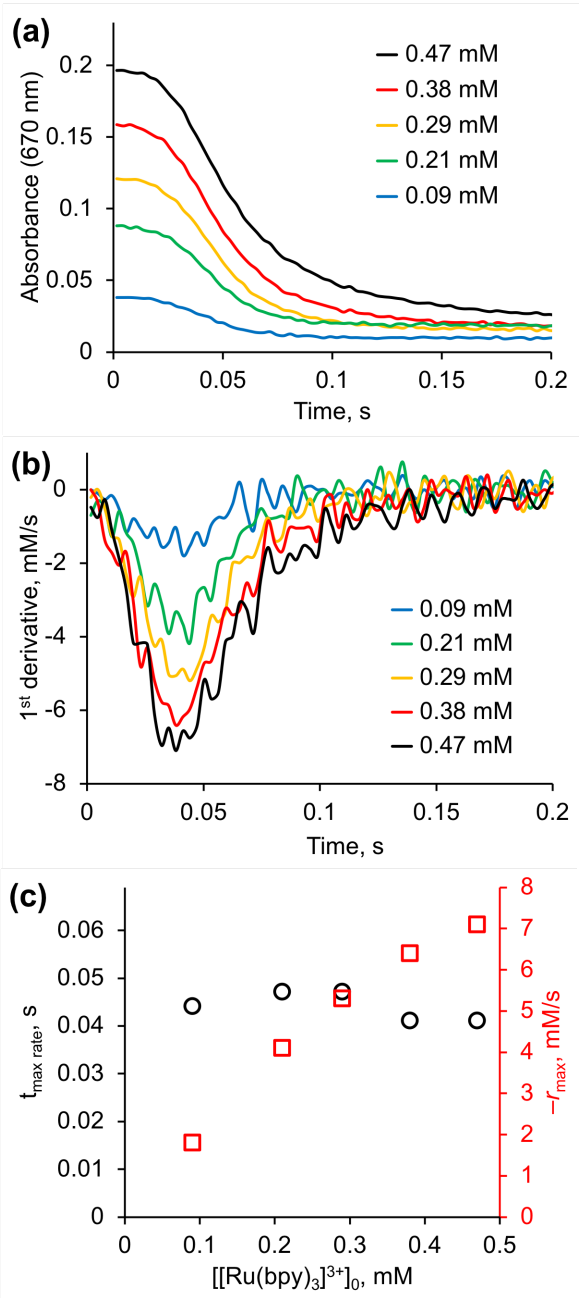

Figure 5.3. (a) Effect of $[[Ru(bpy)_3]^{3+}]_0$ on the kinetics of water oxidation by Co^{2+}_{aq} (labels are $[[Ru(bpy)_3]^{3+}]_0$). (b) First-derivative kinetic curves (labels are $[[Ru(bpy)_3]^{3+}]_0$). (c) Dependence of the induction periods (black) and maximum rates (red) on $[[Ru(bpy)_3]^{3+}]_0$. Conditions: $[Co^{2+}_{aq}]_0 = 5\ \mu M$, 50 mM NaB_i, pH 9.0, 25 °C.

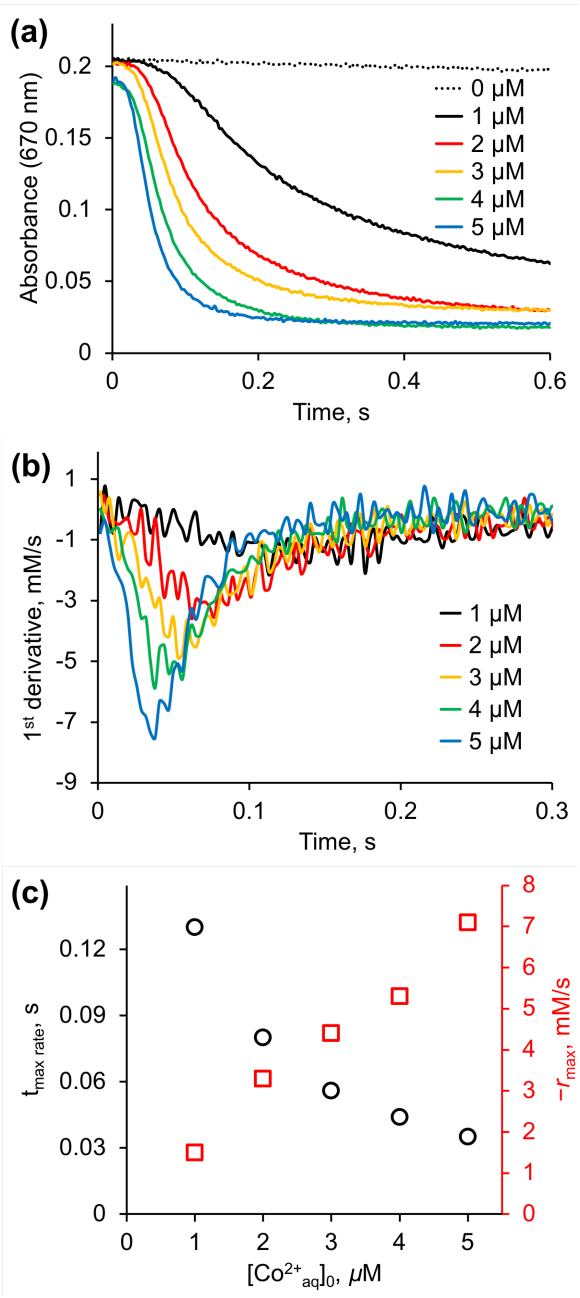

Figure 5.4. (a) Effect of $[Co^{2+}_{aq}]_0$ on the kinetics of water oxidation catalyzed by Co^{2+}_{aq} (labels are $[Co^{2+}_{aq}]_0$). (b) First-derivative kinetic curves (labels are $[Co^{2+}_{aq}]_0$). (c) Dependence of the induction periods (black) and maximum rates (red) on $[Co^{2+}_{aq}]_0$. Conditions: $[[Ru(bpy)_3]^{3+}]_0 \approx 0.5$ mM, 50 mM NaB_i, pH 9.0, 25 °C.

To measure the induction period, we used the time required to reach maximum rates. The first derivative ($d[[Ru(bpy)_3]^{3+}]/dt = 420 \times dA_{670}/dt$) of the kinetic curves as a function of time were used to quantify the induction periods and the maximum of the reaction rates. The maximum reaction rates depend linearly on $[[Ru(bpy)_3]^{3+}]_0$ up to ~ 0.4 mM; however, the induction periods are largely independent of $[[Ru(bpy)_3]^{3+}]_0$ as clearly seen in Figures 5.3(b) and (c). Thus, the initial concentration of $[Ru(bpy)_3]^{3+}$ has no influence on the aggregation of Co species under catalytic conditions ($[[Ru(bpy)_3]^{3+}]_0 >> [Co^{2+}_{aq}]_0$). Analysis of the initial-rate dependence on $[Co^{2+}_{aq}]_0$ in Figure 5.4, was conducted using the same approach as in Figure 5.3. The induction period exhibits an inverse linear dependence on $[Co^{2+}_{aq}]_0$ unlike the dependence on $[[Ru(bpy)_3]^{3+}]_0$, and the maximum rates depend largely linearly in the range of low $[Co^{2+}_{aq}]_0$. On the basis of these findings, we propose the reaction mechanism along with corresponding simulation results for the possible formation of Co-multimers which are responsible for the induction periods and the potential active catalysts.

The first step is oxidation of Co(II) to Co(III) by Ru(III). Here, only the oxidation states Co and Ru are used for simplicity.

$$Co(II) + Ru(III) \rightleftarrows Co(III) + Ru(II) \qquad (5.5)$$

The Co(II) speciation at pH 9 was discussed earlier. We assume that this reaction is thermodynamically favorable by 120 mV: the rate constant of the forward reaction is taken as 1.0×10^9 $M^{-1}s^{-1}$ and that of the reverse reaction is 1.0×10^7 $M^{-1}s^{-1}$. Aggregation of Co(III) species is assumed to be irreversible, and the rate constants of all reactions are described by a single rate constant. We assume that the rate in the induction period is controlled by the water exchange rate and use the rate constant 1.0×10^5 $M^{-1}s^{-1}$. In our

analysis we considered dimers and trimers as the two most dominant species, with the formation of dimer and trimer are based on the Co(III) species when $[[Ru(bpy)_3]^{3+}]_0 >> [Co^{2+}_{aq}]_0$. The following reactions are included in our model.

$$Co(III) + Co(III) \rightarrow Co(III)\text{-}Co(III) \quad (5.6)$$

$$Co(III)\text{-}Co(III) + Co(III) \rightarrow Co(III)\text{-}Co(III)\text{-}Co(III) \quad (5.7)$$

$$Co(IV)\text{-}Co(III) + Co(III) \rightarrow Co(IV)\text{-}Co(III)\text{-}Co(III) \quad (5.8)$$

$$Co(IV)\text{-}Co(IV) + Co(III) \rightarrow Co(IV)\text{-}Co(IV)\text{-}Co(III) \quad (5.9)$$

$$Co(II) + Co(III)\text{-}Co(IV) \rightarrow Co(III)\text{-}Co(III)\text{-}Co(III) \quad (5.10)$$

Eq 5.6 is the formation of dimer and eqs 5.7 – 5.10 are the formation of trimers. The reaction rate constants for oxidation of species containing Co(III) are assumed to be the same and close to the diffusion controlled limit, $1.0 \times 10^9\ M^{-1}s^{-1}$. These reactions are considered to be thermodynamically neutral, therefore the reverse reactions are taken to be $1.0 \times 10^9\ M^{-1}s^{-1}$ as well.

$$Co(III)\text{-}Co(III) + Ru(III) \rightleftarrows Co(IV)\text{-}Co(III) + Ru(II) \quad (5.11)$$

$$Co(III)\text{-}Co(III)\text{-}Co(III) + Ru(III) \rightleftarrows Co(IV)\text{-}Co(III)\text{-}Co(III) + Ru(II) \quad (5.12)$$

The reaction rate constants for oxidation of species containing Co(III) and Co(IV) are assumed to be slightly slower than those for oxidation of species containing Co(III), so rate constants of $1.0 \times 10^8\ M^{-1}s^{-1}$ are used. Again, however, the reverse reactions are assumed to be $1.0 \times 10^8\ M^{-1}s^{-1}$ in the same approach.

$$Co(IV)\text{-}Co(III) + Ru(III) \rightarrow Co(IV)\text{-}Co(IV) + Ru(II) \quad (5.13)$$

$$Co(IV)\text{-}Co(III)\text{-}Co(III) + Ru(III) \rightleftarrows Co(IV)\text{-}Co(IV)\text{-}Co(III) + Ru(II) \quad (5.14)$$

The complexes containing two Co(IV) atoms react with water to form hydroperoxyl intermediate, HOO-Co(III). The rate constant *cannot* be predicted, so we used this rate constant as a variable parameter for simulation.

$$\text{Co(IV)-Co(IV)} \rightarrow \text{HOO-Co(III)-Co(III)} \quad (5.15)$$

$$\text{Co(IV)-Co(IV)-Co(III)} \rightarrow \text{HOO-Co(III)-Co(III)-Co(III)} \quad (5.16)$$

The final step is the fast oxidation of the hydroperoxyl intermediates by two Ru(III) to release O_2.

$$\text{HOO-Co(III)-Co(III)} + 2\,\text{Ru(III)} \rightarrow \text{Co(III)-Co(III)} + O_2 + 2\,\text{Ru(II)} \quad (5.17)$$

$$\text{HOO-Co(III)-Co(III)-Co(III)} + 2\,\text{Ru(III)} \rightarrow \text{Co(III)-Co(III)-Co(III)} + O_2 + 2\,\text{Ru(II)} \quad (5.18)$$

On the basis of the above reaction mechanism, we calculated the maximum rates of $[[Ru(bpy)_3]^{3+}$ consumption and the time to achieve the maximum rates as a function of [Co(II)]. The simulated data are in good agreements with experimental data as shown in Figure 5.5. This analysis shows that the contribution of the trimer is minimal.

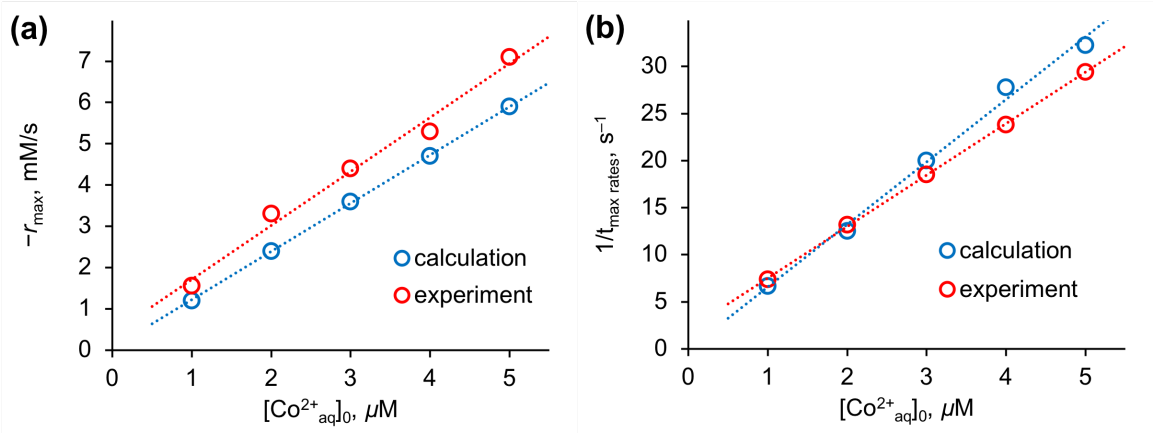

Figure 5.5. (a) Dependence of the maximum reaction rates on $[Co^{2+}_{aq}]_0$. (b) Dependence of the inverse induction periods (the time reached maximum rates) on $[Co^{2+}_{aq}]_0$. Conditions: $[[Ru(bpy)_3]^{3+}]_0 \approx 0.5$ mM, 50 mM NaB_i, pH 9.0, 25 °C. The calculated and experimental data are colored in blue and red, respectively.

5.3.4 Double Mixing Stopped-Flow Kinetic Study

The above observation alone, however, is not sufficient to fully explain the behaviors and identification of polynuclear Co species. To study the formation of Co-multimers and the corresponding catalytic water oxidation activities further, a double mixing stopped-flow method was used: both aging times and $[Co^{2+}_{aq}]_0$ were varied. The time-resolved kinetics are presented in Figure 5.6. The reaction rates apparently decrease as the aging time increases while the kinetic curves exhibit similar reaction rates at the very short aging times (~ 0.01 – 0.1 s) in the presence of both 5 and 10 μM $Co(II)_{aq}$ (Figures 5.6(a) and (b), respectively). However, the rate is becoming similar or a bit slower at higher

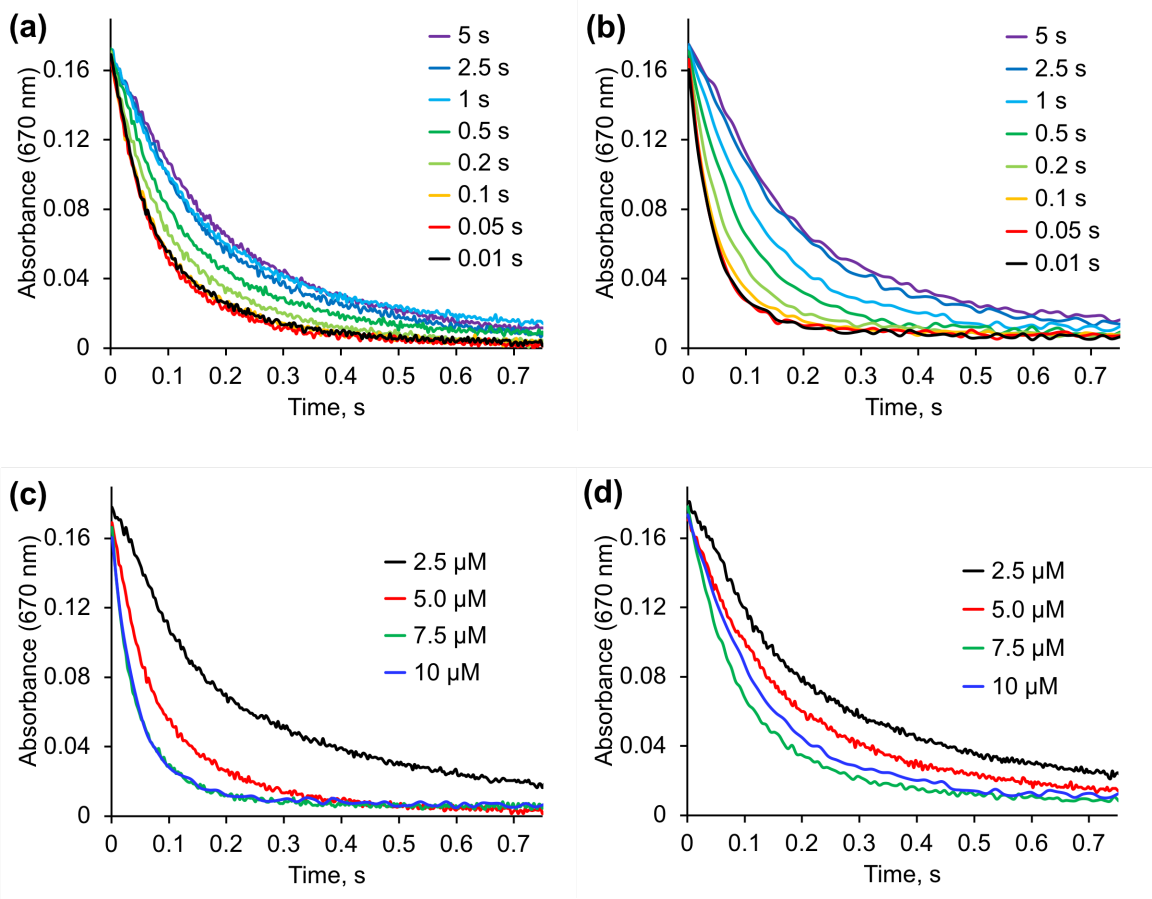

Figure 5.6. Effect of aging times in kinetics of water oxidation catalyzed by (a) 5 μM $[Co^{2+}_{aq}]_0$ and (b) 10 μM $[Co^{2+}_{aq}]_0$ (labels are the aging times). Effect of $[Co^{2+}_{aq}]_0$ on the kinetics with (c) 0.01s and (d) 1s aging times (labels are $[Co^{2+}_{aq}]_0$). Conditions: $[[Ru(bpy)_3]^{3+}] \approx 0.45$ mM, 80 mM NaB_i, pH 9.0, 25 °C in all cases.

$[Co^{2+}_{aq}]_0$ as the aging time increases. For more detailed analysis, the effect of $[Co^{2+}_{aq}]_0$ in water oxidation kinetics is given in Figures 5.6(c) and (d). At the aging time of 0.01 s, the reaction is getting faster with increase of $[Co^{2+}_{aq}]_0$, but nearly identical for 7.5 and 10 μM $[Co^{2+}_{aq}]_0$ (Figure 5.6(c)); a similar trend is observed for the reactions with 1 s aging times.

In this case, however, the reaction with 10 μM $[Co^{2+}_{aq}]_0$ is faster than that with 7.5 μM $[Co^{2+}_{aq}]_0$ at the 0.01 s aging time. A similar trend is observed in the kinetic curves at relatively long aging times (~ 1 – 5 s) (Figures 5.6(a) and (b)). The reaction proceeds faster in the presence of lower concentration ($[Co^{2+}_{aq}]_0$ = 5 μM, Figure 5.6(a)) than higher ($[Co^{2+}_{aq}]_0$ = 10 μM, Figure 5.6(b)).

On the basis of the observation, the dependence of the rates on aging time increases at higher $[Co^{2+}_{aq}]_0$, revealing growth of Co-multimers is time- and concentration-dependent. One can be simply concluded that more efficient water oxidation by Co species is mainly responsible for the low degree of Co-multimer formation, an inference consistent with our model (dimer and trimer are largely dominant). Furthermore, the high degree of Co aggregation inhibits (or slows down from loss of active sites in Co clusters) the reaction based on decrease of reaction rates with increasing aging time. The kinetics at lower $[Co^{2+}_{aq}]_0$ (2.5 μM) in Figures 5.6(c) and (d) have short induction periods, showing that some aggregation of Co species in necessary for high catalytic activity. Importantly, the induction period almost disappears after a very short time (0.01 s), which is considerably shorter than a typical induction period under turnover conditions (> 0.05 s). Our expectation regarding kinetic trends is that higher concentrations of $Co(II)_{aq}$ and longer aging times should lead to more aggregation of Co-multimers, resulting in slower reactions, with the trends becoming nearly independent of these parameters at some point. However, the kinetic trend at longer aging times (> 1 s) remains unclear as shown in Figure 5.6(d). One possible explanation here is that there is breakdown of higher-order aggregates into smaller species such as dimers, which are mainly responsible for efficient catalytic water oxidation.

We propose the reaction mechanism in eqs 5.19 and 5.20 to explain the effect of the aging time on the induction period. When Co^{2+}_{aq} and $[Ru(bpy)_3]^{3+}$ are mixed in 1:1 ratio in the premixing event, both Co(II) and Co(III) are present in solution. In consequence, two additional reactions in eqs 5.19 and 5.20 are included in the kinetic model.

$$\text{Co(II)} + \text{Co(III)} \rightarrow \text{Co(II)-Co(III)} \tag{5.19}$$

$$\text{Co(II)-Co(III)} + \text{Ru(III)} \rightleftarrows \text{Co(III)-Co(III)} + \text{Ru(II)} \tag{5.20}$$

Since the water exchange rate is much faster for Co(II) complexes that for those containing Co(III), the reaction in eq 5.19 is much faster than that in eq 5.6. The simulated kinetic curves with $k_{19} = 1.0 \times 10^9$ $M^{-1}s^{-1}$ are shown in Figure 5.7. The change of the

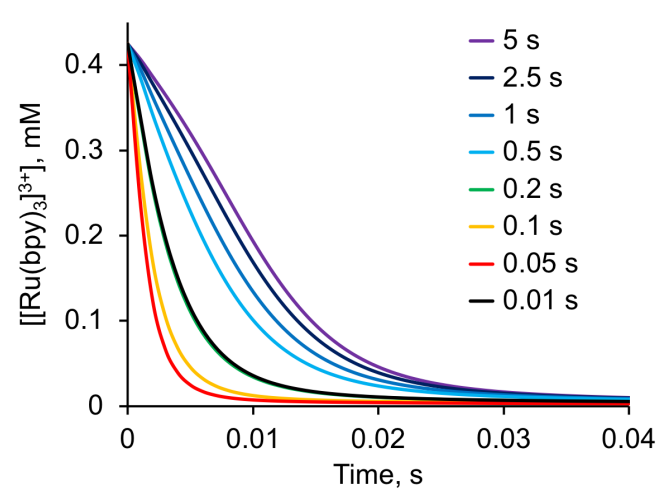

Figure 5.7. Effect of aging times on the simulated kinetics of catalytic water oxidation initiated on addition of Co^{2+}_{aq}. The labels are the aging times (the time intervals between the first and second mixing events). Conditions: $[Co^{2+}_{aq}]_0 = 5$ μM, $[Ru(bpy)_3]^{3+}]_0 = 5$ μM (for the pre-mixing), $[[Ru(bpy)_3]^{3+}]_0 = 0.42$ mM (for the second mixing).

simulated kinetic curve shapes is qualitatively consistent with the experimentally obtained curves. The reaction proceeds faster as the aging time increases up to 0.05 s, then slower with longer aging times, indicating that the addition of reactions in eqs 5.19 and 5.20 to our kinetic model should be considered in evaluating the double-mixing stopped-flow data. The proposed model requires further development along with more detailed information and reasonable rate constants for better results;[48] however, the kinetic model qualitatively explains water oxidation catalyzed by Co^{2+}_{aq}.

Since Co(II) has a significantly faster water exchange rate, the formation of the dimer Co(II)-Co(III) is much faster than dimerization of Co(III). As a result, dimerization of Co-species during premixing is faster under the condition $[[Ru(bpy)_3]^{3+}]_0 \approx [Co^{2+}_{aq}]_0$. If

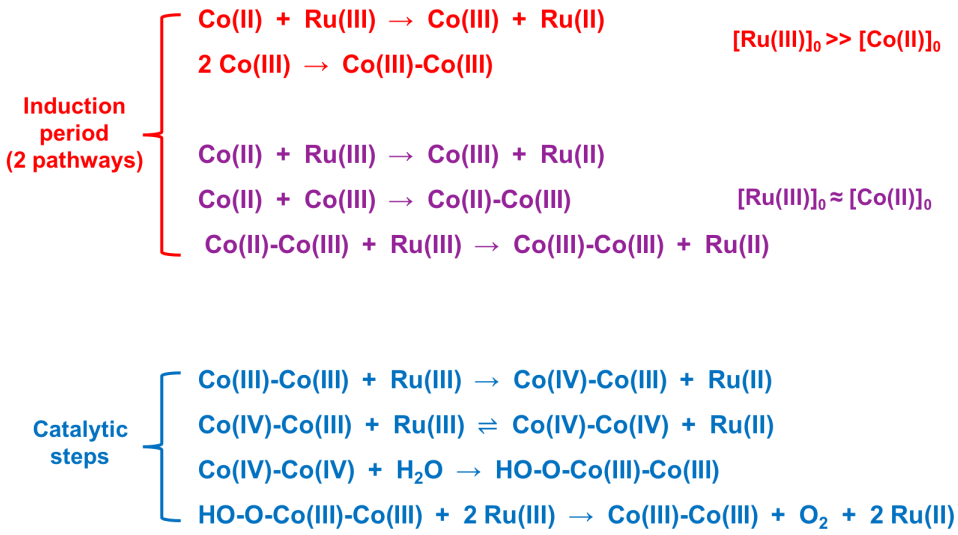

Scheme 5.2. The simplified reaction mechanism of water oxidation catalyzed by $Co(II)_{aq}$.

the large excess of $[Ru(bpy)_3]^{3+}$ is added ($[[Ru(bpy)_3]^{3+}]_0 >> [Co^{2+}_{aq}]_0$), then $Co(II)_{aq}$ is present in very low concentration and the aggregation proceeds through a slow dimerization of Co(III). The overall reaction can be simply described in Scheme 5.2.

5.4 Conclusions

The **Co_4V_2** has been clearly identified as a true WOC on the basis of our kinetic studies. The early-time kinetic measurements clearly distinguish the catalytic water oxidation rates of **Co_4V_2** and $Co(II)_{aq}$. The distinctive kinetic feature for water oxidation catalyzed by Co^{2+}_{aq}, namely the induction period, was studied to probe the true catalyst originating from $Co(II)_{aq}$ under homogeneous conditions. Time-resolved kinetics using a double-mixing stopped-flow method provided detailed insight into induction period. Co-dimer appears to be the principal efficient water oxidation catalyst on oxidation by $[Ru(bpy)_3]^{3+}$. The formation of Co-dimer explains the induction period in kinetic curves consistent with two pathways: Co(II)-Co(III) dimer forms when $[Ru(III)]_0 \approx [Co(II)]_0$, and Co(III)-Co(III) forms directly from two Co(III) when $[Ru(III)]_0 >> [Co(II)]_0$. The kinetic modeling effectively describes the experimental data based on the proposed mechanism. Further studies are required to support our hypothesis in detail and to provide a more detailed mechanism. These studies are in progress.

5.5 References

(1) Lewis, N. S.; Nocera, D. G. *Proc. Natl. Acad. Sci.* **2006,** *103*, 15729.

(2) Barber, J. *Chem. Soc. Rev.* **2009,** *38*, 185.

(3) Gray, H. B. *Nat. Chem.* **2009,** *1*, 112.

(4) Hurst, J. K. *Science* **2010,** *328*, 315.

(5) Blakemore, J. D.; Crabtree, R. H.; Brudvig, G. W. *Chem. Rev.* **2015,** *115*, 12974.

(6) Garrido-Barros, P.; Gimbert-Surinach, C.; Matheu, R.; Sala, X.; Llobet, A. *Chem. Soc. Rev.* **2017,** *46*, 6088.

(7) Roger, I.; Shipman, M. A.; Symes, M. D. *Nat. Rev. Chem.* **2017,** *1*, 0003.

(8) Shafirovich, V. Y.; Khannanov, N. K.; Strelets, V. V. *Nouveau J. de Chim.* **1980,** *4*, 81.

(9) Brunschwig, B. S.; Chou, M. H.; Creutz, C.; Ghosh, P.; Sutin, N. *J. Am. Chem. Soc.* **1983,** *105*, 4832.

(10) Kanan, M. W.; Nocera, D. G. *Science* **2008,** *321*, 1072.

(11) Jiao, F.; Frei, H. *Angew. Chem. Int. Ed.* **2009,** *48*, 1841.

(12) Yin, Q.; Tan, J. M.; Besson, C.; Geletii, Y. V.; Musaev, D. G.; Kuznetsov, A. E.; Luo, Z.; Hardcastle, K. I.; Hill, C. L. *Science* **2010,** *328*, 342.

(13) Zhong, D. K.; Gamelin, D. R. *J. Am. Chem. Soc.* **2010,** *132*, 4202.

(14) Artero, V.; Chavarot-Kerlidou, M.; Fontecave, M. *Angew. Chem. Int. Ed.* **2011,** *50*, 7238.

(15) Gerken, J. B.; McAlpin, J. G.; Chen, J. Y. C.; Rigsby, M. L.; Casey, W. H.; Britt, R. D.; Stahl, S. S. *J. Am. Chem. Soc.* **2011,** *133*, 14431.

(16) Huang, Z.; Luo, Z.; Geletii, Y. V.; Vickers, J.; Yin, Q.; Wu, D.; Hou, Y.; Ding, Y.; Song, J.; Musaev, D. G.et al. *J. Am. Chem. Soc.* **2011,** *133*, 2068.

(17) McCool, N. S.; Robinson, D. M.; Sheats, J. E.; Dismukes, G. C. *J. Am. Chem. Soc.* **2011,** *133*, 11446.

(18) Shevchenko, D.; Anderlund, M. F.; Thapper, A.; Styring, S. *Energy Environ. Sci.* **2011,** *4*, 1284.

(19) Surendranath, Y.; Lutterman, D. A.; Liu, Y.; Nocera, D. G. *J. Am. Chem. Soc.* **2012,** *134*, 6326.

(20) Yamada, Y.; Yano, K.; Hong, D.; Fukuzumi, S. *Phys. Chem. Chem. Phys.* **2012,** *14*, 5753.

(21) Zidki, T.; Zhang, L.; Shafirovich, V.; Lymar, S. V. *J. Am. Chem. Soc.* **2012,** *134*, 14275.

(22) Blakemore, J. D.; Gray, H. B.; Winkler, J. R.; Müller, A. M. *ACS Catal.* **2013,** *3*, 2497.

(23) Nakazono, T.; Parent, A. R.; Sakai, K. *Chem. Commun.* **2013,** *49*, 6325.

(24) Pintado, S.; Goberna-Ferrón, S.; Escudero-Adán, E. C.; Galán-Mascarós, J. R. *J. Am. Chem. Soc.* **2013,** *135*, 13270.

(25) Song, F.; Ding, Y.; Ma, B.; Wang, C.; Wang, Q.; Du, X.; Fu, S.; Song, J. *Energy Environ. Sci.* **2013,** *6*, 1170.

(26) Deng, X.; Tüysüz, H. *ACS Catal.* **2014,** *4*, 3701.

(27) Lv, H.; Song, J.; Geletii, Y. V.; Vickers, J. W.; Sumliner, J. M.; Musaev, D. G.; Kögerler, P.; Zhuk, P. F.; Bacsa, J.; Zhu, G.et al. *J. Am. Chem. Soc.* **2014,** *136*, 9268.

(28) Ullman, A. M.; Liu, Y.; Huynh, M.; Bediako, D. K.; Wang, H.; Anderson, B. L.; Powers, D. C.; Breen, J. J.; Abruña, H. D.; Nocera, D. G. *J. Am. Chem. Soc.* **2014,** *136*, 17681.

(29) Burke, M. S.; Kast, M. G.; Trotochaud, L.; Smith, A. M.; Boettcher, S. W. *J. Am. Chem. Soc* **2015,** *137*, 3638.

(30) Han, J.; Wang, D.; Du, Y.; Xi, S.; Hong, J.; Yin, S.; Chen, Z.; Zhou, T.; Xu, R. *J. Mater. Chem: A* **2015,** *3*, 20607.

(31) Aiyappa, H. B.; Thote, J.; Shinde, D. B.; Banerjee, R.; Kurungot, S. *Chem. Mater.* **2016,** *28*, 4375.

(32) Mondschein, J. S.; Callejas, J. F.; Read, C. G.; Chen, J. Y. C.; Holder, C. F.; Badding, C. K.; Schaak, R. E. *Chem. Mater.* **2016,** *29*, 950.

(33) Ullman, A. M.; Brodsky, C. N.; Li, N.; Zheng, S.-L.; Nocera, D. G. *J. Am. Chem. Soc.* **2016,** *138*, 4229.

(34) Kinastowska, K.; Barroso, J.; Yate, L.; Pavlov, V.; Chuvilin, A.; Bartkowiak, W.; Grzelczak, M. *Photochem. Photobiol. Sci.* **2017,** *16*, 1771.

(35) Shi, H.-T.; Li, X.-X.; Wu, F.-H.; Yu, W.-B. *Dalton Trans.* **2017,** *46*, 16321.

(36) Xie, L.; Zhang, R.; Cui, L.; Liu, D.; Hao, S.; Ma, Y.; Du, G.; Asiri, A. M.; Sun, X. *Angew. Chem. Int. Ed.* **2017,** *56*, 1064.

(37) Zhang, L.; Mi, T.; Ziaee, M. A.; Liang, L.; Wang, R. *J. Mater. Chem. A* **2018,** *6*, 1639.

(38) Kanan, M. W.; Surendranath, Y.; Nocera, D. G. *Chem. Soc. Rev.* **2009,** *38*, 109.

(39) Lutterman, D. A.; Surendranath, Y.; Nocera, D. G. *J. Am. Chem. Soc.* **2009,** *131*, 3838.

(40) Kanan, M. W.; Yano, J.; Surendranath, Y.; Dincă, M.; Yachandra, V. K.; Nocera, D. G. *J. Am. Chem. Soc.* **2010,** *132*, 13692.

(41) McAlpin, J. G.; Surendranath, Y.; Dinca, M.; Stich, T. A.; Stoian, S. A.; Casey, W. H.; Nocera, D. G.; Britt, R. D. *J. Am. Chem. Soc.* **2010,** *132*, 6882.

(42) Vickers, J. W.; Lv, H.; Sumliner, J. M.; Zhu, G.; Luo, Z.; Musaev, D. G.; Geletii, Y. V.; Hill, C. L. *J. Am. Chem. Soc.* **2013,** *135*, 14110.

(43) Folkman, S. J.; Finke, R. G. *ACS Catal.* **2017,** *7*, 7.

(44) Li, B.; Yan, Y.; Li, F.; Xu, L.; Bi, L.; Wu, L. *Inorg. Chim. Acta* **2009**, 2796.

(45) Baes, J., Charles F.; Mesmer, R. E. *The Hydrolysis of Cations*; John Wiley & Sons: New York, 1976.

(46) Barnum, D. W. *Inorg. Chem.* **1983,** *22*, 2297.

(47) Richens, D. T. *The Chemistry of Aqua Ions: Synthesis, Structure, and Reactivity: A Tour through the Periodic Table of the Elements*; John Wiley & Sons: Chichester, 1997.

(48) The overall kinetic modeling is in progress to obtain better results. Therefore, we do not provide the exact values of reaction rate constants.